ABSTRACT

Title of Document: EFFECTS OF BAR FORMATION ON CHANNEL STABILITY AND SEDIMENT LOADS IN AN URBAN WATERSHED

Zachary David Blanchet,
Master of Science, 2009

Directed By: Dr. Karen L. Prestegaard,
Department of Geology

This study investigates channel adjustment due to urbanization in the Little Paint Branch creek of the Anacostia River watershed. In the past 15 years, large gravel bars have formed in the channels, more than doubling the active channel width of some reaches. Field data was collected to analyze downstream hydraulic geometry and the effects of gravel bars on shear stress, turbidity, and morphological change. The watershed was gauged at three locations to document the contributions of discharge and sediment to the downstream Anacostia Estuary. The results indicate that Little Paint Branch Creek generates proportionally more runoff per basin area than the watershed does as a whole, even though the impervious surface area is lower in the upstream tributaries, like Little Paint Branch Creek. Bar formation induces channel widening, which decreases flow depth and thus shear stress for bankfull and higher stages. This shoaling limits bed transport and will eventually limit bank erosion.

EFFECTS OF BAR FORMATION ON CHANNEL STABILITY AND SEDIMENT LOADS IN AN URBAN WATERSHED

By

Zachary David Blanchet

Thesis submitted to the Faculty of the Graduate School of the
University of Maryland, College Park, in partial fulfillment
of the requirements for the degree of
Master of Science
2009

Advisory Committee:
Professor Karen L. Prestegaard, Chair
Professor Saswata Hier-Majumder
Professor Wenlu Zhu

Acknowledgements

I would like to thank my advisor, Dr. Karen Prestegaard, and my committee, Dr. Saswata Hier-Majumder and Dr. Wenlu Zhu for their help writing and editing this thesis. Much appreciation also goes to Erik Hankin, Marcie Occhi, Achyut Dangol, and Andrew Kosiba for their help with data collection, and to the Anacostia Watershed Society and EPA for funding my research.

Table of Contents

List of Tables

List of Figures

List of Symbols

A	bankfull area
B	surface width
C	dimensionless sediment concentration
d	depth
D	grain size
D_{50}	Median Grain Size
D_{84}	84^{th} percentile grain size
D_c	center channel depth
DA	drainage area
H	depth
H*	dimensionless depth
P	wetted perimeter
P_{bank}	bank wetted perimeter
P_{bed}	bed wetted perimeter
q_b	unit sediment transport
q*	Dietrich (1989) Sediment Availability
Q	discharge
Q*	Dimensionless Discharge
Q_b	total channel width sediment transport
Q_s	total sediment discharge
S	water surface gradient
SF_{bank}	shear force on the bank
TSS	Total Suspended Sediments (mg/l)
u	velocity
u*	shear velocity
U*	Dimensionless Velocity
W	width
W*	Dimensionless Width
Y_0	max water depth
u*	shear velocity
R	hydraulic radius
$\mathcal{R}$	submerged specific gravity of sediment
τ_b	shear stress
τ_c	critical shear stress
τ_{cs}	critical shear stress for surface sediment
τ_{css}	critical shear stress for subsurface sediment
τ^*_c	critical dimensionless shear stress
ρ_s	sediment density
ρ_w	water density
μ'	dimensionless bed/bank strength relationship
Φ'	bank strength
Φ	angle of repose for loose sediment
θ	bank angle

Chapter 1: Scope and Approach

1.1 Introduction

As coastal cities expand into once natural watersheds, urbanization-driven changes in stream discharge and sediment supply can significantly affect stream channel morphology and behavior (Hammer, 1972; Morisawa and LaFlure, 1979; Arnold et al., 1982; Neller, 1988). Stored sediment can be mobilized by larger and more frequent peak flows, which can increase both sediment transport and localized deposition in low gradient downstream reaches (Wolman and Schick, 1967). Flooding and sediment problems have become prominent in coastal cities around the Chesapeake Bay Watershed and the fine sediment yield from urban watersheds causes damage to aquatic ecosystems (Brush, 1989; Cronin and Vann, 2003; Kemp et al., 2005). Sediment pollution is a major problem in coastal areas around the world and the impacts can be as difficult to reverse as they are far reaching. (Chesapeake Bay Foundation, 2006).

Over the span of several hundred years, land use in the Anacostia River watershed has replaced the original forested land cover with agricultural and subsequently urban/suburban land uses (Allmendinger, 2007). Agricultural land uses affected water runoff and soil erodibility, which resulted in head-ward erosion of stream channels and facilitated the movement of fine sediment from the hillslopes to downstream reaches (Wolman, 1967) Urbanization increases the amount of overland flow runoff, but fine sediment production from paved surfaces is low in comparison with the intensive agricultural land uses in the early 1900's (Dawdy,

1967; Wolman, 1967; Wolman and Schick, 1967). Sediment stored in streambanks can become sediment sources as part of the channel widening adjustments to urbanization (Allmendinger et al., 2007).

A sediment budget constructed for the Good Hope Tributary, a Piedmont tributary of the Anacostia River, indicates that land use changes can be tracked through three distinct fluvial stratigraphic units: a basal deposit of fine-grained organic rich sediment, overlaid by coarse angular sediment, that is overlain by sediment derived from agricultural sources (Allmendigner, 2007). The Little Paint Branch creek originates in the Piedmont, but it is primarily in the Coastal Plain Province. Dangol (2009) found these same three stratigraphic units in the Little Paint Branch tributary.

Urbanization affects the magnitude of frequent (low recurrence interval) flood events (fig. 1), which form the bankfull channel, A common consequence of an increase in the bankfull flood ($\sim Q_{1.5}$) is an increase in channel width to accommodate the new flow regime (e.g. Hammer, 1972).

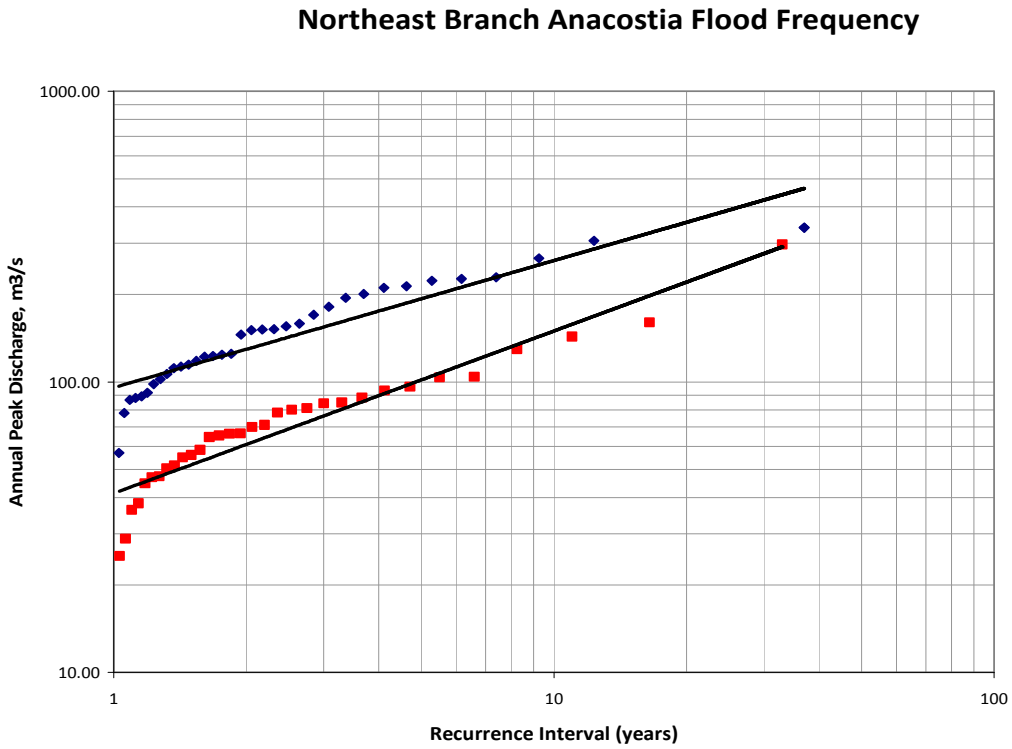

Figure 1: Flood frequency curve for the NE branch Anacostia River between 1933 and 1969 (red) and 1970 and 2006 (blue). The bankfull discharge has doubled at this site.

A flow regime in a river is an adjusted condition. It occurs when the flood discharges, including both water and sediment, do not vary significantly over large periods of time, from decades to centuries. The channel geometry, flow, and sedimentary processes become adjusted to the flood discharges and only minor changes occur in the channel condition with changing flow stage (Bridge, 2003).

In his work, Hammer proposed that stream channels would take about 30 years to develop new bankfull channels that could accommodate the new flow regime. The research by Hammer (1972) and others who have examined channel enlargement due to urbanization have focused primarily on the adjustment of the

channel due to changes in discharge. They suggest that stream channels accommodate the increase in discharge primarily by channel widening. This maintains the channel bankfull depth and shear stress. Thus, if the channel was a threshold channel prior to urbanization (i.e. it initiates bedload transport at bankfull stage) then it remains a threshold channel because the dimensionless shear stress, which is the ratio of the shear stress of the water to the bed or bank grain resisting forces, has not changed. These changes are summarized in fig. 2.

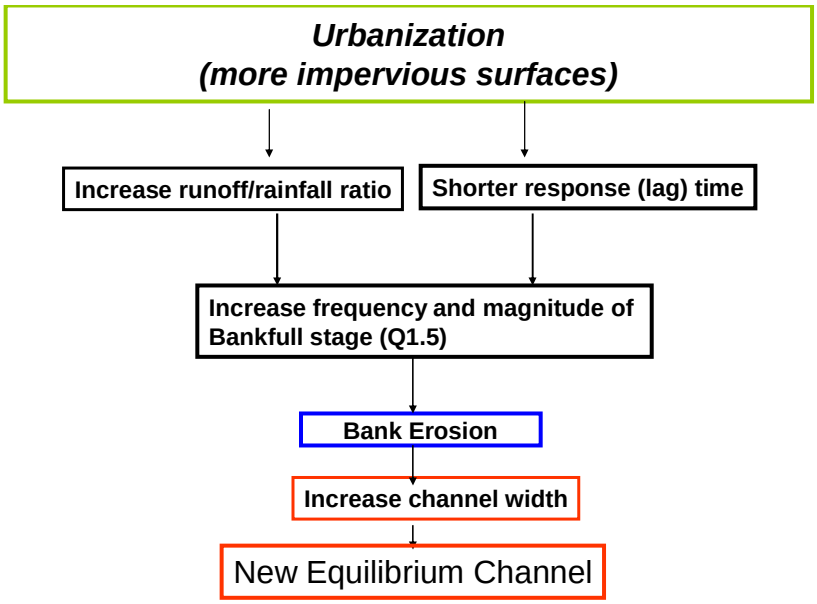

Land use changes in green, hydrological and hydraulic changes in black, sediment transport changes in changes blue, morphological changes in red.

Figure 2: Flow diagram of the effects of urbanization on channel morphology with the assumptions: a) that urbanization primarily affects discharge, and b) that bed sediment is at the threshold of motion at bankfull stage.

The morphology of a stream channel is dependent on two independent variables: the sediment supply and the flow regime. Urbanization may affect the

amount and size of sediment delivered to stream channels by a variety of erosion processes including: gully erosion, bank erosion, and increased mobilization of bed sediment. This change in sediment supply can affect bedload transport and bedload deposition rates (Wilcock, 2001). The bankfull channel shear stress can be increased by bed erosion and depth increases or decreases, and the bankfull dimensionless shear stress can be affected by both bankfull shear stress and bed grain size changes. These considerations suggest that not all stream channels that undergo urbanization will respond by adjusting from one threshold channel to a slightly larger one primarily by bank erosion.

Tributaries of the NE branch of the Anacostia River contain large gravel bars, which indicate sediment transport and deposition rates above threshold conditions. These gravel bars became prominent features of downstream reaches of Little Paint Branch and Paint Branch Creeks (fig. 3) by the early 1990's (Behrns, 2007; Kosiba, 2008) The formation of central gravel bars in the channel has accelerated bank erosion and channel widening, potentially releasing fine-grained bank sediments to downstream locations (Berhns, 2007). Behrns (2007) evaluated channel changes on Paint Branch Creek, and found that although channel widening and deepening have both occurred, the major morphological change is due to channel widening. Also, where gravel bars have formed, channel widening is significantly greater than adjacent reaches, although widening around gravel bars is associated with a decrease in depth (Kosiba, 2008).

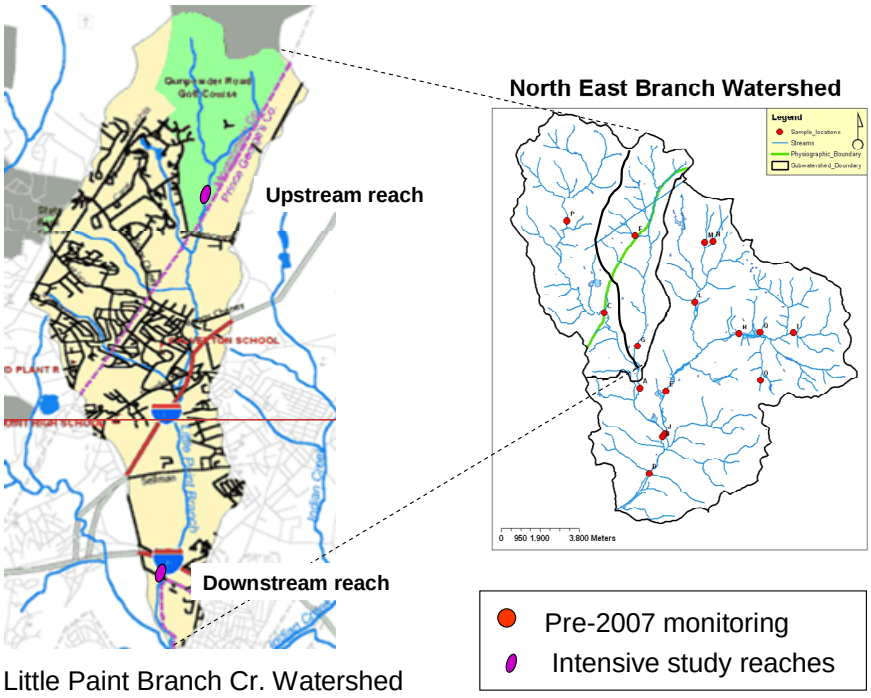

Figure 3: Map of the Little Paint Branch Creek Watershed

These findings suggest that Hammer's model is not applicable to the channel changes being observed in the Anacostia watershed. Fig. 4 demonstrates a revised model of channel change, giving consideration to changes in sediment supply and storage resulting from increased erosion of both the bed and banks. In this model, gravel bar formation produces a negative feedback on channel depth and subsequently bed shear stress. The purpose of this research is to evaluate stream adjustment processes suggested by this model.

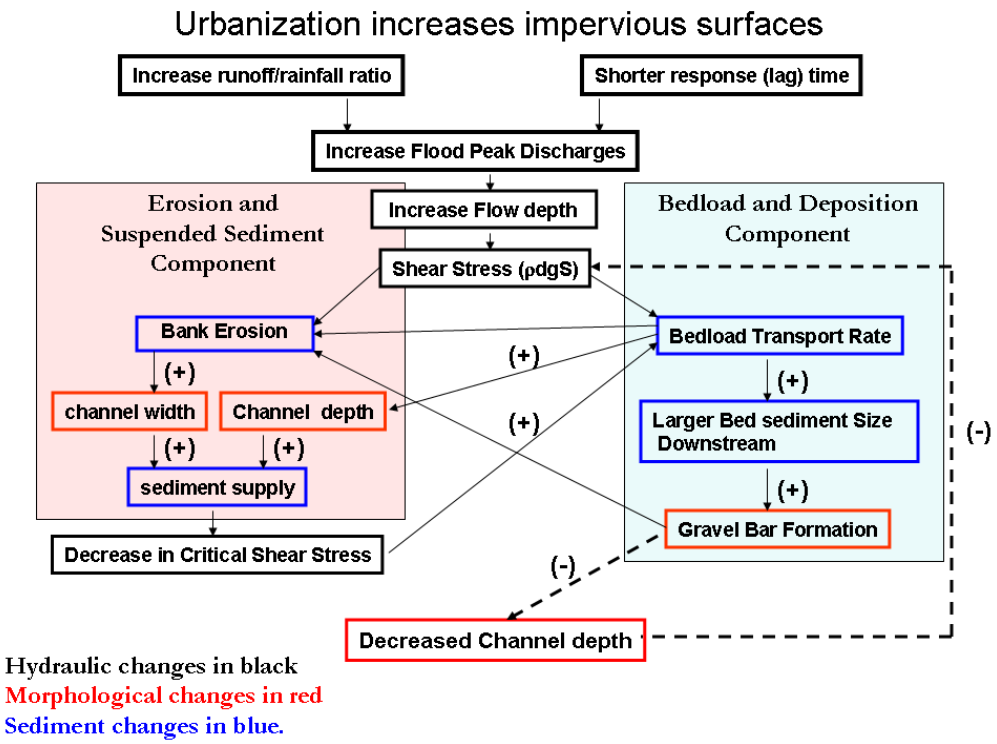

Figure 4: The effects of urbanization on channel morphology with the assumption that an increase in the magnitude of bankfull flow affects flow depth and thus shear stress, this generates bank and bed erosion which affects bedload transport rate. Note negative feedback loop.

1.2 Previous Work

There have been many studies on the impact of urbanization and human land use on watersheds in recent years. Using physical data from lowland streams in western Washington, Booth and Jackson (1997) measured the relationship between channel stability and watershed urbanization, as well as the effectiveness of storm detention ponds.

The study found that a strong correlation exists between channel stability and urbanization. At approximately ten percent impervious surface area, a watershed displays loss of aquatic system function that is demonstrable, and potentially

irreversible. Additionally, it was found that storm detention ponds, a commonly used means of temporarily storing runoff from storm events, succeed at mitigating the peak discharge of storm events, but fall short of reducing the duration of storm flows. In order to reduce storm flow durations, storm detention ponds would need volumes that in most cases would be prohibitively large.

The long term consequences of human settlement in Auckland, New Zealand were studied by Gregory et al. (2008). They examined the evolution of the small, 61 km^2, Twin Streams catchment since European colonization began in the 1840's. Reaches in the catchment were delineated by their setting in the valley, planform, geomorphic features, and bed material texture using procedures outlined by Brierley and Fryirs (2005).

The catchment has undergone four distinct phases of development: 1) the clear cutting of the region's Kauri trees for lumber, 2) settlers arriving to extract the gum of the kauri trees from the soil, 3) the regeneration of native vegetation in the upper parts of the catchment and agricultural/viticultural/horticultural use in the middle and lower reaches, and 4) post WWII urban development which has continued in the middle and lower reaches to the present day.

It was found that there is a spatial variance in channel response that reflects the pattern and rate of past land uses. The most sensitive reaches were those in lowland areas as they had been subject to multiple phases of disturbance further upstream in the catchment. The lowland streams received the bulk of the sediment caused by erosion throughout the catchment, and with their low stream gradient they have a diminished capacity to transport the sediment flux from upstream. As a result,

the lowland streams are continually responding to the legacy of past events to this day. In the upstream reaches that were not channelized, the stream is restoring itself to a natural condition with geomorphic forms consistent with those that existed prior to European colonization.

Studies on watershed urbanization's impact on channel hydraulics and sediment transport mechanics are less common. Recently developed approaches integrate hydraulic geometry and sediment transport considerations to develop models of stable channels. These models include factors such as bank strength and bed material that may change significantly within a short distance downstream. It is therefore possible to more accurately locate the reaches of a stream that are vulnerable to changes in morphology due to erosion or deposition in the near future and to identify those that are currently undergoing a change.

This information is invaluable for the study of Paint Branch Creek because the sediment transport regime has changed over the past ten years. The deposition of new sediment into gravel bars will cause a further change in the storage or transport of sediment. With the potential for this feedback, channel morphology and sediment transport must be modeled as a single dynamic system. There doesn't appear to be an existing model that will accurately account for the small scale and non-threshold channels characteristic of the current state of the Little Paint Branch watershed. As such, most analysis will be done using calculations of dimensionless critical shear stress and sediment composition.

1.3 Hypotheses

1. Urbanization has increased flood discharges, which increases bankfull discharge and bankfull channel area. Channel widening increases the amount of sand-sized bed material, which causes an increase in bedload transport potential in downstream reaches.
2. Gravel bar formation causes shoaling of the bed, which decreases bed shear stress and stabilizes gravel sediment. Gravel bar formation selectively stores fine-grained bed material, coarsening of the bed in the adjacent channels can also stabilize the channel bed around the bars.
1. The formation of gravel bars causes flow divergence and bank erosion. Therefore, turbidity and suspended load are significantly higher at the downstream of the bar complex than upstream of the bar complex.

1.4 Scope

Channel morphology changes in the downstream direction in Little Paint Branch Creek. The downstream reaches with significant gravel bars are very different than the single-thread upstream reaches. Therefore, the approach to this study is designed to examine the channel morphology and sediment characteristics at three different scales (fig. 5**)**. A brief description of these three scales of measurement and the types of data collected at each scale are described below.

1. Watershed Scale. This is the largest scale. I will examine downstream changes in channel morphology and bed sediment characteristics. These data

will be used to calculate sediment flux downstream from the headwaters to the downstream depositional reach. Morphological data will be compared with regional non-urban stream data sets (Prestegaard et al., 2001) to determine the amount of sediment mobilized by urbanization.

2. Bar Complex Scale. Continuously monitored data on turbidity and gauge height were collected at two sites, located upstream and downstream of the bar complex (fig. 6). Water surface gradients and flow velocities were measured at high flows. These data are used to evaluate the over-all effects of the gravel bar complexes on net bedload and suspended loads.

3. Individual Bar or Reach Scale. The last and smallest is at individual channel bars that have formed within the gravel bar complex near Cherry Hill Road (fig. 6), studying short term morphological changes and sediment size distributions relative to shear stresses. In addition to morphological measurements, field measurements of bedload transport, shear stress, and morphological change at individual gravel bars. These data will be used to test the hypothesis that there is a negative feedback between gravel bar formation, channel depth, and shear stress, which causes bed stabilization

The study of the river on these three scales will allow us to understand the morphological and hydrological changes occurring comprehensively, without overlooking smaller changes and interactions.

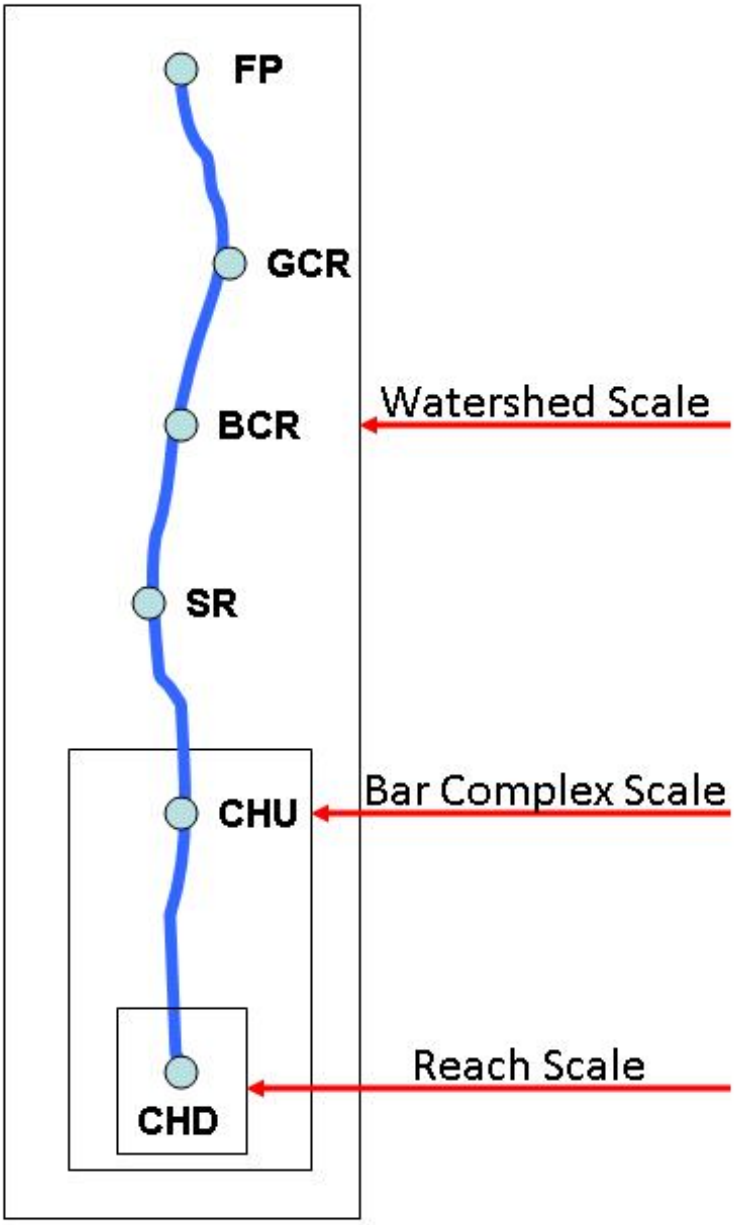

Figure 5: The nested scales of study on Little Paint Branch Creek. FP = Fairland Park, GCR = Greencastle Road, BCR = Briggs Chaney Road, SR = Sellman Road, and CHU = Cherry Hill upstream, CHD = Cherry Hill downstream sites.

Figure 6: Overhead view of the bar complex reach. Gravel bars and their influence on the river are particularly evident in this stretch of the river.: 2009 Tele Atlas, USGS, obtained via Google Earth.

1.5 Importance

Previous work suggests that sediment in urbanized watersheds is from overland flow, bank erosion, and street sources (Allmendinger, 2007; Hession et al., 2003; Wolman and Schick, 1967). For the NE branch of the Anacostia, bank erosion supplies 70-80% of the total sediment load. Flow from overland flow sources appears to provide the remainder (Devereux and Prestegaard, 2008). In the Little Paint

Branch Creek, the size of material stored in the channel banks increases upwards, reflecting deposition by large magnitude floods in recent years (Dangol, 2009). The grain size also changes in the downstream direction. In regions of active bank erosion, the average grain size being eroded from the banks is medium sand (~0.3 mm; Dangol, 2009). During storms events, these particles can be mobilized and moved downstream primarily as suspended load, increasing the water's turbidity and eventually contributing to siltation and water quality problems in the Chesapeake Bay (Kemp et al., 2005).

The EPA has established a total maximum daily load (TMDL) for total suspended sediment (TSS) in the Anacostia, with the goal reducing sediment loads and the movement of various contaminants to levels that meet the accepted water quality standard. The TMDL establishes daily and annual weight of suspended solids allowed to pass through the system.

The Prince George's County Department of Environmental Resources (DER) uses a modeling approach to determine options to sediment load reduction in the portions of the Anacostia under its jurisdiction. The model chosen was the Best Management Practice – Decision Support System (BMP-DSS). It is based off of a GIS platform and uses various water quality models, such as HSPF and SWMM to predict runoff and sediment loads. These models primarily use land use to model water and sediment fluxes. Mitigation procedures (best management practice (BMP) solutions) based on user inputs of various watershed parameters and cost constraints are evaluated. Prince George's has a goal to lower TSS by 96% and TN (total nitrogen) by 80% in future years. At one site in a tributary to the Anacostia, Prince

George's County has begun a project to try to meet these goals. The approach to do this is to minimize bank erosion by channel stability measures or by use of "stream restoration" practices that rely on the Rosgen classification system (Rosgen, 1994).

The validity of the work of Rosgen and the use of his classification system for restoration design has been debated since it was first published (e.g. Simon et al. 2007, Smith and Prestegaard, 2005). Rosgen's classification and restoration models are of the same linear channel progress model that can be seen in fig. 2. The major problem with this type of model is that it disregards any possible change in the hydrology or sediment input into a stream system. It is for this reason that for watersheds that have undergone a change in hydrology and/or sediment supply, linear channel progression models will not accurately predict future morphologies and may actually cause further damage if they are used to plan restoration efforts.

In this thesis, the impact of hydrological and sediment supply alterations to the urbanized Little Paint Branch is analyzed in order to better understand the progression of its downstream channel form. A new conceptual model of changes in channel morphology, hydraulics, and sediment supply is proposed and can be seen in fig. 4. This model has multiple feedbacks, both positive and negative, that take into consideration the effects of bar formation and sediment supply alterations.

Chapter 2: Effects of urbanization on channel morphology, bed sediment characteristics, and bed mobility in a Coastal Plain Watershed.

2.1 Introduction

As erosional and depositional agents, rivers modify the landscape and deliver sediment to downstream locations. The supply of water and sediment to a river influences the spatial and temporal placement of sediment in both the channel and the floodplain. Urbanization causes an increase in impervious surfaces in a watershed, which increases the amount of overland flow during storms. This commonly results in an increase in the magnitude of floods for the same-sized storm event (Pizzuto et al., 2000). These hydrological changes are observed to cause adjustments to river morphology (e.g. channel widening, Hammer, 1972) and erosive power (Hay, 1987). Much of the previous work on the effects of urbanization on stream behavior has focused on changes in channel morphology rather than changes in sediment characteristics and channel mobility.

Rivers transport sediment in different modes: dissolved load, wash load, suspended load, and bed load. Bed load is material that is transported in contact with the bed, so that it travels at a slower velocity than the surrounding flow as it rolls, slides, or saltates along the bed (Church, 2006). Suspended particles are entrained from the bed and transported in the water column by turbulent mixing processes (Mclean, 1991). Sediment transport rates, therefore, depend upon excess shear stress available to transport bedload material and turbulence to transport suspended load.

Both excess shear stress and turbulence can be either determined or estimated from flow variables and sediment characteristics.

Bed mobility and bedload transport rates are difficult to predict (Church, 2006; Barry, 2004). Recent research on initiation of motion and bedload transport indicates that bed substrate surface heterogeneities and the size of subsurface material can significantly affect initiation of motion and sediment transport rates (Wilcock and Crowe, 2003, Dietrich, 1989). Urbanization can affect bed surface and subsurface material due to bed scour or by increasing the supply of sand due to surface erosion and channel widening. In the Little Paint Branch, channel widening has been observed to be a widespread consequence of urbanization. Bank sediment released into the stream system from channel widening can cause morphological changes downstream. The purpose of this chapter is to examine the morphological and sediment mobility changes that have been induced by urbanization.

Hypotheses

1. Stream channels in Little Paint Branch watershed have higher bankfull discharges and larger bankfull channel dimensions than adjacent streams in non-urban watersheds of similar basin area.
2. Coastal Plain channels adjust primarily by widening, which affects the downstream hydraulic geometry.

3. Channel erosion due to urbanization (channel widening and deepening) results in the depletion of subsurface material in headwater reaches, which reduces bedload transport potential in upstream regions.
4. Channel widening increases the amount of sand-sized bed material mobilized in the watershed, which causes an increase in bedload transport potential in downstream reaches.

2.2 Previous Work

2.2.1 Channel morphology and Downstream Hydraulic Geometry

Hydraulic geometry describes the relationship between channel morphology and stream discharge. In their groundbreaking research, Leopold and Maddock (1953) developed an empirical model where the width, depth, and velocity of water flowing through cross sections are expressed as power functions of discharge. The data set of streams examined by Leopold and Maddock (1953) consisted of stream channels without braided or highly meandering reaches. The hydraulic geometry relationships they developed are applicable primarily to single thread, threshold channels.

Leopold and Maddock (1953) presented two ways to examine hydraulic geometry relationships. At-a-station hydraulic geometry indicates the change in channel dimensions with discharge at an individual cross section. For at-a-station hydraulic geometry, depth and velocity accommodate most of the increase in discharge. The downstream changes in channel dimensions (width, depth, velocity)

during an event with a constant frequency, such as the bankfull discharge, is termed the downstream hydraulic geometry. In the downstream case, width and depth accommodate most of the increase in discharge and width generally increases the most with a downstream increase in discharge. The hydraulic geometry relationships are as follows (Leopold and Maddock, 1953):

$$w = aQ^b \quad (1)$$

$$d = cQ^f \quad (2)$$

$$v = kQ^m \quad (3)$$

The hydraulic geometry exponents and the coefficients are also constrained by the continuity equation, thus:

$$Q = ackQ^{b + f + m} \quad (4)$$

$$b + f + m = 1 \quad (5)$$

$$a*c*k = 1 \quad (6)$$

where w = width, d = depth, and v = velocity. In log-log plots of w, d, and v against Q (discharge), a, c, and k are the intercepts of their respective lines against the y-axis, and b, f, and m are the slopes of the lines.

In 1978, Gary Parker examined the empirical hydraulic geometry concept introduced by Leopold and Maddock (1953) and compared them to the conditions required to generate a stable, threshold gravel-bed channel. Stability calculations require information on bed sediment grain size and shear stress (ρgRS). Thus, the

consideration of threshold conditions affects the relationship between bankfull depth and bankfull width. If stream gradient, S, and grain size (D_{50}) and center channel depth (d_c) are determined, then any other pair of parameters can be used to calculate the rest. In order to compare streams of various sizes including laboratory channels, Parker (1978) expressed hydraulic geometry variables as dimensionless numbers by normalizing most channel dimensions by grain size.

$$R = 0.0553\ S^{-1.01} \tag{7}$$

$$\tilde{Q} = 4.97R^{1.70}\ S^{0.50}\ B^{*}\ (1-2.23\ /\ \text{ﬂ}) \tag{8}$$

$$Q^{*} = 1.02\ X\ 10^{-5}\ R^{0.275}\ B^{*}\ (1-4.52\ /\ \text{ﬂ}) \tag{9}$$

Where $R = d_c/D_{50}$ ($8 < R < 140$), ﬂ $= B / D_c$ (ﬂ > 15), d_c = depth at center of channel, $\tilde{Q} = Q/[(\mathcal{R}gD_s)^{0.5}\ D^2_s]$, $Q^{*} = Q_s/[(\mathcal{R}gD_s)^{0.5}\ D^2_s]$, $\mathcal{R} = \rho_s/\rho - 1$ ($\mathcal{R} = 1.65$ for natural rivers with quartz sediment), $B^{*} = B/D_s$, B = bankfull channel width, S = water surface gradient, and Q_s = volumetric sediment discharge.

Parker's (1978) analysis explicitly presented downstream hydraulic geometry considerations as a consequence of downstream changes in grain size and discharge, which are required to maintain threshold conditions. His approach, however, does not address the development of channel bed forms (e.g. channel bars) during sediment transport conditions that are greater than the threshold condition.

2.2.2 Sediment Transport

Much progress has been made in developing parameters to define sediment transport in gravel-bed rivers in the past twenty years. The bedload transport rate q_b is commonly expressed as a power function of excess channel shear stress, as originally defined by Meyers-Peters and Muller:

$$q_b = k(\tau_b - \tau_c)^n \qquad (10)$$

where k and n are determined empirically (n is variable but is commonly expressed as 1.5), τ_b is the shear stress of the bed, and τ_c is the critical shear stress required to move the median grain size of the bed. The coarsening of the surface grains is believed to come about when the local sediment transport rate exceeds the supply rate. In rivers with homogenous sediment this would increase bed erosion, but where the sediment is poorly sorted it can create locally armored channels that will only respond to high shear stresses (Dietrich et al., 1989). Once formed, a coarse surface layer serves to regulate the mobility of finer adjacent and subsurface material.

Dietrich et al. (1989) noted that in streams with heterogeneous bed sediment, the bedload grain size is much closer to the subsurface size distribution than the surface. Thus, consideration of surface grain size alone can not evaluate the sediment available for bedload transport. They established the parameter q^*, the transport rate for the coarser surface grains normalized by the transport rate for the fine sub-surface grains.

$$q^* = \left[\frac{\tau_b - \tau_{cs}}{\tau_b - \tau_{css}} \right]^{1.5} \quad (11)$$

where τ_{cs} is the critical shear stress of the surface particles, and τ_{css} is the critical shear stress of the subsurface particles. τ_{cs} and τ_{css} are estimated using the relationship:

$$\tau_C^* = \tau_c \left[(\rho_s - \rho_w) g D_{50} \right]^{-1} = 0.045 \quad (12)$$

where τ^*_c is critical dimensionless shear stress, ρ_s is sediment density and ρ_w is fluid density. Thus q* takes into account the disparity of the median grain sizes in the surface and subsurface of a gravel bed river and will range from zero to one. At zero, there is low bedload sediment supply and the channel will be very well armored, while at one there is a high bedload supply and the channel will be completely unarmored. The parameter q* does not measure absolute armoring, but "is a relative index that describes armoring as a function of bed load supply relative to boundary shear stress and transport capacity" (Barry et al., 2004).

Barry et al. (2004) used the q* concept to develop a sediment transport equation that includes a consideration of the position of the stream in the watershed. This equation is site-specific, although the approach can be applied to other watersheds:

$$q_b = 257 A^{-3.41} Q^{(-2.45q^* + 3.56)} \quad (13)$$

where A is drainage area. The equation is a refinement of the more traditional bedload transport equation $q_b = \alpha Q^{\beta}$, where α is inversely related to drainage area and β describes the absolute magnitude of bedload transport (Leopold and Maddock, 1953). They found that q* is able to "accurately predict the rating curve (power function relationship between bedload transport and discharge) exponent over a range

of discharges, despite any change in stage-dependent grain sizes, as well as different climates, lithologies, and bedload sampling methods" (Barry et al., 2004). When compared with five other transport equations, including Meyers-Peters and Muller, it performed the best for 17 different test sites.

2.2.3 Hydraulic Geometry with Sediment Transport

Parker (1978) provided a link between threshold channel behavior and downstream hydraulic geometry; Millar (2004) developed a model to calculate the optimum geometry for gravel rivers. Natural rivers will adjust to optimum dimensions for a given flow regime, allowing it to transport sediment without net deposition or scour. Such models have also been produced in the past, empirically by Leopold and Maddock (1953), and theoretically by Parker (1978, 1979), Yang et al. (1981), and Huang et al. (2002). The major difference in Millar's model is that the stability of the river bank is very important factor in determining the depth and width of the channel. He begins by defining the maximum sediment transport efficiency, η:

$$\eta = G_b/(\rho Q_{1.5} S) \quad (14)$$

$$\eta = C/S,\ C = \text{dimensionless sediment concentration} \quad (15)$$

where G_b is bed load transport rate at the formative (bankfull) discharge (kg/s), ρ is the density of water (kg/m^3), $Q_{1.5}$ is the formative discharge (m^3/s), and S is the channel gradient. The variable ρQS is also known as stream power. Maximizing η is also maximizing G_b, which in turn minimizes stream power.

Critical dimensionless bank shear stress, τ^*_{bankc}, for the gravel particles of the bank is determined by an equation developed by Flintham and Carling (1993), that partitions shear stress into bed and bank components:

$$\tau^*_{bankc} = \tau_{bankc}/(\rho g(s - 1)d_{50} = 0.048\tan\Phi'\sqrt{(1 - (\sin^2\theta/\sin^2\Phi')} \quad (16)$$

$$\tau^*_{bedc} = 0.048\ \tan\Phi \quad (17)$$

where τ_{bankc} is the critical shear stress for bank materials (N/m2), τ^*_{bedc} is the critical dimensionless shear stress for bed sediment, s is specific gravity (assumed to be 2.65), g is gravity, d_{50} is the median particles size of the bank, Φ' is bank strength, Φ is the angle of repose for loose sediment, and θ is bank angle.

The equations for this method were derived using a tilting flume with a bed of well sorted gravels. Because of this, they were originally intended for determining the shear stress in straight, symmetrical channels that were either rectangular or trapezoidal. These conditions can be approximated in straight reaches with little to no bank roughness, which is what exists at the study sites.

Weaker banks will form wider channels, so this approach can be very useful in determining channel geometry. Stability decreases with increases in bank angle for any given bank material. For given values of discharge, sediment load, and median grain size, the optimum geometry becomes narrower, deeper, and less steep with increasing bank strength. Using the latter two equations, we can solve for μ'.

$$\mu' = \tau_{bankc}/\tau_{bedc} = \tau^*_{bankc}/\tau^*_{bedc} = \tan\Phi'/\tan\Phi \quad (18)$$

As can be seen, μ' is a dimensionless number describing the relationship between bank strength and bed strength. This is the critical difference in Millar's approach that sets it apart from previous models. Using this variable, we can calculate the "optimal" width and depth of a theoretical river:

$$W^* = 16.5Q^{*0.70} S^{0.60} \mu'^{-1.10} \quad (19)$$

$$D^* = 0.125Q^{0.16} S^{-0.62} \mu'^{0.64} \quad (20)$$

$$W/D = 155Q^{*0.53} S^{1.23} \mu'^{-1.74} \quad (21)$$

where $W^* = W/d_{50}$, $Q^* = Q/(d_{50}^2 \sqrt{g d_{50}(s-1)})$, and $D^* = D/d_{50}$. Millar found that the ratio between W and Q can be stated as $W:Q^{0.5}$. When using this model, a one order of magnitude variation can be expected from variations in d_{50} and μ', therefore there are a wider variety of possible channel widths for any given discharge.

Expanding on Millar's past model, a paper by Eaton and Millar (2004) furthered rational regime sediment modeling with constraining bank stability constants.

$$\log SF_{bank} = -1.4026 \log (P_{bed}/P_{bank} + 1.5) + 2.247 \quad (22)$$

$$\tau_{bank}/ \gamma Y_0 S = SF_{bank}/100 ((W + P_{bed}) \sin\theta / 4Y_0) \quad (23)$$

$$\tau_{bed}/ \gamma Y_0 S = (1 - SF_{bank}/100) (W/2P_{bed} + 0.5) \quad (24)$$

where SF_{bank} is the shear force acting on the bank, P_{bed} is the wetted perimeter of the channel bed, P_{bank} is the wetted perimeter of the channel banks, Y_0 is the maximum water depth, S is the water gradient, γ is specific weight of water (ρg), and W is the width of the channel. Through these equations we now have the shear stresses of both the bank and the bed.

The stability of the bank can be assessed by comparing τ_{bank} with a bank stability criterion based on the bank friction angle (Φ') and sediment size:

$$\tau_{bank}/(\gamma_s-\gamma)\, D_{50bank} \leq c \tan\Phi' \sqrt{(1 - (\sin^2\theta/\sin^2\Phi'))} \qquad (25)$$

c is a coefficient dependent on the properties of an unconsolidated and non-cohesive sediment with bank strength unmodified by vegetation. It is defined as $c = \tau^*_c/\tan\Phi$, where Φ is the angle of repose. In this equation the value of Φ' varies from being equivalent to Φ, to a high value of ninety degrees, the equivalent of a non-erodible bank. For the results of the paper, the c value was set to 0.069 for sand ($\Phi = 30°$) and 0.048 for gravel rivers ($\Phi = 40°$).

Sediment transport can then be estimated through the dimensionless value G, a function of the dimensionless bed shear stress and a reference shear stress:

$$5474\left(1 - 0.853\left(\frac{\tau^*_{bed}}{\tau^*_r}\right)^{0.45}\right) \qquad \frac{\tau^*_{bed}}{\tau^*_r} > 1.59 \qquad (26)$$

$$G\left(\frac{\tau^*_{bed}}{\tau^*_r}\right) = \quad Exp\left(14.2\left(\frac{\tau^*_{bed}}{\tau^*_r}-1\right)-9.28\left(\frac{\tau^*_{bed}}{\tau^*_r}-1\right)^2\right) \qquad 1 \le \frac{\tau^*_{bed}}{\tau^*_r} \le 1.59 \quad (27)$$

$$\left(\frac{\tau^*_{bed}}{\tau^*_r}\right)^{14.2} \qquad \frac{\tau^*_{bed}}{\tau^*_r} < 1 \qquad (28)$$

where $\tau_{bed}* = \tau_{bed} / \gamma s - \gamma) D_{50}$. This can then be put into dimensional form as:

$$q_b = G\ (0.0025(\tau_{bed}/\rho)^{3/2}/g(s\ -1)) \qquad (29)$$

Where s is the specific sediment weight, q_b is the volumetric sediment transport rate ($m^3/s/m$). The transport rate for the entire channel, Q_b can be calculated through the product of the active channel width and q_b. The model proved to be effective at modeling the widths of gravel bed rivers, especially when compared to models without a bank constraining parameter.

2.2.4 Channel Widening and Bed Mobility in the Little Paint Branch Gravel Bar Complex

For his senior thesis at the University of Maryland, Achyut Dangol studied the sediment composition of the gravel bars and banks at Sellman Road and in the Cherry Hill Bar Complex. He found that the grain size of bank material decreases in the lower portions of the watershed (from Sellman road to Cherry Hill), suggesting sand

sized material is usually not carried as suspended sediment load in the Cherry Hill Bar Complex reach. This suggests that it is usually either stored and/or transported as bedload between the sites.

Dangol (2009) also examined the composition of the gravel bars and discovered that they are formed of alternating layers of sand and gravel with a final coarse layer on the surface. These data suggest that the gravel was transported over a sand bed. Dangol (2009) used data from Wilcock (2001) to estimate the critical dimensionless shear stress for layers with variable sand content. Wilcock demonstrated that critical dimensionless shear stress for gravel mobility decreases from 0.045 to as low as 0.02 as the sand percentage increases past 30% (Wilcock, 2001). The increase in the percentage of sand and fine material in the gravel bars observed by Dangol (2009) may represent high rates of gravel and sand bedload transport associated with an increased the mobility of the bed. Sequential deposition of gravel and sand layers on the bars however, causes shoaling of the bed which decreases shear stress and would lead to a decrease in bedload transport. Dangol (2009) concluded that gravel bars become stabilized due to accretion and shoaling of the bed.

2.3 Study Sites and Methods

2.3.1 Study Sites

Study sites were selected that met the following criteria: a) they were distributed throughout the length of Paint Branch Creek, b) they were not

significantly modified by rip-rap, restoration projects, etc., and c) they were bordered by floodplain, so that they could migrate freely. Very few sites within Little Paint Branch Creek met these criteria and most were contained within MNCPPC parkland. A brief description of the sites follows.

Fairland Park (FP) is located in the Piedmont province and has a history of use as agricultural pasture land. The region surrounding the site has been reforested. Extensive stormwater management projects upstream and to the East of the site limit direct stormwater runoff to the creek. The drainage area upstream of the site is 4.4 km^2, which is in suburban development with stormwater management and forest.

The Greencastle Road (GCR) site is about 1 km downstream from Fairland Park. It has a drainage area of 9.6 km^2. The region adjacent to the site is riparian forest and parkland. Several new housing subdivisions have been built in the past 5 years between site FP and the GCR site. The site has forested but incised banks and an unusually sandy bed. A gauging station was also placed at this site.

The Briggs Chaney Road (BCR) site is on a golf course, with a stormwater mitigation pond adjacent to the site. Upstream of site, the channel flows through a hexagonal culvert. It has a drainage area of 14 km^2 and is 2 km downstream from the previous site.

The Sellman Road site (SR) is located in forested Little Paint Branch Park. The site is downstream of an extensive channelized reach that brings the stream past interstate 95. The channelized reach is both steep and straight. This has caused extensive erosion upstream of the study reach. Stream restoration work that had been done on this site previously created flumes to decrease stream power and erosion,

however the attempt failed. Large boulders are now found on the edge of the bank and gravel bars are once again forming. As a result of the restoration effort the channel cross-section area is now uncommonly large. It is located about 3 km downstream of the BCR site and has a drainage area of 16 km^2.

The two sites upstream and downstream of the Cherry Hill Bar Complex (CHBC) are also known as CHU and CHD. They have a common drainage area of 25.9 square kilometers, and are respectively a total distance of 8.6 and 9.1 kilometers downstream from the Fairland Park (FP) site. In this area the stream runs next to the Little Paint Branch Trail through the Cherry Hill Neighborhood Park. The bar complex is one of the areas of concentration for this study, and was further subdivided to study bar complex processes.

2.3.2 Field measurements of channel morphology and bed grain sizes

A. Channel morphology measurements.

At each site, the channel cross sectional form was surveyed. Cross sections were measured at the downstream end of a riffle (Leopold and Maddock, 1953). From these data, total channel area, surface width, and average depth (area/width) were determined.

B. Water Surface (Energy) Gradient Measurements.

At baseflow conditions, the bed topography and the gradient of the surface of the water is measured by placing a stadia rod at the water surface and measuring elevation at intervals of 2m along the channel using surveying techniques. For

selected high flow events, flags were placed at the water level along the bank, and the elevations are determined after the storm using surveying techniques. Gradient is calculated by plotting elevation against distance and determining the average gradient over the reach.

C. Measurement of surface and subsurface grain size material

Surface grain size distributions were collected by the Wolman pebble count method (Wolman, 1955). Each pebble count included 100 random samples within a 10 meter reach of the stream centered over the cross section. Subsurface materials have been collected by removing the top sediment layer of a 6" by 6" square area, and sampling underlying subsurface material. Samples were collected at cross-section locations and at least three samples of subsurface material were obtained in each cross section. Grain size distribution data were plotted from the pebble count data. They were converted to weight percent for comparison with subsurface size distributions by assuming spherical shapes and quartz density (these are spherical, quartz-dominated sediments. From the grain size distribution data, median (D_{50}) and D_{84} were determined for surface and subsurface size samples.

D. Field measurement of Velocity

Velocity measurements were made at the gauged locations (Cherry Hill Upstream, Downstream, and Greencastle Road). These measurements were used

to define a rating curve. At other sites, velocity was estimated from relative roughness d/D_{84}. For relatively straight gravel-bed streams with relatively little bar formation, the relationship between velocity and relative roughness can be expressed as:

$$\frac{u}{u*} = 2.8 + 5.75 \times \log\left(\frac{d}{D_{84}}\right) \quad (30)$$

This equation matched measured values of discharge quite accurately at gauged locations, and has been shown to accurately model velocity in natural, straight, gravel-bed rivers at bankfulll (Wolman and Leopold, 1956) and low flow (Stoner, 2002) conditions.

E. Calculation of Fluid Shear Stress

At all locations bankful shear stress was determined using duBoys equation:

$$\tau = \rho g R S \quad (31)$$

Where ρ is fluid density, g is gravitational acceleration, R is hydraulic radius, and S is bankfull energy gradient (water surface gradient for a straight reach).

F. Calculation of Dimensionless Shear stress.

Dimensionless shear stress (τ^*) is the ratio of the fluid shear stress to the grain resisting forces $(\rho_s-\rho_w)gD84$. ρ_s is channel bed sediment density and ρ_w is the density of water. Values of critical dimensionless shear stress have been

evaluated for homogeneous sediment (0.06; Shields, 1938), for heterogeneous gravel streams (0.045; Bray, 1978; Church, 2006, and for sand and gravel mixtures (0.045 -0.02; Wilcock, 2004. See Dangol (2009)) Values of critical dimensionless shear stress for these gravel channels likely ranges from 0.045 to 0.01 depending upon the sand content. Critical dimensionless shear stress for each site was estimated using bed grain size distribution data and calibration with bedload transport observations.

G. Calculation of Excess Shear Stress.

Excess shear stress is calculated by subtracting the shear stress of the water from the critical shear stress required to mobilize the bed material within a transect. The critical shear stress required to mobilize the sediment is calculated assuming a constant D_{84} value for the site.

Figure 7. Aerial photographs of the study sites on the Little Paint Branch and within the CHBC (Source: Tele Atlas, US Geological Survey).

2.4 Results

2.4.1 Urbanization-induced Changes in morphology and sediment mobility at the Watershed Scale

The changes immediately evident at the watershed scale are channel widening and deepening which can be seen in figs. 8 and 9. Channel widening can have many unforeseen effects on system morphology, and it can alter the sediment transport regime, riparian function, as well as hydraulic characteristics. Channel deepening can coarsen channels, increase shear stress, induce bank erosion, and increase localized sediment transport.

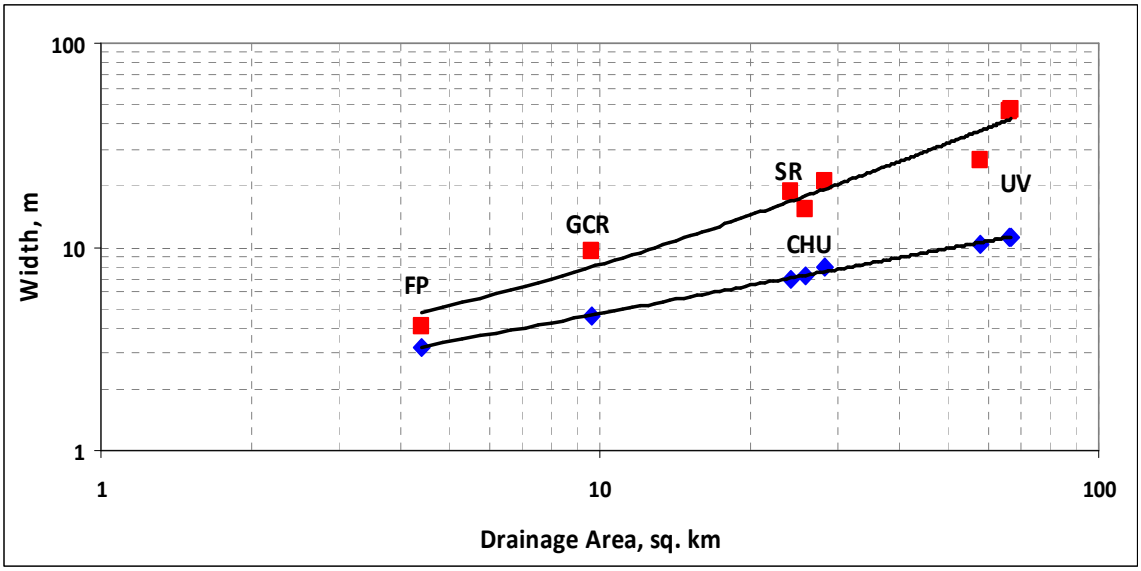

Figure 8. Paint Branch and Little Paint Branch bankfull width vs. drainage area. The red data points are post urbanization and the blue data points are pre urbanization. UV is the University View Apartment Complex adjacent to the University of Maryland campus in College Park

The channels showed both channel widening and channel deepening when compared with reference reaches (figs. 8 and 9). The amount of channel widening,

however is greater than the amount of deepening and rate of channel widening increases in the downstream direction. The sediment released through channel widening of Little Paint Branch Creek is carried by either bedload or suspended load in the system. Channel widening and deepening can not only release sediment into the system, but also increases channel cross sectional area, which should result in an increase in the size of the bankfull discharge that can be contained within the channel banks.

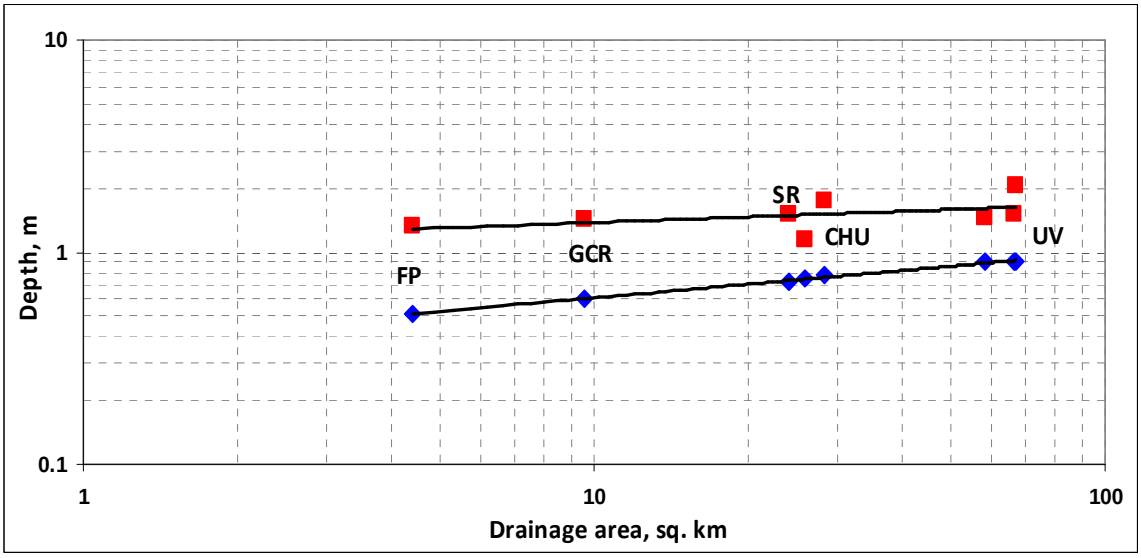

Figure 9. Paint Branch and Little Paint Branch bankfull depth vs. drainage area. The red data points are post urbanization and the blue data points estimated values for pre-urbanization. (Based on regional data from Prestegaard et al., 2001; Behrns, 2007)

The channel cross sectional area for Little Paint Branch Creek is compared with Coastal Plain reference reaches in fig. 10. These diagrams show a significant increase in channel capacity, for example the channel for a drainage area of ten square kilometers, in Little Paint Branch Watershed is approximately thirty percent larger than the reference streams. The increased channel area corresponds to a

significant increase in bankfull discharge, shown in fig. 11. Velocity increases along with an increase in channel depth, therefore, bankfull discharge of the urbanized Little Paint Branch creek is significantly higher than the reference reaches. For the ten square kilometer example, bankfull discharge in Little Paint Branch Creek is over seventy percent greater than the Coastal Plain reference streams. The equations that describe the relationships between discharge and basin area are compared in table 1. These equations predict that streams with this amount of urbanization (11-20% impervious surfaces) will have higher bankfull discharges for watersheds of 1,000 km^2 or less in area (the average Coastal Plain Watershed is several hundred kilometers in area).

Table 1. Comparison of channel dimensions versus basin area for the urbanized Paint Branch Creek with non-urban reference reaches from Prestegaard et al., 2001

Site	**Bankfull Q**	**Bankfull Area (A)**	**Bankfull Width (W)**
Urban Paint Branch, 2008	$Q = 1.45DA^{0.73}$	$A = 1.32\ DA^{0.58}$	$W = 3.33\ DA^{0.43}$
Non-urban reference reaches of Western Coastal Plain.	$Q = 0.18DA^{1.05}$	$A = 0.98DA^{0.54}$	**$W = 1.64\ D.A.^{0.46}$**

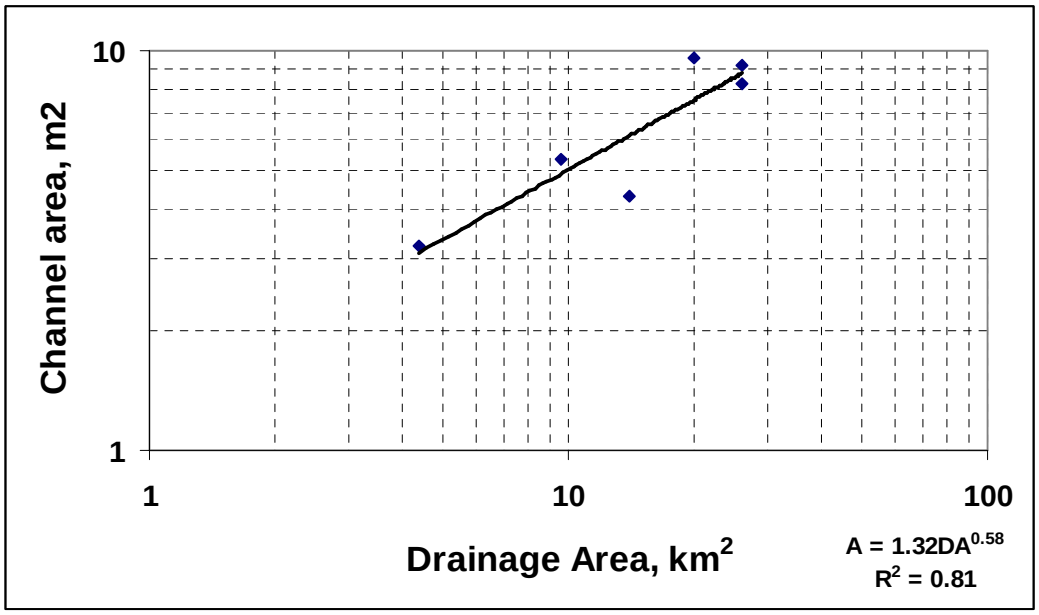

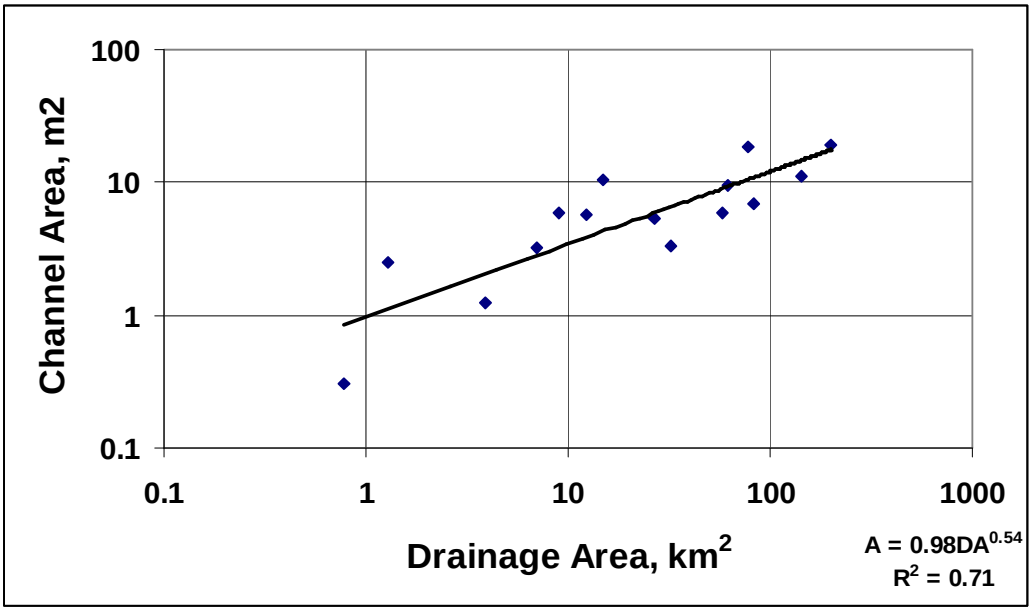

Figure 10. Relationships between Drainage area and channel area for a) Little Paint Branch 2008 (this study) b) Western Coastal Plain non-urban data (Prestegaard et al., 2001)

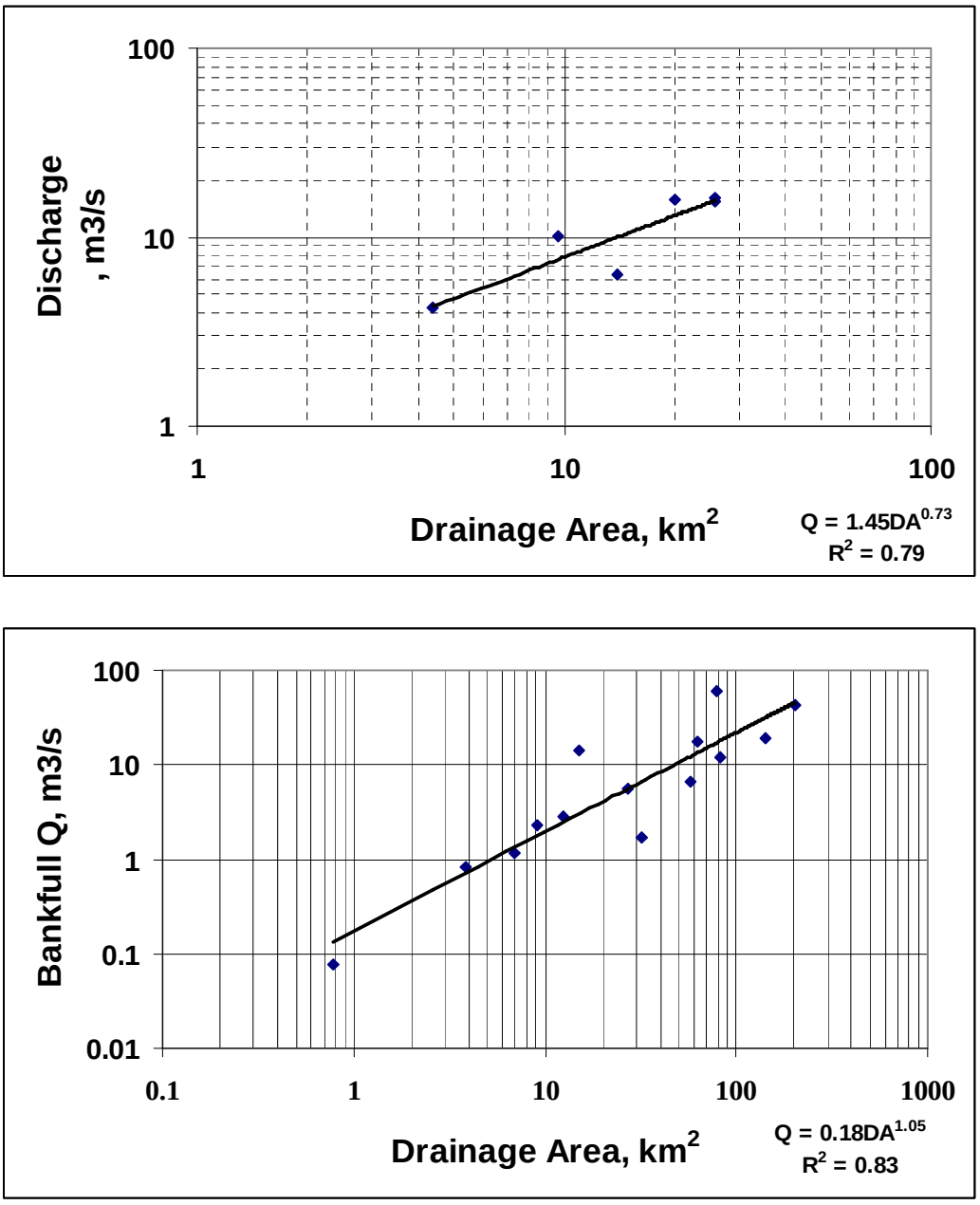

Figure 11. Relationship between drainage basin area and bankfull discharge A: Little Paint Branch Creek; B: Non-urban Western Coastal Plain Streams (Prestegaard et al., 2001). Note the much larger bankfull discharges for Little Paint Branch, particularly for smaller drainage basin areas.

2.4.2 Downstream Hydraulic Geometry for Little Paint Branch Creek

The downstream hydraulic geometry describes the rate of increase in width, depth and velocity in the downstream direction to accommodate the downstream increase in bankfull discharge. Widening of Little Paint Branch creek has affected the downstream hydraulic geometry relationships. The Little Paint Branch Creek downstream hydraulic geometry relationships are best constrained for channel width; these are shown in fig. 12. Note that the urbanized reach data plot generally within the trend of the non-urban data, suggesting that the stream accommodate to the discharge by widening to the size of a stream expected in a larger watershed. The depth and velocity relationships were derived from the original regression equations and further constrained by the regression relationship of discharge to width and the continuity equation.

The exponents for the downstream hydraulic geometry relationships for the Paint Branch Creek, Western Coastal Plain (Prestegaard et al., 2001) and Midwestern United States (Leopold and Maddock, 1953) are shown in Table 2. The largest exponent in the hydraulic geometry relationship indicates that the corresponding stream dimension increases at a faster rate downstream than the other dimensions. Little Paint Branch primarily accommodates to a downstream increase in discharge by channel widening (probably due to base-level controls). Coastal plain streams of similar watershed area increase in width and velocity almost equally, and the Midwestern streams both widen and deepen in the downstream direction.

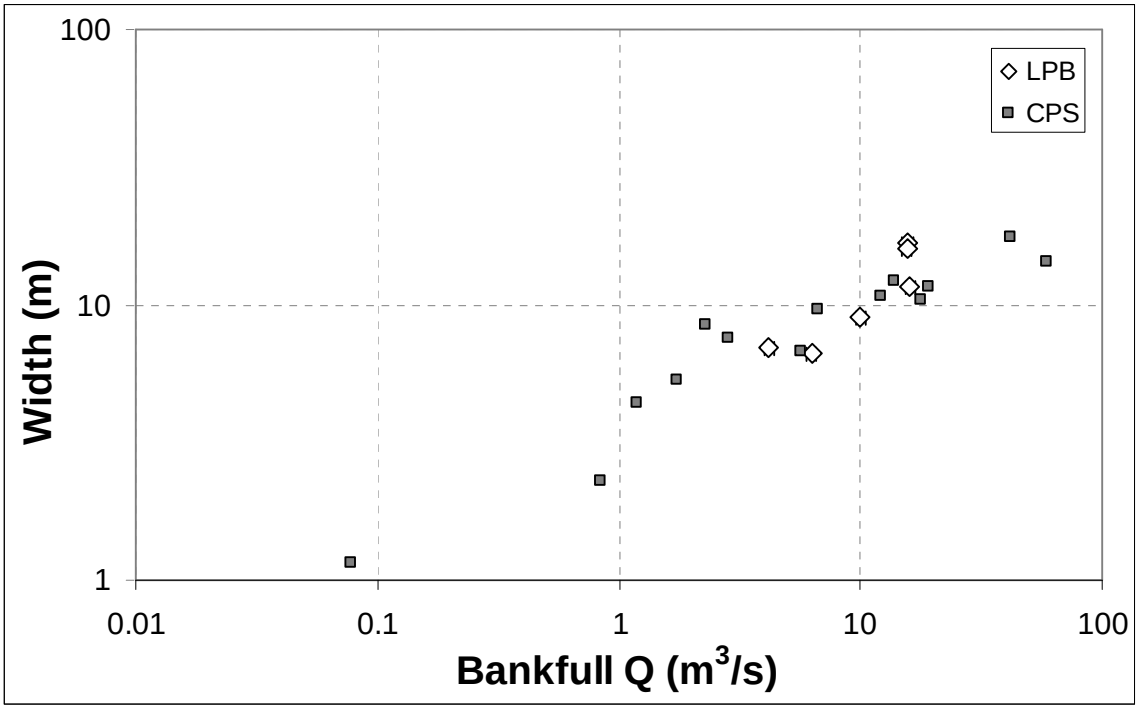

Figure 12. Downstream Hydraulic Geometry in the Little Paint Branch and Maryland Coastal Plain Streams, Bankfull Discharge vs. Bankfull Width. The regression equation for the Little Paint Branch sites is $W = 2.4Q^{0.64}$ and for the Coastal Plain is $W = 3.83Q^{0.40}$.

Table 2. Downstream Hydraulic Geometry Exponents

Region	**width**		**depth**	**velocity**
L. Paint Branch, 2008	0.64	(R^2 = .80)	0.17	0.19
W. Coastal Plain[1]	0.40	(R^2 = 0.90)	0.20	0.40
Midwestern U.S.[2]	0.5		0.4	0.1

[1] Prestegaard et al., 2001; [2] Leopold and Maddock, 1953

2.4.3 Little Paint Branch Sediment Data

Surface and subsurface grain size analyses were conducted for each station. Coarse surface sediment can act as a mobile armored layer, which then regulates the mobility of the finer subsurface material (Parker et al., 1982). Streams with mobile armored beds are usually threshold channels that commonly only move bed sediment during bankfull or larger flood events (Parker, 1979). This mobilization of the surface allows subsurface material to move, and bedload material becomes a mixture of surface and subsurface grain sizes (Parker and Klingeman, 1982; Dietrich, et al., 1989).

The surface grain size distribution data are shown in fig. 13. These data indicate that the upstream site, Fairland Park had coarse surface material, but the surface grain size was similar to that found at the two furthest downstream locations (Sellman and CHU). This suggests that coarse sediment may be mobile at many sites throughout the watershed and its presence on the bed surface is related primarily availability and the history of transport events. Although Greencastle Road is only a kilometer downstream from Fairland Park, it contains the finest surface sediment distribution. The region upstream of Greencastle road has recently been suburbanized. This fine sediment may reflect recent disturbances in both the watershed and the channel.

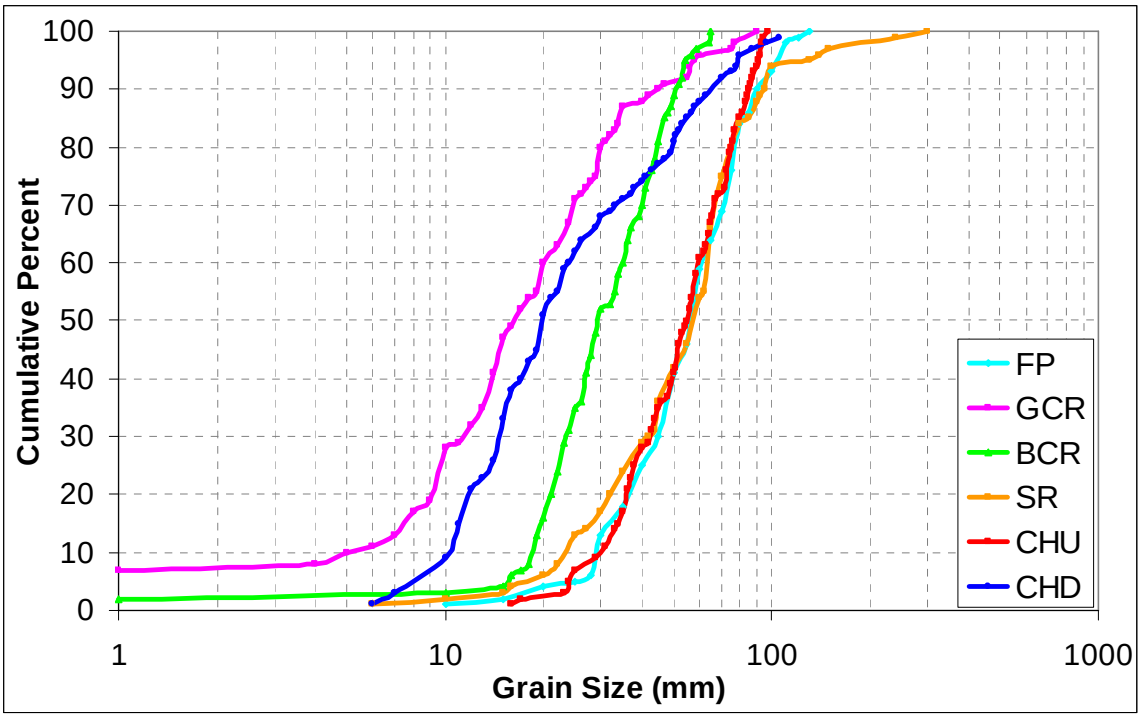

Figure 13. Surface Sediment Distributions measured at Little Paint Branch sites.

The range of subsurface sediment is much smaller than the range of surface grain sizes and there does not seem to be a relationship between surface grain size and subsurface grain size (fig. 14). Downstream Cherry Hill (CHD) has the coarsest subsurface sediment distribution but among the smallest surface grain size distributions. Sellman Road had one of the coarsest surface sediment distributions, but has finer subsurface sediment than most other sites. A summary of the data can be found in Table 3.

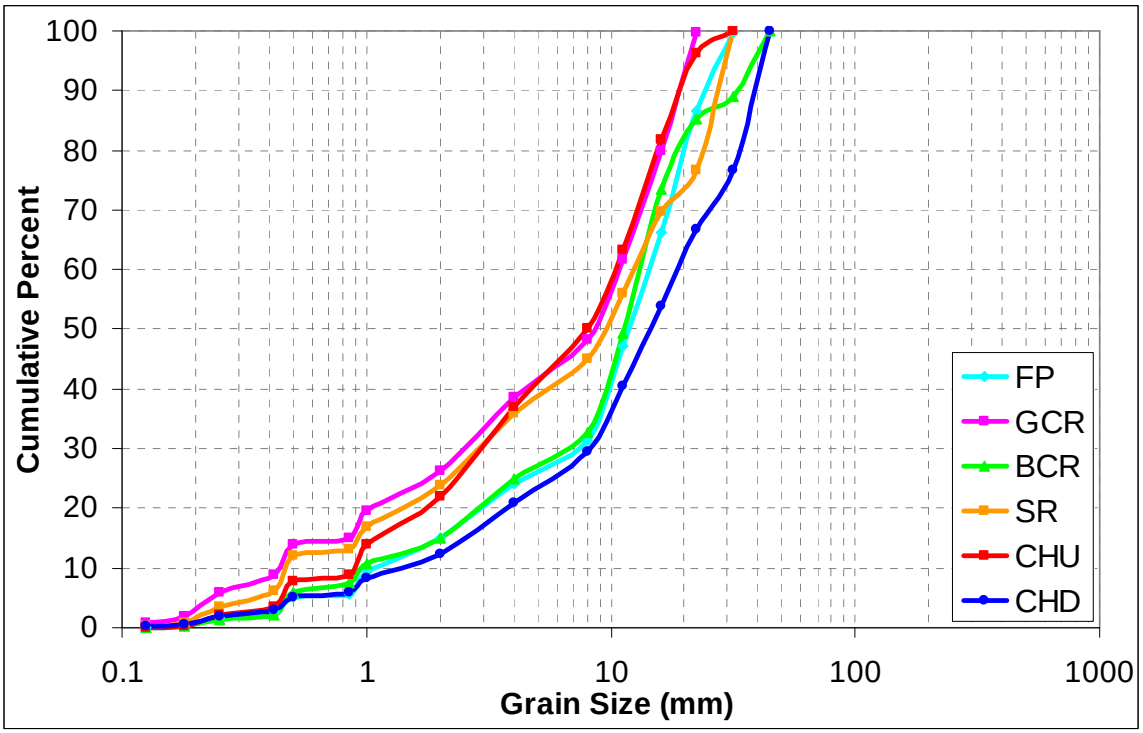

Figure 14. Subsurface Sediment Distributions measured from Little Paint Branch sites.

In most sediment transport theory a characteristic grain size is used to calculate bed mobility rather than the grain size distribution (e.g. Dietrich, 1989). Grain sizes that are commonly used for flow resistance and sediment transport equations are the median D_{50} or D_{84}, one standard deviation above the mean. The median grain size is often used in sediment transport relationships, while D_{84} has a large role in bed roughness and is sometimes used to determine stability for channels with mobile armored beds. Table 3 and Fig. 15 show the surface and subsurface D_{50} and D_{84} values for every site in the watershed. These data indicate that there is not a systematic downstream increase in median surface or subsurface sediment size.

Table 3. Watershed scale sediment data (mm).

Site	$D50_s$	$D50_{ss}$	$D84_s$	$D84_{ss}$
FP	60	14	80	22
GCR	17	10	34	16
BCR	30	12	47	21
SR	60	15	80	27
CHU	55	8	78	17
CHD	20	15.7	52	34

The graphs of surface to subsurface grain size ratios indicate that the size of subsurface material decreases downstream, perhaps reflecting an increase in the amount of sand derived from bank erosion in the subsurface (Fig. 16). This regional trend rapidly changes over the gravel bar reach (between CHU and CHD). The high ratio of Surface to subsurface material at CHU indicates the possible role of sand in gravel bar formation, while the low ratio at CHD (values near one) indicates a depletion of fine-grained subsurface material at the downstream Cherry Hill site, which might lead to channel bed stability at CHD. The role of gravel bar formation in sediment supply and bed sediment characteristics will be examined in more detail in the next chapter.

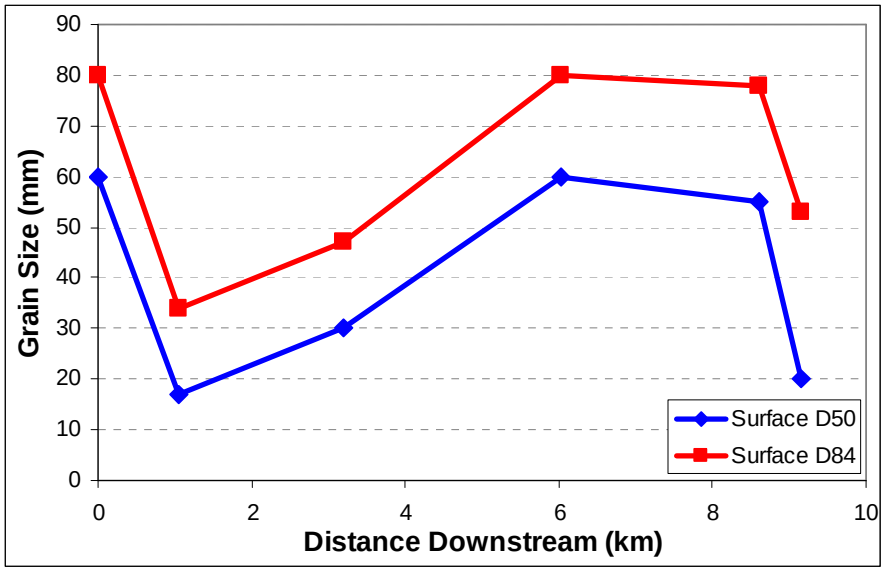

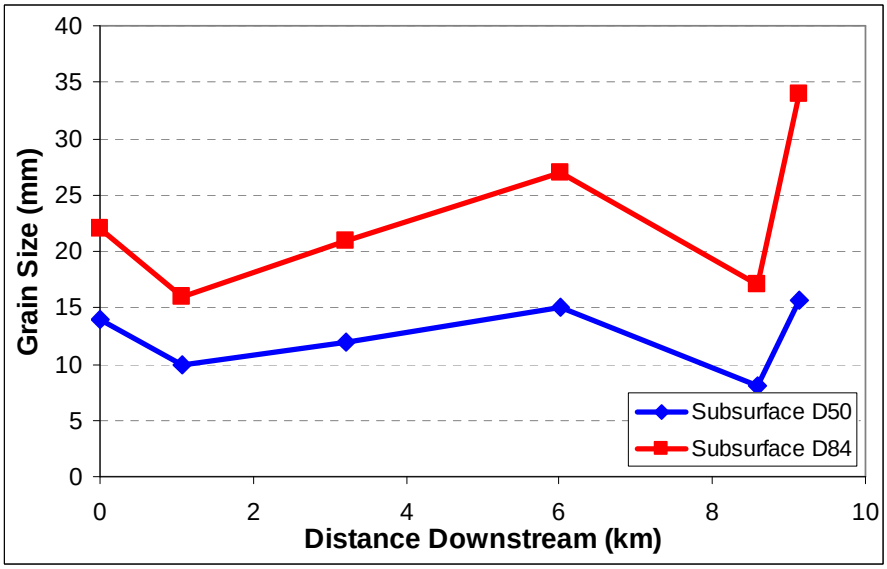

Figure 15 a: Surface D_{50} and D_{84} values; b: Subsurface values. Variance due to error is contained within the data points.

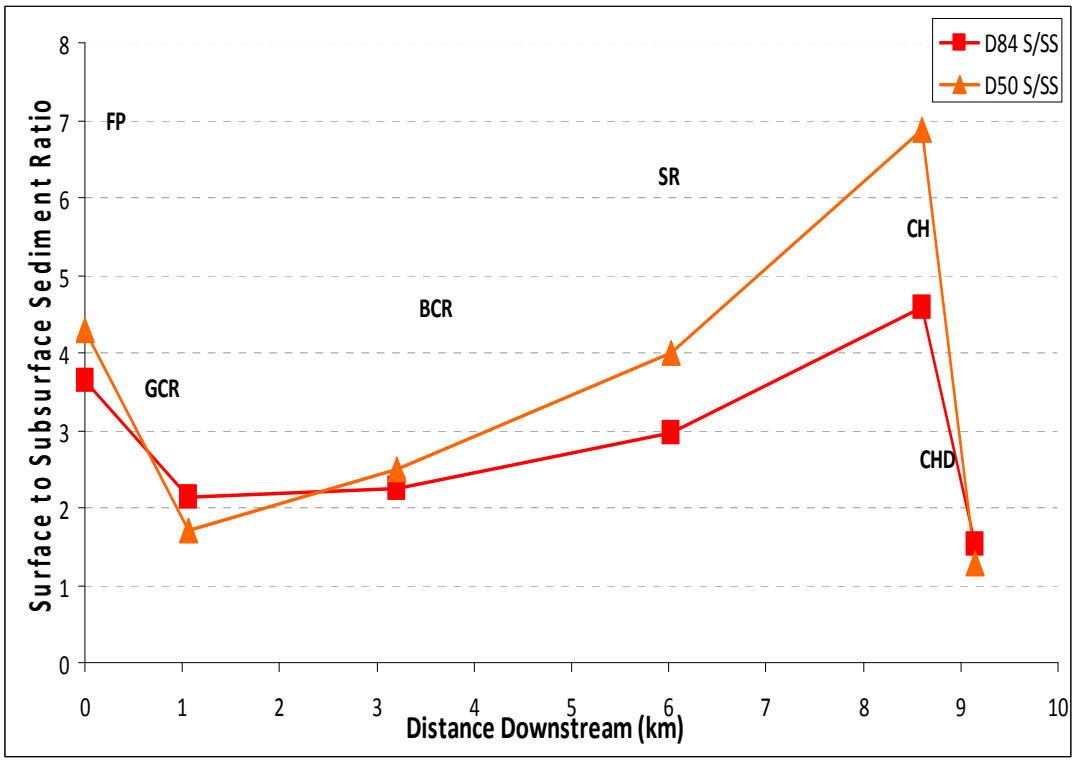

Figure 16. Surface and subsurface ratios (for both D_{50} and D_{84}) versus distance downstream.

2.4.4 Dimensionless Hydraulic Geometry Relationships

In a 1979 paper, Gary Parker first introduced dimensionless hydraulic geometry relationships for gravel-bed rivers. Although Parker has made several revisions to the original relationships, he uses grain size to generate dimensionless numbers to evaluate width, depth, and discharge in hydraulic geometry expressions:

$$Q^* = \frac{Q_{BF}}{\sqrt{gD_{50}}D_{50}^2} \qquad H^* = \frac{H_{BF}}{D_{50}} \qquad W^* = \frac{W_{BF}}{D_{50}} \qquad U^* = \frac{Q^*}{(H^*W^*)} \qquad (32)$$

where Q* is dimensionless discharge, Q_{BF} is the bankfull discharge, H* is dimensionless depth, W* is dimensionless width, and U* is dimensionless velocity.

These analyses are useful for qualitatively assessing the amount of change has occurred in the sediment composition of the Little Paint Branch. For the data sets

used by Parker for several gravel bed rivers around the world, an average relationship between W* and Q* was found to be $W^* = 4.87Q^{*0.461}$. Fig. 12 shows the equation for the Maryland Coastal Plain streams to be very similar: $W^* = 3.9Q^{*0.44}$. In contrast, the regression equation for the sites in the Little Paint Branch in fig. 11 is $W^* = 10.95Q^{*0.35}$.

The two sets are plotted together in fig. 17 which indicates the difference in the dimensionless hydraulic geometry equations, the larger surface sediment composition of the Little Paint Branch causes the dimensionless values to be much lower than those of the coastal reference streams. The impact of the sediment size is more visible when fig. 17 is compared with fig. 11, the dimensional hydraulic geometry width plot.

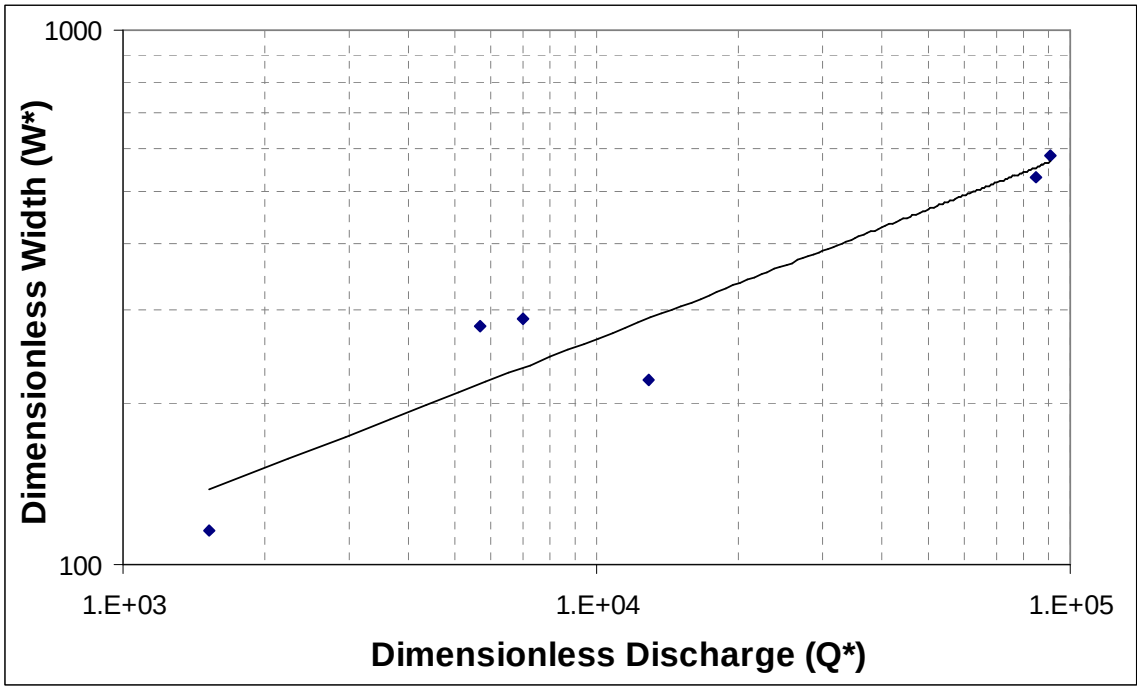

Figure 17a. Little Paint Branch (urban) dimensionless hydraulic geometry . $W^* = 10.95Q^{*0.35}$, $R^2 = 0.88$.

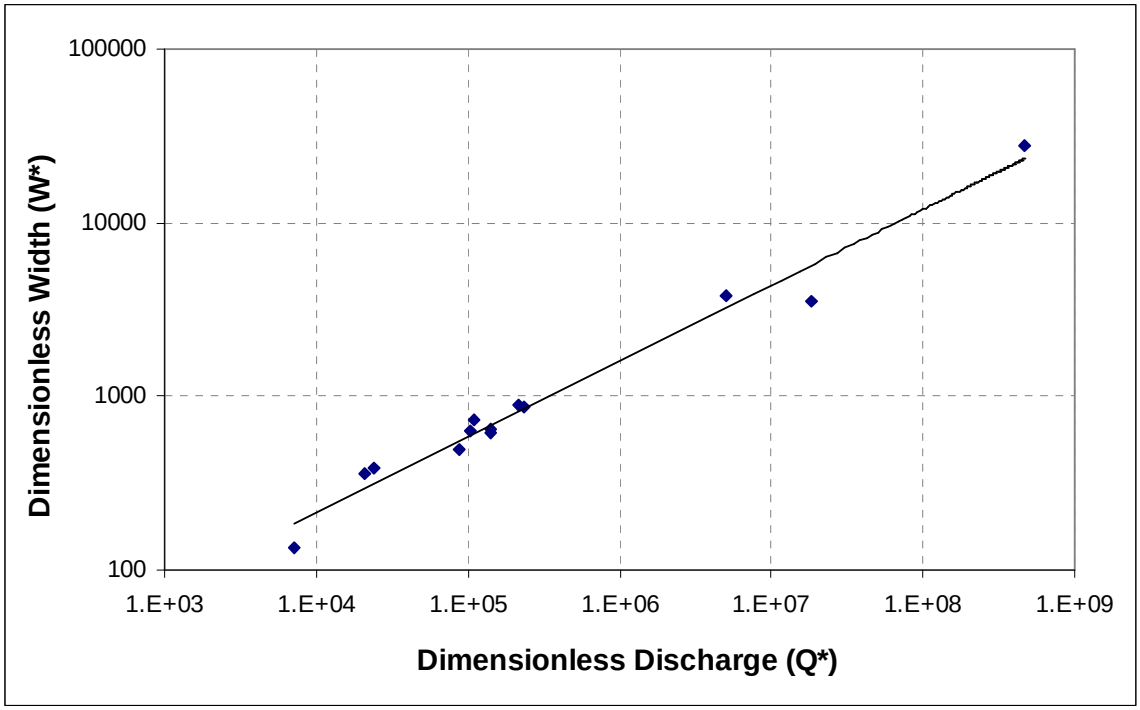

Figure 17b. Maryland Coastal Plain : non-urban stream dimensionless hydraulic geometry.

$W^* = 3.9Q^{*0.44}$, $R^2 = 0.97$

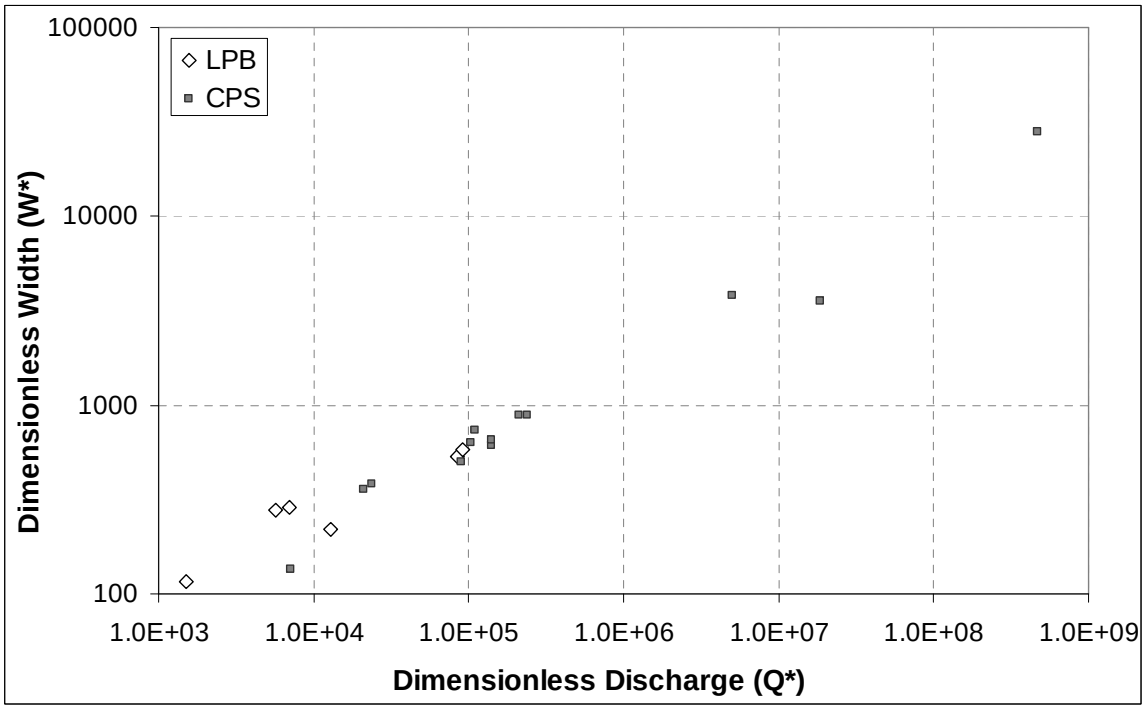

Figure 17c. Dimensionless Width v. Dimensionless Discharge for the Little Paint Branch and Maryland Coastal Plain reference streams. LPB $W^* = 10.95Q^{*0.35}$, CPS $W^* = 3.9Q^{*0.44}$

2.4.5 Determination of Critical Dimensionless Shear Stress and Bed Mobility

Evaluation of Bankfull shear stress ratios

The bankfull shear stress ratio $\tau^*_{bf}/\tau^*_{crit}$ can be used to determine whether the channel is mobile at the bankfull stage. The critical dimensionless shear stress, τ^*_{crit} is the ratio between t_{fluid} (ρgRS) and t_{grain} ($(\rho s-\rho w)gD_{50}$)at the initiation of motion (Shields 1938). Shields (1938) found that the critical dimensionless shear stress for homogenous sediment is 0.06. For heterogeneous gravel-bed streams with naturally sorted bed material, the critical dimensionless shear stress for sediment transport has been found to be around 0.045 (Neill, 1978), With high amounts of sand in the bedload, the critical dimensionless shear stress can drop as low as 0.01 (Wilcock, 2001). Table 4 shows the bankfull dimensionless shear stress ratios for the Little Paint Branch study sites. Values of critical dimensionless shear stress values based upon the percentage of subsurface sand found at each sites are also indicated in this table

Table 4. Bankfull Dimensionless Shear Stress and Stream Gradient of Little Paint Branch Sites. T*crit is based on percent sand content, these numbers were derived from Wilcock (2001).

Site	% sand	T*crit	T*max	T*/T*crit	Gradient	Distance Downstream (km)
FP	15%	0.038-0.042	0.023	0.58	0.0104	0
GCR	26%	0.013-0.017	0.007	0.47	0.0063	1.06
BCR	15%	0.028-0.032	0.007	0.23	0.0037	3.20
SR	17%	0.023-0.027	0.036	1.44	0.0122	6.02
CHU	22%	0.018-0.022	0.015	0.75	0.0055	8.60
CHD	5%	0.043-0.045	0.016	0.36	0.007	9.14

Sediment Supply and Bed Mobility

As mentioned previously, Dietrich's q* the ratio of the excess shear stress calculated based on mean surface grain size to the excess shear stress calculated using the mean subsurface material. The q* value ranges from zero to one. Near zero there is likely to be little bedload sediment supply due to channel armoring , values near one indicate that surface and subsurface grain sizes are similar, indicating either little armoring or very little subsurface material. Fig. 18 shows the q* value versus the distance downstream. The furthest upstream site has a q* value close to zero, but the value increases to near 1 at Greencastle (which has fine sediment in the subsurface and on the bed). Most of the values for other sites are consistent with values for mobile armor, but values between CHU and CHD go from near zero to near 1, due to the depletion of fine-grained material at CHD. Thus, q* is not a very accurate measure of sediment supply in this reach.

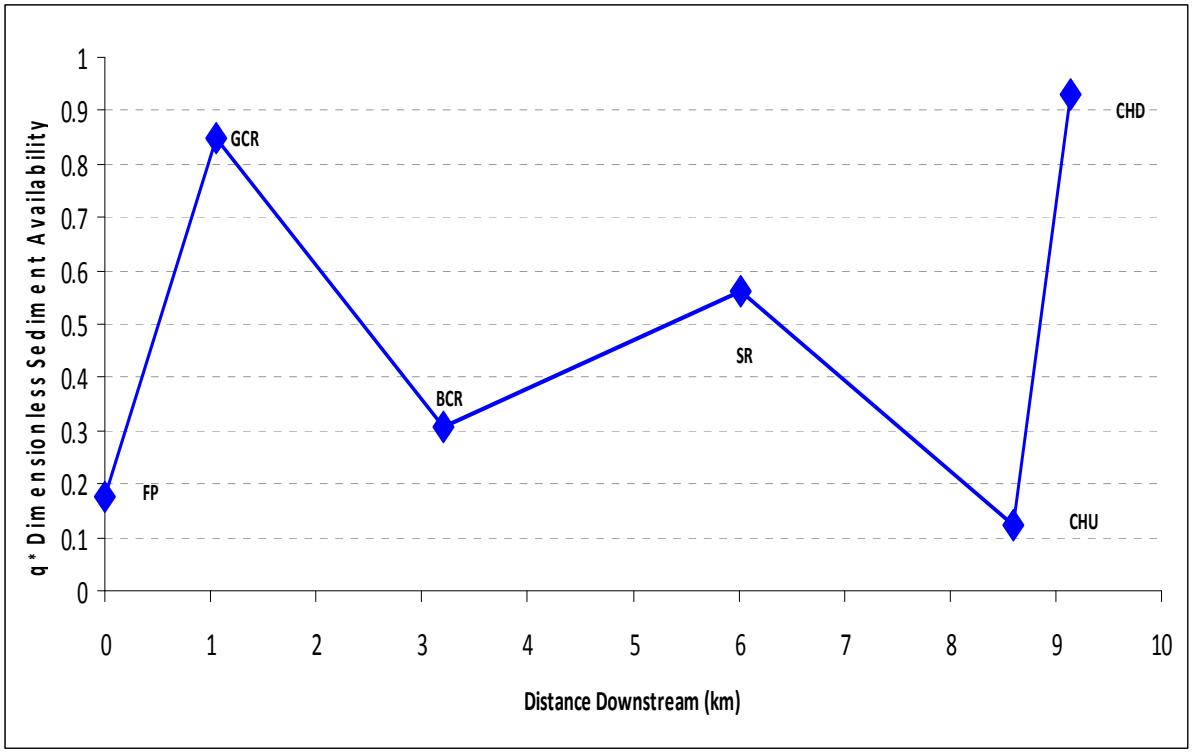

Figure 18. q* values versus distance downstream in the Little Paint Branch.

Bedload transport and bed sediment supply characteristics (q*, bedload per unit width at bankfull, and percent fine sediment) are summarized in Table 5 for all measured sites at the watershed scale. Bedload transport per unit width was calculated using an equation developed by Meyer-Peter and Muller in 1948. The q_b is bedload in kilograms per meter width per second and is calculated as follows:

$$q_b = 8\left[\frac{\rho_s}{\rho_s - \rho}\right]\sqrt{\frac{g}{\rho}}\left[\left(\frac{n'}{n_t}\right)^{3/2}\rho S D - 0.047(\rho_s - \rho)D50_{ss}\right]^{3/2} \qquad (33)$$

where $n_t = \frac{S^{1/2}R^{2/3}}{V}$ and $n' = \frac{D90_s^{1/6}}{26}$, D_{90s} and D_{50ss} are the 90th percentile of the surface sediment and the 50th percentile of the subsurface sediment, respectively, and V is the flow velocity in meters per second. Calculated values of bedload

transport are shown in fig. 19, which indicates similar values at all locations, with an exception of Sellman road reach. The Sellman Road reach recently underwent a channel stabilization procedure due to the adjustment of gradient along Interstate 95 which concentrated elevation changes in the reach above Sellman Road. This increases shear stresses within this reach and has caused significant erosion downstream of 95 and some localized deposition of gravel sediment.

In the bar complex reach, upstream Cherry Hill has a higher percentage of fine sediment, but a lower q* value and a lower q_b than Downstream Cherry Hill. The other sites with the highest q*, Greencastle and Downstream Cherry Hill, are second only to Sellman Road in bedload discharge, q_b. The change in bed mobility and sediment composition within the Cherry Hill Bar Complex is further investigated in the next section.

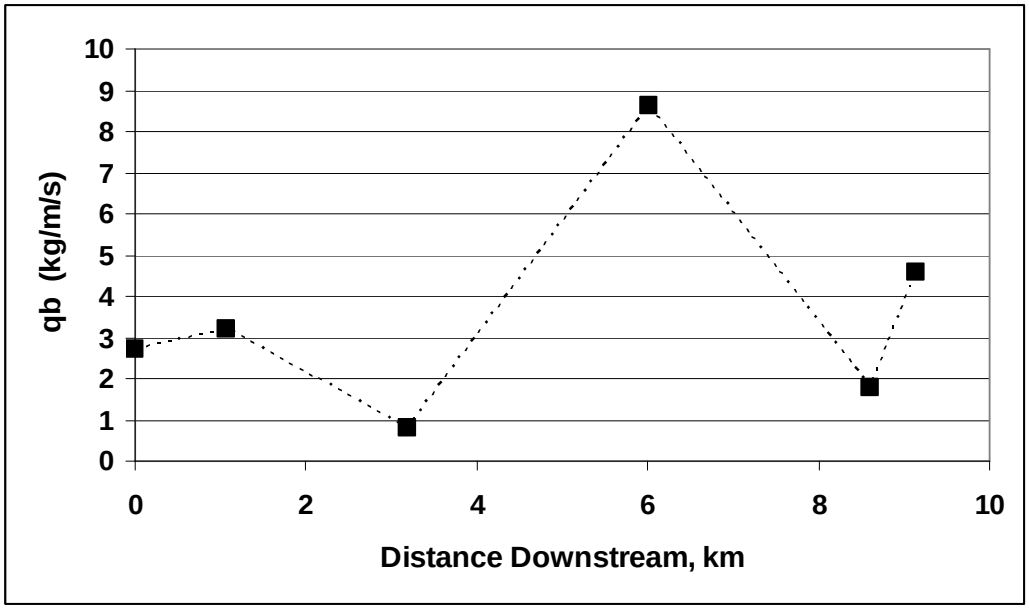

Figure 19. q_b versus distance downstream in the Little Paint Branch

Table 5 Watershed Scale q*, q_b, and percent fine sediment.

Site	q*	q_b at Q_{bf} (kg/m/s)	Percent Fine Sediment (<2 mm)
Fairland Park	0.178	2.694	15%
Greencastle Rd	0.850	3.207	26.3%
Briggs Chaney Rd.	0.309	0.784	15.1%
Sellman Rd.	0.560	8.609	17%
Upstream Cherry Hill	0.124	1.786	21.9%
Downstream Cherry Hill	0.928	4.575	12.2%

2.5 Discussion

2.5.1 Effects of urbanization on channel dimensions and hydraulic geometry

With increasing drainage area, the Little Paint Branch accommodates increased discharge dominantly by channel widening, the rate of which increases in the downstream direction. The reference, non-urbanized coastal streams also did this, but to a lesser extent. The increase in depth with drainage area wasn't significant in either data set, though it slightly greater in the Little Paint Branch, but this is likely a byproduct of the increased potential for channel scour caused by a greater bankfull discharge.

The accelerated channel widening of the Little Paint Branch results in a greater relative channel area to non-urbanized rivers, and consequently it has an increasingly greater bankfull discharge downstream. For the same ten square kilometer drainage area in both data sets the Little Paint Branch has a thirty percent

greater bankfull channel area than the reference streams. Channel widening is accommodated by bank erosion which introduces fine and coarse sediment to the system and likely inhibits the effects of channel scouring caused by the greater shear stress of a larger bankfull discharge.

Hydraulic geometry relationships show that in addition to widening, the reference coastal plain streams increase in velocity downstream, something that is not nearly as significant in the Little Paint Branch. Data from Midwestern streams show that the dominant accommodating parameters to increasing discharge are both width and depth. The dimensionless hydraulic geometry calculations indicate the significance of the difference in sediment composition of the urban and non-urban channels of the area.

2.5.2 Fine sediment and bedload transport potential

Channels have widened and deepened as a direct result of urbanization. This has changed the sediment supply to the entire system. Bank erosion mobilizes both sand and gravel to cobble sized sediment, but increases the ratio of sand in the bed sediment over most of Little Paint Branch Creek. The shear stress at bankfull has been increased at most locations due to an increase in channel depth. There is some indication that coarse grain sizes have been moved downstream, which affects local dimensionless shear stress.

The ratio of surface/subsurface sediment had a definitive increase downstream until the bar complex. Within the bar complex, there are significant changes in the amount of sand in the subsurface. Surface D_{50} and D_{84} values are highest at Sellman

Road, the most erosive site. .Values of subsurface D_{50} and D_{84} values are at their lowest at Upstream Cherry Hill. The fine subsurface material found at that site and the surrounding reach could very well be instrumental in bar formation. This will be examined in the next section.

2.5.3 Model and Parameter Limitations

The assessment of the usefulness of q* as a parameter in this study is affected by two complications in the Little Paint Branch watershed. The Dietrich et al. (1989) q* formulation uses 0.045 as the critical dimensionless shear stress. Thus the formulation is intended for channels with heterogeneous gravel beds, but not significant amounts of bed sand. The critical dimensionless shear stress was not adjusted at each reach, although this could be done. In addition, q* values near 1 will occur when the subsurface material has a size close to that of the surface. This can occur for very different reasons, either due to large amounts of fine material in both locations or due to depletion of subsurface material and thus similar (coarse) size in both surface and subsurface material.

The model developed by Barry, et al. (2004) does not estimate channel geometry and uses drainage area as a surrogate for both channel slope sediment supply within the watershed, which is not applicable to a watershed as altered from its original condition as the Little Paint Branch. The hydraulic geometry models of Parker (1978) and Millar (2004) are designed for threshold, gravel-bed channels, which limit the applicability of these models for reasons very similar to those of Dietrich's q* parameter. Because the watershed has been so removed from its natural

threshold conditions and may not return to such a state for decades, empirical approaches that were designed for natural streams can not be applied without significant manipulation. As such, shear stress based approaches remain a practical and accurate means of assessment.

Chapter 3: Channel Changes, Sediment Storage, and Bed Mobility within the Bar Complex Reach

3.1 Introduction

Many non-urban streams in the mid-Atlantic region are threshold streams, which commonly do not have significant sediment storage bars along or within the channel. The lower reaches of Little Paint Branch Creek contain both mid-channel and alternate bars that cause flow divergence, channel widening, and bank erosion. Processes that cause bank erosion are generally considered to have negative impacts on a river system. The process of bar formation, however, may be beneficial to the long-term sediment budget of the channel by shoaling the reach and resulting in more frequent overbank flooding and storage of sediment on the floodplain. The purpose of this chapter is to examine sediment and channel morphology changes that are associated with bar formation.

Hypotheses

1. Gravel bar formation causes shoaling of the bed, which decreases bed shear stress and stabilizes channel sediment around the gravel bars.
2. Fine-grained bed material is selectively stored in gravel bars, while coarse-grained sediment lines the channels around the bars.
3. The limited amount of subsurface material in channels adjacent to bars decreases the sediment supply (Dietrich, 1989, q*) and the bedload transport rate (Q_b) for a given discharge

3.2 Previous Work

Research on the effects of gravel bar formation on channel form and hydraulics is primarily limited to flume studies of bar evolution. There is little to be found on the sediment composition and hydraulics of gravel bar reaches. Observations of the conditions of gravel bar development and its consequences are more common, however.

According to Church (2006), sediment accretion and thus the major bed form features in a channel are controlled by the dominant sediment transport mode, which can be either suspended sediment or bedload sediment transport. When the dominant mode is bedload, as is the case with the Little Paint Branch, deposits within the channel slowly accumulate and force flow around them. Because of this the channel remains shallow as the channel width increases as banks are eroded, giving rise to lateral instability. Concurrently, suspended sediments such as sand are deposited on the accumulating bed forms and build vertically, fining upward nearest the surface. In the case of center channel bars, also known as braid bars, Ashworth et al. (1992) noted that these may form downstream of channel constrictions, as is the case with site CHB in this study.

3.3 Study Reach and Methods

The study reach is in the lower portion of Little Paint Branch Creek and it contains a series of sediment bars (fig.20). Gauging stations were installed at the upstream and downstream ends of the reach, which were gauged for turbidity and depth. The general methods used to determine surface and subsurface grain size,

channel morphology, gradient, and the calculation of hydraulic variables are discussed in the previous chapter.

The Cherry Hill Bar Complex was studied in detail, with measurements of sediment size distributions at seven sites evenly distributed through the bar complex reach (fig. 20). The seven study sites are numbered in descending order from upstream to downstream. In addition, sediment and morphological data were collected at cross section locations distributed around the first gravel bar.

In the case of this study, particles directly on the surface of the channel or gravel bar are considered surface sediment. Particles one inch beneath the surface are considered subsurface sediment; the one inch buffer is to ensure equal depth of measurement at all sampling locations. Surface samples were collected using Wolman Pebble Counts. In the case of the channel surface, a ten meter long sample area was used encompassing the entire width, and measurements were made. On the bar surface similar technique was used, though the bar boundary width was used rather than that of the entire channel. No difference was made between subsurface sampling in the channels and gravel bars. Three subsurface sample replicates were obtained for each sample site.

.

Figure 20. Aerial photo of the bars measured within the Cherry Hill Bar Complex. CHU and CHD are included to aid orientation. Source: Google Earth, USGS, Tele Atlas, 2009.

3.4 Results

3.4.1 Channel Surface and Subsurface Grain Size Data

Analyses of the surface grain size distributions in the bar complex reach show that there is a general fining of surface particles in the downstream direction (fig. 21). Fig. 21 indicates that Upstream Cherry Hill has the coarsest surface sediment. The two sites that, were the furthest downstream (CH1 and CHD) had the finest grain size of the sites measured. The downstream trends in the median (D_{50}) coarse (D_{84}) grain size fractions are shown in fig. 22. The coarse size fraction (D_{84}) decreases more rapidly downstream than the median grain size. Site CH2 appears unusually coarse in all of the grain size distributions.

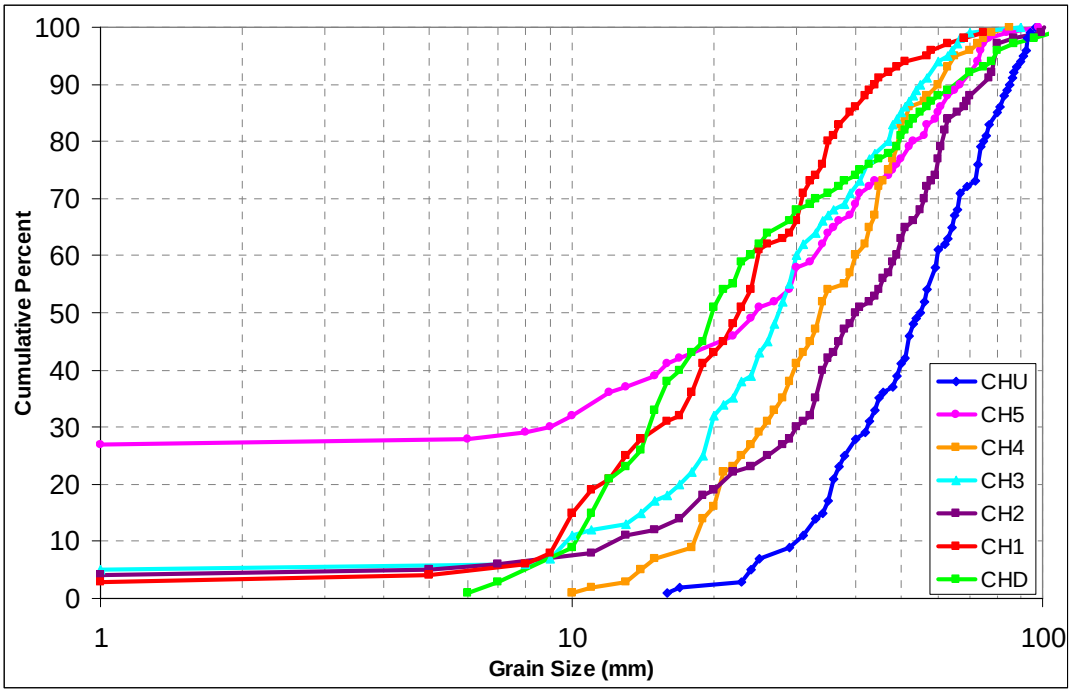

Figure 21. Bar Complex Channel Surface Sediment Distributions Sites are organized from upstream to downstream in the legend.

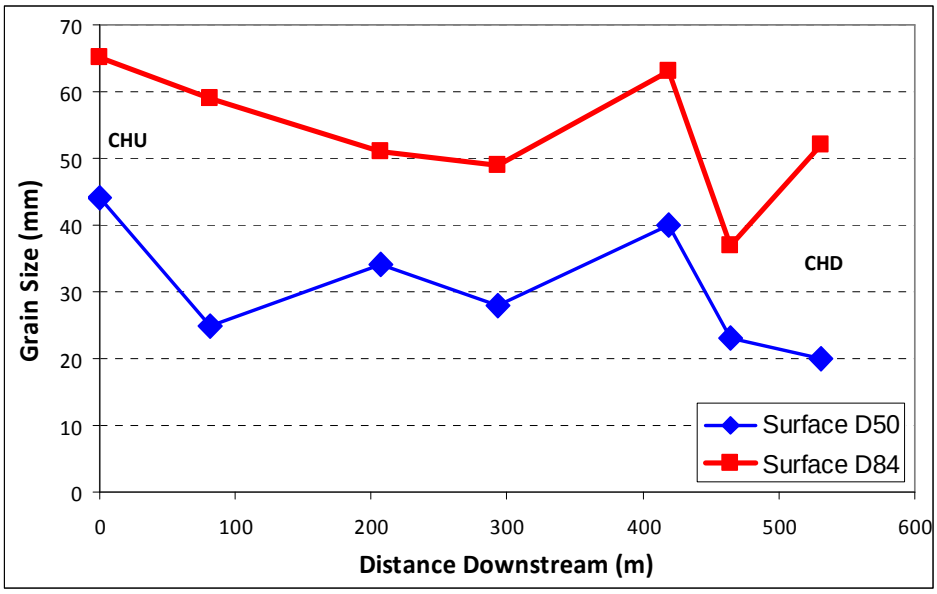

Figure 22. Downstream trend in channel surface grain size.

The distributions of subsurface sediment size for the channel sites in the bar complex reach did not vary as widely as with the surface sediment (fig. 23). The standard deviation for the grain sizes are shown in Table 6, and indicate that there are higher standard deviations for surface grain sizes than subsurface grain sizes. The Upstream Cherry Hill site had one of the coarsest surface size distributions, but one of the finer subsurface sediment distributions. The coarsest subsurface sediment was found at CH1, near the downstream end of the gravel bar complex. This general inverse relationship between surface size distribution and subsurface size distribution is particularly evident for the D_{84} values of each, shown in fig. 24.

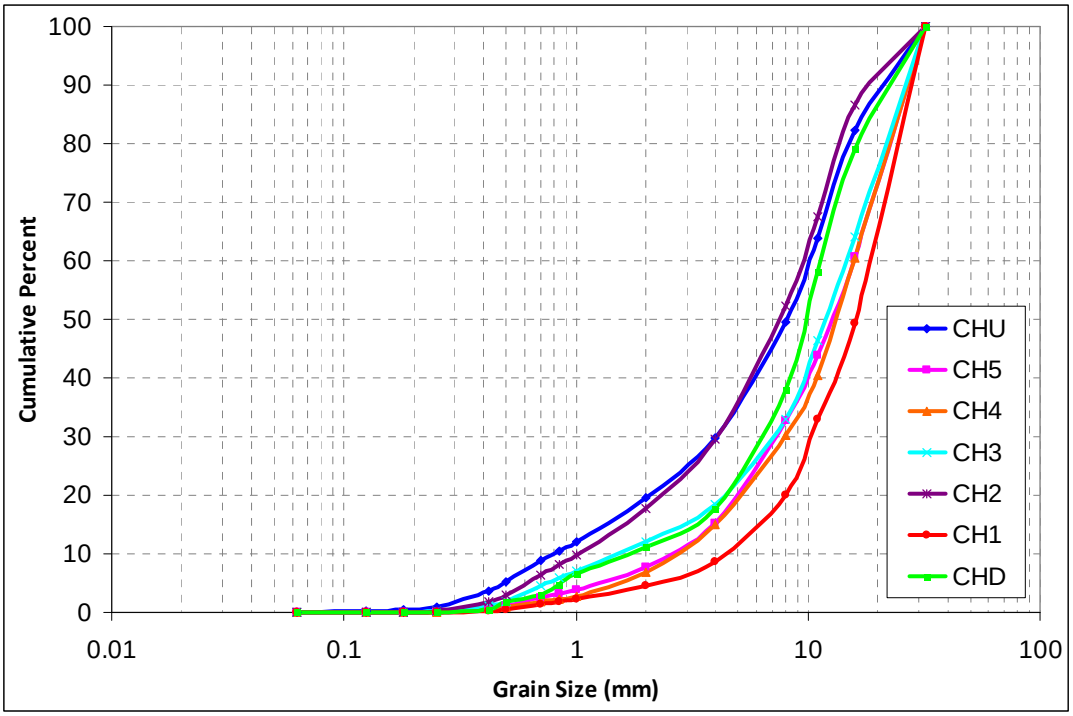

Figure 23. Channel Subsurface Sediment Distributions for grain sizes in the bar complex reach.

Legend lists the sites in order, from upstream to downstream locations.

Table 6. Cherry Hill Bar Complex Channel Grain Size Data

Site	D_{50s}	D_{50ss}	D_{84s}	D_{84ss}
CHU	55	8	78	17
CH5	25	13	59	25
CH4	34	14	51	25
CH3	28	13	49	24
CH2	40	7.5	63	15
CH1	23	16	37	26
CHD	20	9.5	53	19
AVE	32.1	11.6	55.7	21.6
ST.Dev	12.2	3.2	12.8	4.5

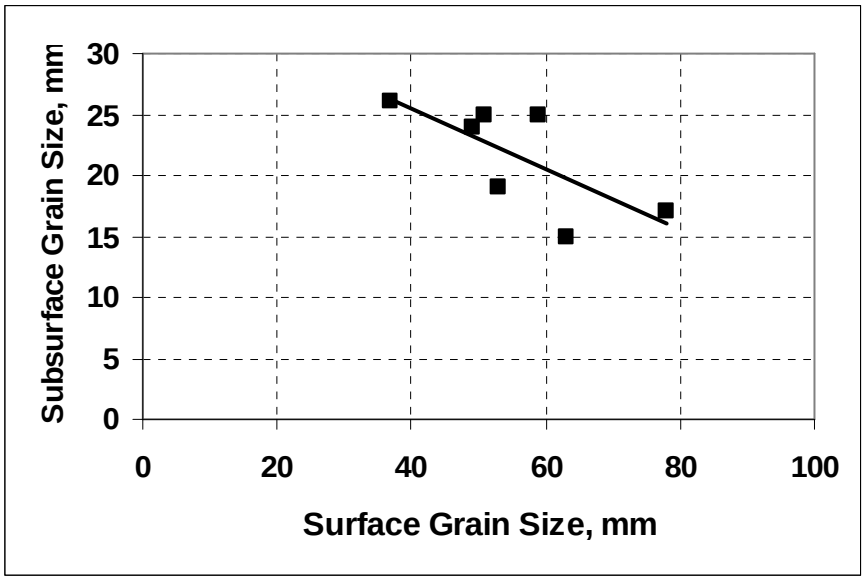

Figure 24. Relationship between D84 of channel surface and subsurface grain size; R^2 value is 0.52.

These two trends: a) the downstream finer in the surface grain size distribution, and b) the downstream coarsening of the subsurface size distribution combine to generate a downstream increase in the similarity of the surface and subsurface grain size distributions. The subsurface and surface sediment distributions for the sites at the upstream and downstream ends of the reach (CHU and CHD) are shown in figs. 25a and b. The difference between the surface and subsurface sediment distributions is much smaller at the downstream end of the reach (after the gravel bar complex) than the site upstream of the gravel bar complex. The pattern throughout the reach is shown as surface/subsurface ratios (fig. 26). These have implications for sediment transport, which will be discussed in the next section.

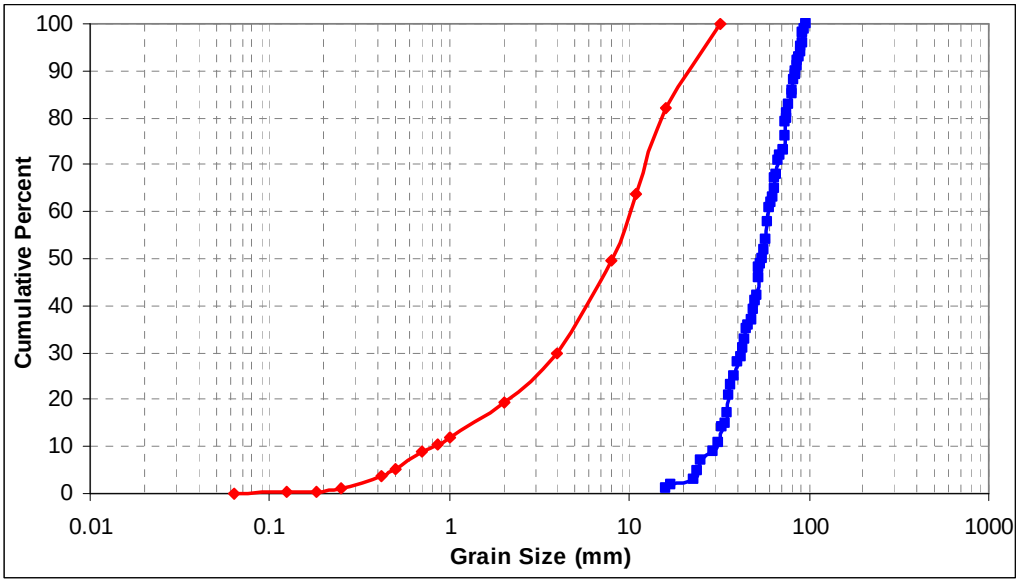

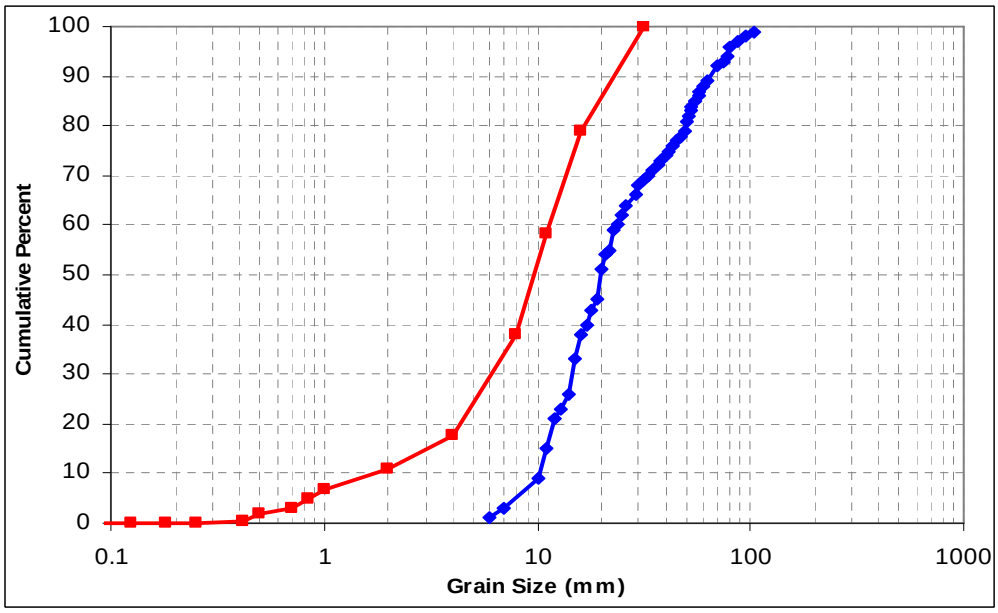

Figure 25. Grain Size Distributions for surface (blue) and subsurface (red) grain sizes at a) the upstream and b) downstream ends of the bar complex reach.

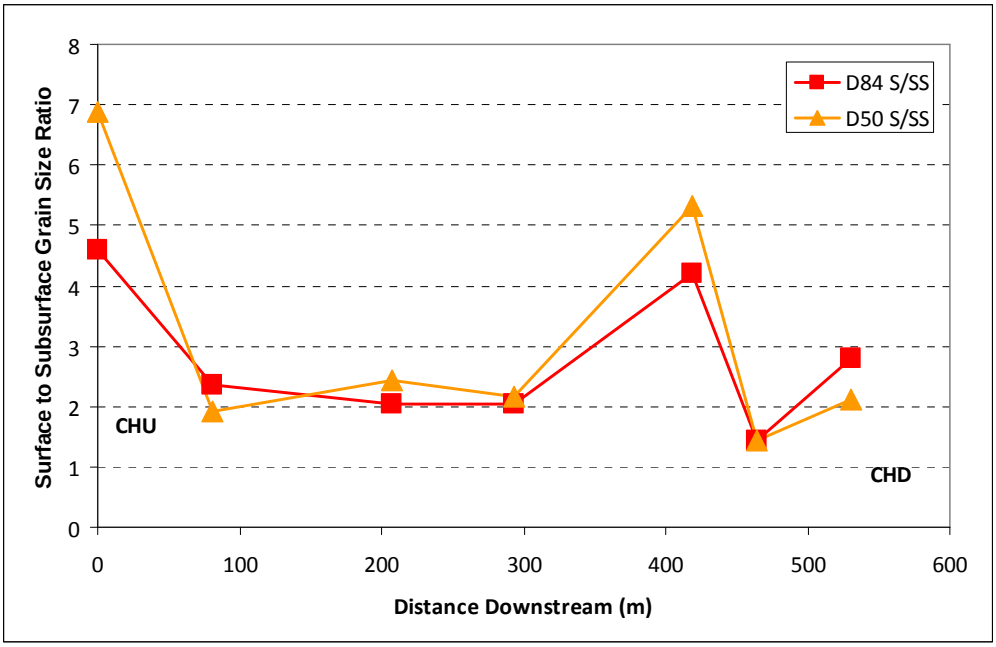

Figure 26. Ratio of surface to subsurface grain size for the median (D50) and one standard deviation above the mean (D84) size fractions.

Dietrich et al. (1989) introduced the concept of q* to describe the amount of armoring in channel bed. This parameter is calculated as follows:

$$q^* = \left[\frac{\tau_b - \tau_{cs}}{\tau_b - \tau_{css}} \right]^{1.5} \qquad (34)$$

In general, the value of q* increases within the bar complex (fig. 27), but this is due primarily to a narrowing in the disparity of surface and subsurface sediment sizes in the downstream direction. The q* value increases greatly after the Upstream Cherry Hill site, and stays elevated with the exception of the CH2 site. As was observed in the watershed as a whole, q* may not be a useful parameter in this river due to high availability of sand-sized and smaller sediment. High values of q* are intended to indicate low amounts of channel armoring, but it actually reflects the condition when similar grain size values are found in the surface and the subsurface. This can result

from fine sediment availability in both the surface and subsurface, or depletion of fine sediment in the subsurface; a condition that probably decreases sediment mobility.

Due to this dual cause of high values of q*, it does not correlate well with the percentage of fine sediment (Table 7). The percentage of fine material in the channel sediment within tends to decrease in the downstream direction. The lowest values occur at the beginning of the complex, before the major bar sites, but the lowest is just before the end at site CH1 with a value of only 4.44%.

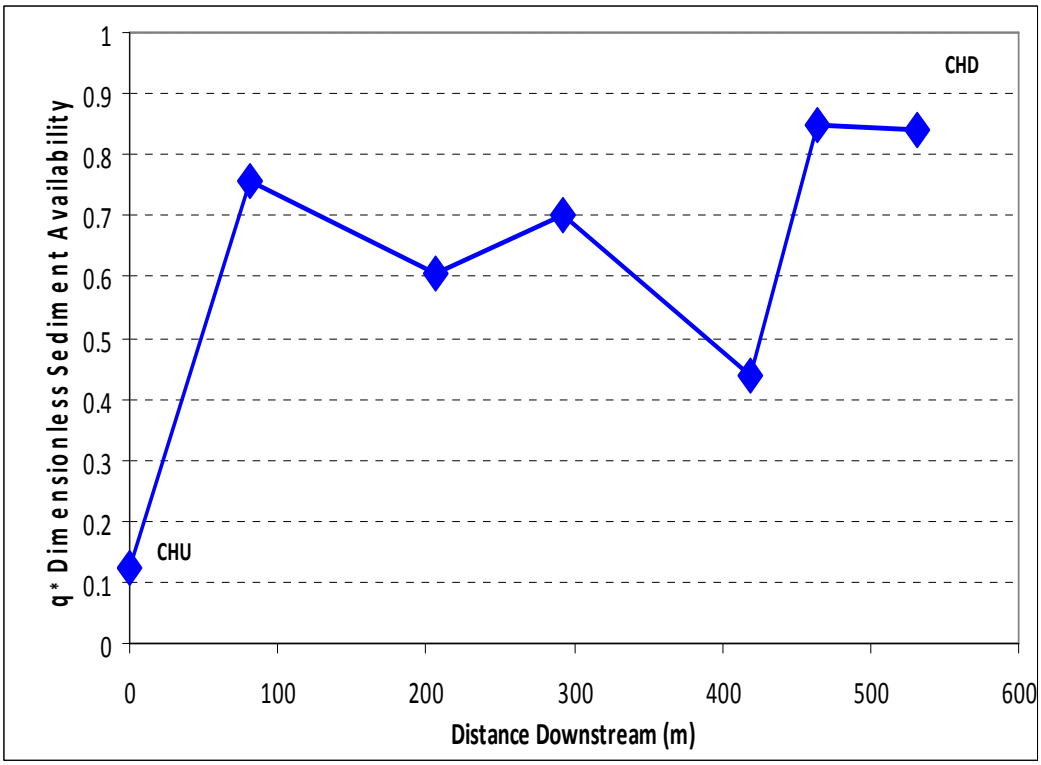

Figure 27. q* values for channel sediments vs. distance downstream in the Cherry Hill Bar Complex.

Table 7. q* and percent fine sediment values in the Cherry Hll Bar Complex.

Site	q*	Percent Fine Sediment (<2 mm)	Estimated T*crit values
CHU	0.124	19.43%	0.020
CH5	0.758	7.72%	0.037
CH4	0.605	6.80%	0.038
CH3	0.701	12.15%	0.035
CH2	0.437	17.64%	0.025
CH1	0.850	4.44%	0.040
CHD	0.839	11.0%	0.035

3.4.2 Comparison of sediment size between gravel bars and their adjacent channels

The channel bed and gravel bars are potentially both a source and reservoir for sediment moving through the system. The size of material stored in gravel bars was determined by measuring the surface and subsurface sediment distributions of the bars and comparing it to the adjacent channels. Five gravel bars were chosen for measurement based on location and the availability of data. Four of them span the length of the Cherry Hill Bar Complex (see Fig. 20) and the fifth is located at the Sellman Road (SR) site. Data was collected for this study and additional data were obtained from Dangol (2009).

Two different relationships were observed between the size of the sediment on the bar and the size of the sediment in the channels. For the large, bankfull bars at Sellman Road and CHB, the channel surface was coarser than the bar surface. The three lower level alternate bars or central bars (Bar 1, 3, and 4) had coarser sediment

than the adjacent channel bed. At all five locations, the bar subsurface was significantly finer than the channel subsurface, indicating selective storage of fine sediment in the channel bars. The amount of material less than 2 mm stored in the channel bed is significantly less than the amount stored in the gravel bars (Table 8). The ratio of the <2mm fractions in the channel and bars is also shown in Table 8. These data indicate that there is significantly more fine sediment stored gravel bars than the adjacent gravel bed (on the average there is 4.6 times more fine sediment in the bars than in the channel).

Table 8. Data Summary for gravel bars and adjacent channels.

Fine Ratio			D_{50s}	D_{50ss}	D_{84s}	D_{84ss}	% <2mm
		bar	38	4	55	15	32.33
SR	2.19	**channel**	58	15	80	28	14.73
		bar	30	4	41	12	30.84
	1.28	**channel R**	42	10	59	22	24.06
CHB	9.76	**channel L**	55	17	78.5	29	3.16
		bar	49	2.2	63	16	49.04
Bar #4	6.35	**channel**	24	14	59	25	7.72
		bar	38	7	54	23	32.47
Bar #3	2.67	**channel**	27	13	49	24	12.15
		bar	45	10	59	24	22.93
Bar #1	5.16	**channel**	23	16	38	25	4.44

For central bar locations, there can be significant variations in sediment characteristics between the two distributary channels. At the CHB site, there is a greater amount of fine material in the right channel then in the left (Figs. 25a and 25b). At the time the samples were collected for analysis, the left channel was the "active" one in that it conveyed most of the water through the reach. The sediment in the left channel became far more coarsened as a result of the greater shear stresses it endured. The right channel received only a fraction of the water, giving it a lower depth and lower overall shear stress values.

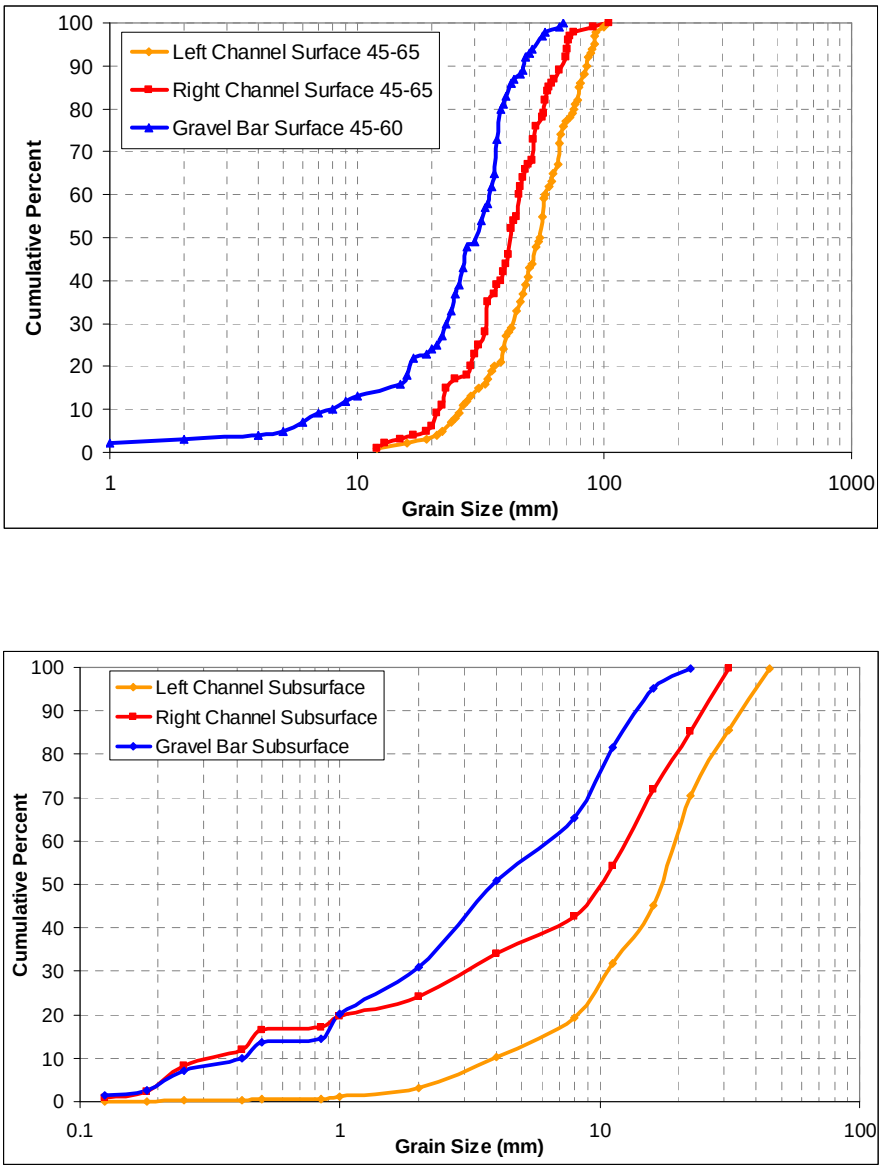

Figure 28 a: Bar vs. Channel surface sediment distributions at CHB. b: Bar vs. Channel subsurface sediment distributions at CHB. Note change in x axis scale between the two graphs.

The selective storage of fine sediment in the gravel bars is illustrated in fig. 29, which is a plot of the percentage of fine material (< 2 mm) in both bar and channel sites versus the distance downstream in the bar complex. The highest values of fine sediment storage in bars are at the upstream end of the system and they gradually taper off towards the end of the complex as the size of the bars themselves decrease (Dangol (2009); Fig. 30). The percentage of fine sediment stored in the channel bed is considerably less throughout the bar complex and it ranges from 2-12% of the channel sediment within the bar complex.

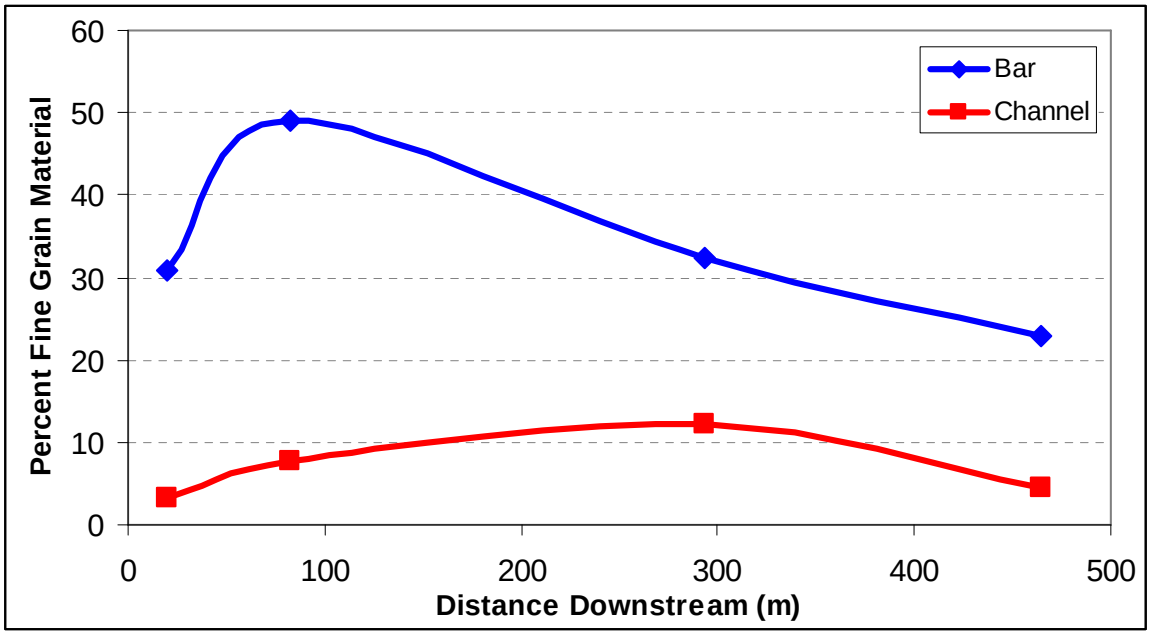

Figure 29. Percent fine material (2 mm) in the channel and gravel bars in the bar complex. Error variance plots within the data points.

These data indicate that the bars are built by layers of sand and gravel, with total sand in the bars ranging from 22-50%. This suggests that the bars were deposited during bedload transport conditions that included significant amounts of

sand moving in the bedload (i.e. associated with bank erosion events). This is significant, because these high proportions of bed sand are associated with significantly lower critical dimensionless shear stress values (Wilcock, 2001). This is consistent with field observations of bar accretion during multiple transport events over a 2-year period.

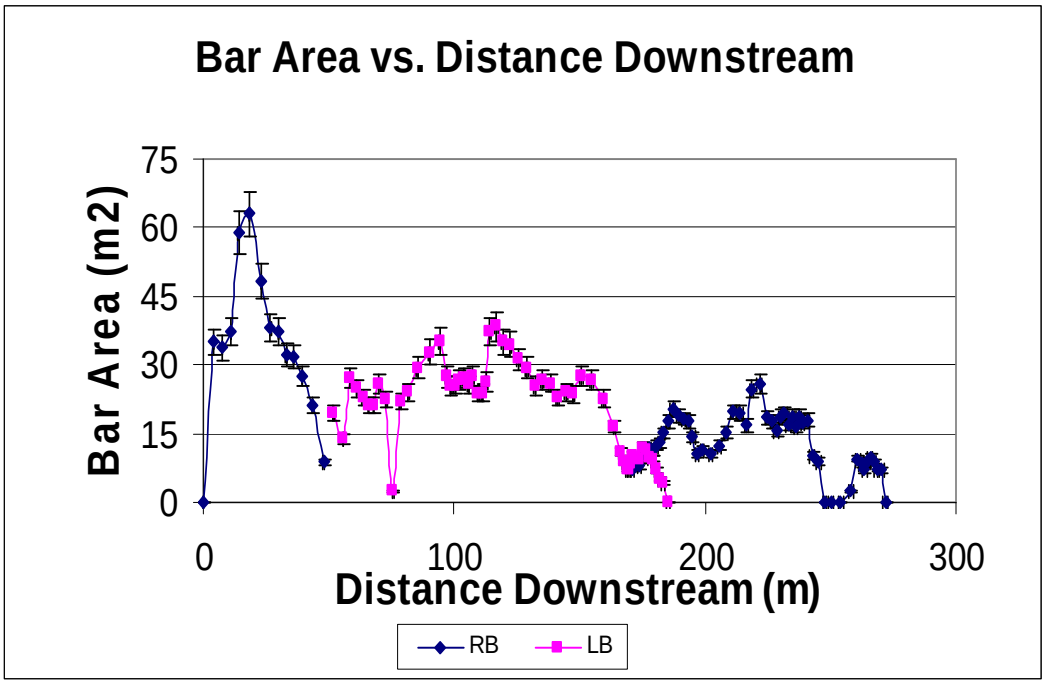

Figure 30. Gravel Bar area versus distance downstream; from Dangol (2009). LB are left bank bars and RB are right bank bars. The upstream gravel bar stores more fine-grained sediment..

3.4.3 The influence of a gravel bar on channel hydraulics and sediment transport

Figure 31. Picture of Cherry Hill Bar near bankfull flow.

To evaluate the effects of central bar on flow and bed mobility, detailed analysis of sediment sizes and bed mobility were evaluated at cross sections distributed around the Cherry Hill Bar (just downstream of CHU), which is shown in fig. 31. Eight cross section sites were located across the channel and bar over a reach of 100 meters. At each site, cross sections were surveyed and surface and subsurface sediment distribution of bar and channel sediment were measured. Water surface gradients were measured during high flow events. These data were used to determine width, depth, gradient, shear stress, and dimensionless shear stress for bankfull events within the reach.

The width to depth ratio versus distance along the channel is plotted for the bar reach in fig. 32. These data indicate the expansion of the channel around the central bar (35-70 m). The increase in width to depth ratio is due to both width expansion and shoaling of the channel bed. The decrease in depth reduces the shear stress on the channel bed during storm flows and forces water out on to the floodplain. This may increase bank erosion, the increased shear stress on the channel banks can be modeled using a shear stress partitioning model by Flintham and Carling (1988):

$$SF_{bank} = 1.77\ \{(P_{bed}/P_{bank}) + 1.5\}^{-1.4} \quad (35)$$

$$\tau_{bank} = \tau_o * SF_{bank}\ (B+P_{bed})/(2*P_{bank}) \quad (36)$$

where SF_{bank} is the shear force on the bank, P denotes perimeter, and B is the surface width. In the model, as the wetted perimeter of the bank decreases the lateral stresses of the river are concentrated on a smaller area. The increase in shear stress on the bank causes it to erode. The application of Flintham and Carling's (1988) model has limitations though, as it was developed for straight, trapezoidal channels.

The surface grain size (D_{84}) values of the channels are significantly coarser than the bar surface (fig. 32b).

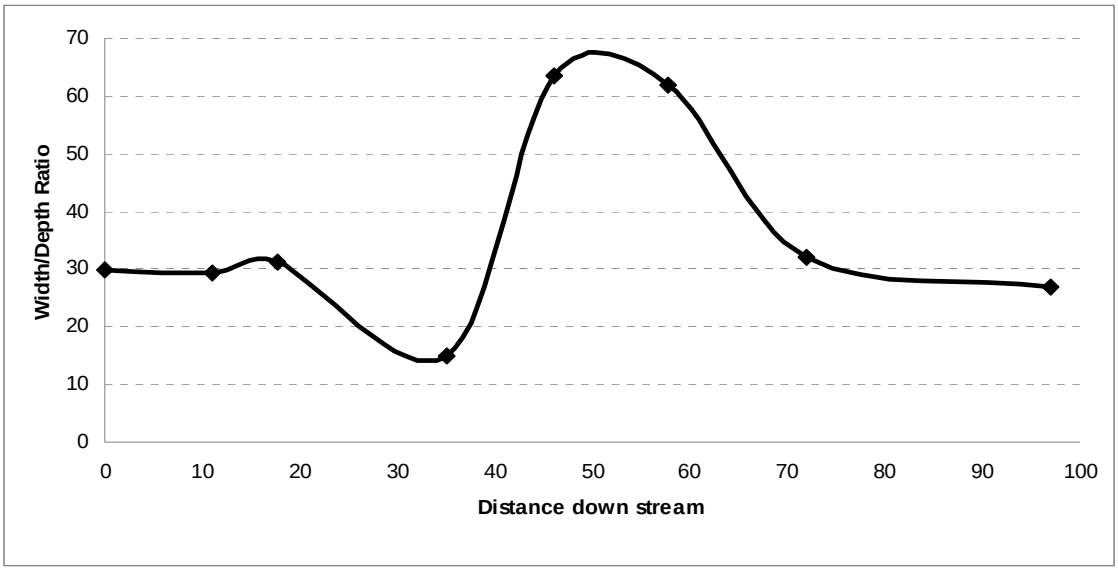

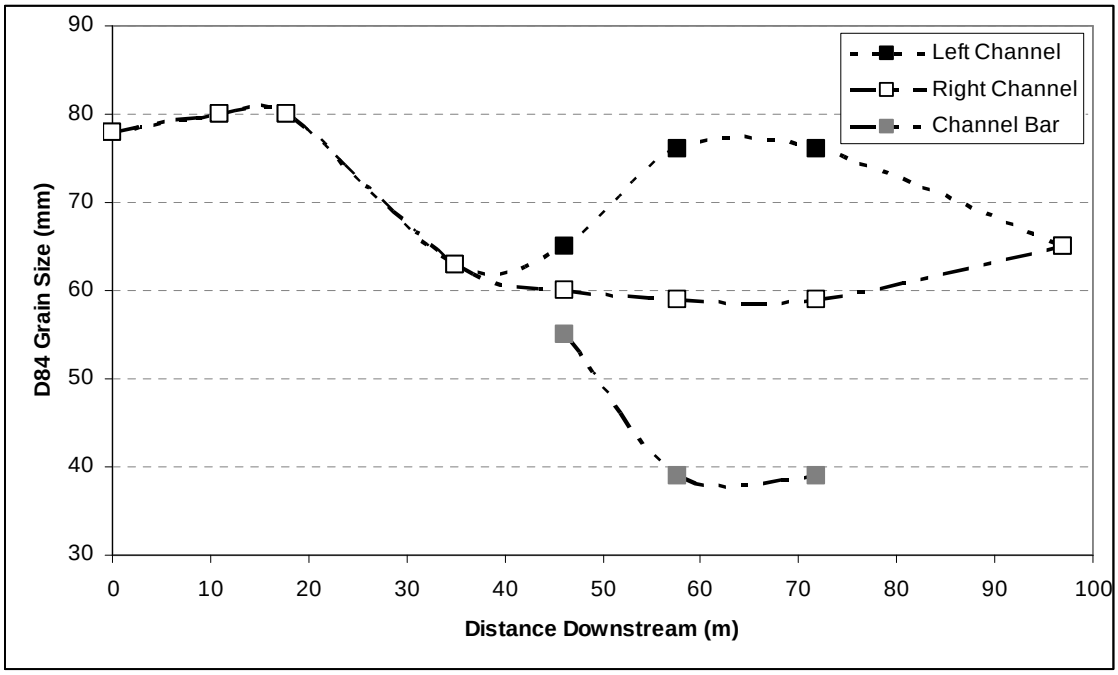

Figure 32. a) Width to Depth ratio in the Cherry Hill Bar reach. B) D_{84} Grain size in the reach. Error is contained within the data points.

The dominant left channel is coarser than the secondary right channel. The D_{84} values of the channel bar are similar in size to the adjacent channels at the upstream end, but bar sediment becomes finer with distance along the bar.

The channel morphology and sediment measurements were used to calculate the dimensionless shear stress of each site was calculated for bankfull flow conditions. These data are summarized in table 9. The cross sectional average dimensionless shear stresses are shown in fig. 33. The solid lines on the graph represent a dimensionless shear stress of 0.045 and 0.03, a common range for critical dimensionless shear stresses for gravel (0.045) and gravel over sand (0.03). For high amounts of sand in the bed, the critical dimensionless shear stress can drop to even lower value (Wilcock, 2001). For this reach, the critical dimensionless shear stress is probably much lower than 0.045.

These data indicate that the gravel bar surface and the right distributary channel are both stable at the bankfull stage; values of τ^*_{avg} and τ^*_{max} are near or below 0.045, with the main exception occurring in the left channel. The dimensionless shear stress over the channel bar reaches a value of 0.032, which is near the threshold of motion for gravel that overlays sand. As seen in fig. 28a, however, the presence of sand on the bar surface is limited. In fig. 33b, the dimensionless shear stress values for the maximum channel depths are shown. This graph indicates that the channels can be mobilized at these locations at bankfull flows. Both maximum and average shear stress data suggest that the downstream portions of the left channel will be the most mobile. This result is consistent with field observations and the resurveys of channel cross sections.

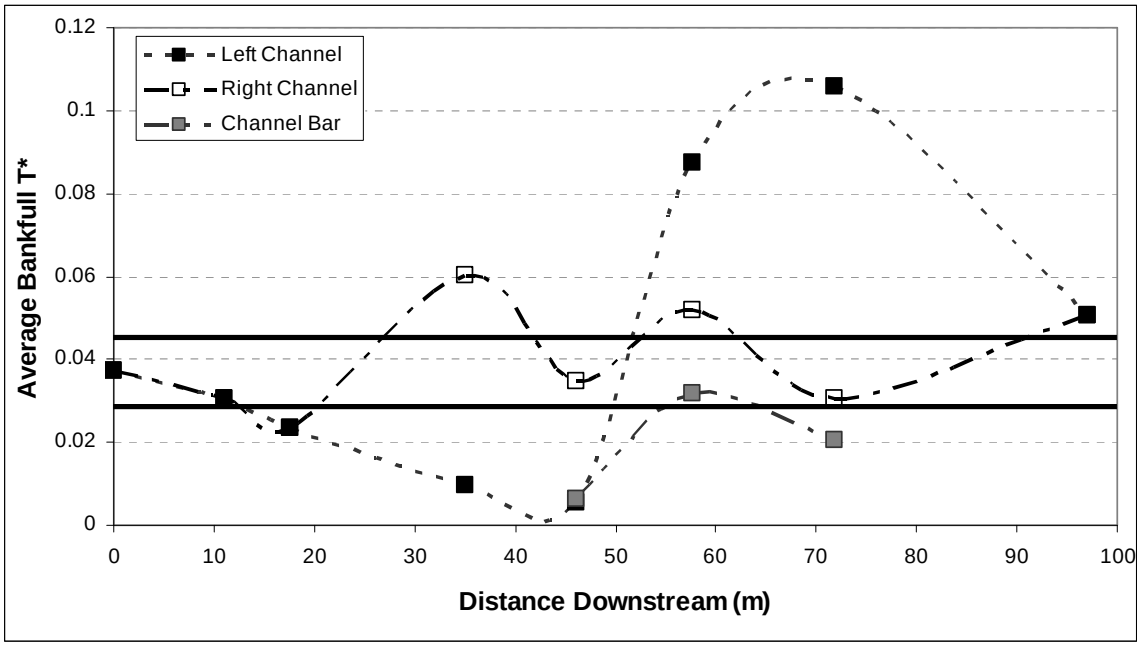

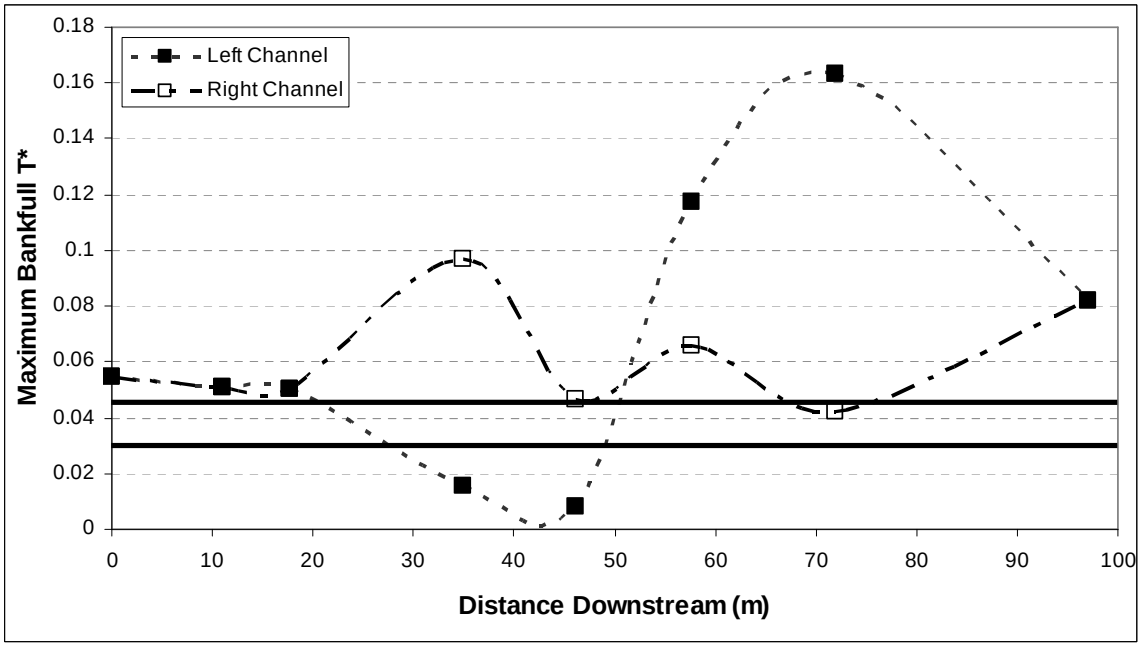

Figure 33 a) Average downstream dimensionless shear stress of the Cherry Hill Bar reach. The upper solid line marks a τ^* of 0.045 and the lower line marks a τ^* of 0.03 b) Maximum downstream dimensionless shear stress of the Cherry Hill Bar reach. The upper solid line marks a τ^* of 0.045 and the lower line marks a τ^* of 0.03.

Table 9 Cherry Hill Bar Data.

Site	Distance	Channel	D84	Gradient	Avg. Depth	Max Depth	Avg. T*	Max T*
1	0		78	0.007	0.68	1.00	0.037	0.054
2	11		80	0.007	0.58	0.96	0.031	0.051
3	18		80	0.007	0.44	0.94	0.023	0.050
4	35	Left	63	0.001	0.89	1.44	0.009	0.015
		Right	63	0.007	0.89	1.44	0.060	0.097
5	46	Left	65	0.001	0.54	0.81	0.006	0.008
		Right	60	0.008	0.45	0.61	0.035	0.047
		Bar	55	0.004	0.13	*	0.006	*
6	58	Left	76	0.022	0.50	0.67	0.088	0.118
		Right	59	0.008	0.67	0.84	0.052	0.066
		Bar	39	0.008	0.27	*	0.032	*
7	72	Left	76	0.011	1.20	1.84	0.106	0.163
		Right	59	0.004	0.76	1.06	0.030	0.042
		Bar	39	0.004	0.34	*	0.020	*
8	97		65	0.007	0.77	1.25	0.051	0.082

In summary, the data indicate that although energy gradient increases due to the formation of the gravel bars, the decrease in channel depth prevents shear stress values from exceeding the threshold of motion in much of the channel and on the bar surface. The formation of the gravel bar serves as a storage reservoir for fine sediment. It also has resulted in the shoaling of the channel bed, which serves to promote overbank flow during bankfull and higher floods events, which reattaches the stream to its flood plain.

3.5 Discussion

3.5.1 Sediment distribution in the Bar Complex

In this chapter, I examined the distribution of sediment grain sizes for surface and subsurface material at both gravel bar and channel locations. Sediment sizes of the channel surface gradually decrease over the bar complex reach while the subsurface sediment shows little variation. This results in a general decrease in surface to subsurface grain size ratios in the gravel bar reach. The downstream site, CHD does not contain gravel bars and it is depleted in fine sediment in the subsurface material. The combination of these two factors provides further evidence of the storage of fine sediment within the gravel bars.

The q* values do not appear to be useful in these reaches with varying amount of sand in both the surface and subsurface grain size distributions. The q* parameter is intended to identify armored reaches, but sites with depleted subsurface material can generate high values of q*. The measure of the amount of sand in the reach and its effect on critical dimensionless shear stress might be a better way of identifying local channel mobility.

3.5.2 Gravel bars as sediment reservoirs

It is quite clear from the gravel bar sediment data shown that gravel bars are major storage sites for fine sediment. The average ratio between the percentage of fine material(<2mm) in bars and in the channels is 4.6, which suggests that the gravel bars store on average 4.57 times more fine sediment than the channels adjacent to them.

The sequestration of this material from the active channel has the effect of increasing the critical dimensionless shear stress for channel sites, which limits the mobility of the sediment in the channels. The shoaling of the bar locations serves to limit the mobility of sediment stored in the bars.

3.5.3 The role of bar formation in sediment mobility

The upstream gravel bar CHB was examined in detail. Around the gravel bar, channel widths are 2-3 times wider than adjacent upstream single thread reaches. The channel initially widens at the bar head, and width decreases downstream. The upstream portion of the divided reach has average bankfull shear stresses at or below critical, but the bar tail is a zone of active bed and bank scour and sediment transport. Shear stresses over the bar top are significantly lower than in the channels. These data suggest that channel bars may initially increase bank erosion, but they also provide a place for the storage of fine sediment, and increase overbank flooding onto the floodplain. Additionally, the storage of fine sediment from reduces the mobility of the coarse sediment that initially forms gravel bars, which may prevent the growth of more gravel bars further downstream.

These data suggest that the geomorphic response of urban stream channels to urban runoff is more complex than earlier envisioned (e.g. Hammer, 1972). In Little Paint Branch Creek, bank erosion has resulted in the mobilization of fine sediment. This fine sediment has increased the mobility of the gravel bed, which has facilitated the formation of gravel bars, which in turn has shoaled the gravel bed and locally stabilized the channel bed. These change pathways are summarized in fig. 34.

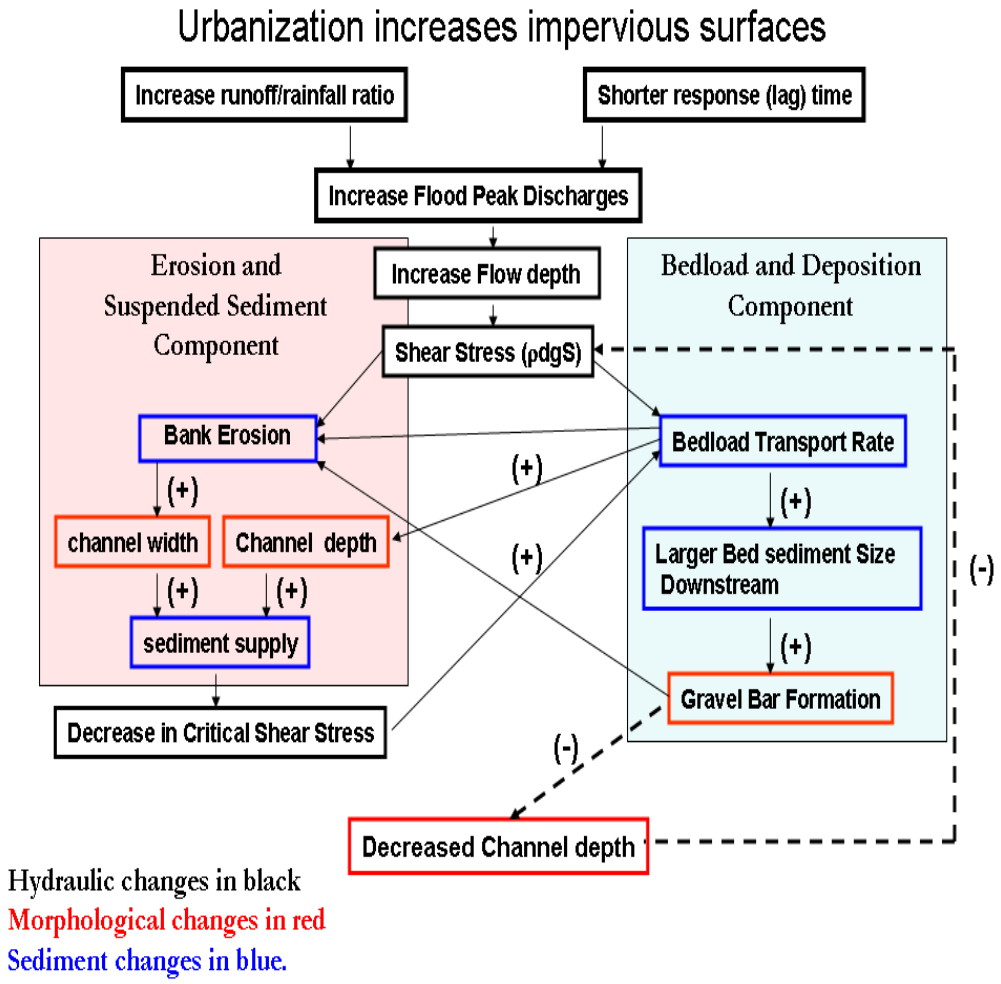

Figure 34. The effects of urbanization on channel morphology with the assumption that an increase in the magnitude of bankfull flow affects flow depth and thus shear stress, this generates bank and bed erosion which affects bedload transport rate. Note negative feedback loop.

Chapter 4: Effects of urbanization on storm response and sediment load in the Northeast Branch watershed and Bar Complex reach

4.1 Introduction

As part of the Chesapeake Bay Program, local and regional governments have set goals to limit the discharge of sediment and associated toxic substances from the Northeast Branch watershed into the tidal reaches of the Anacostia. These goals are part of the Total Maximum Daily Load (TMDL) regulations enforced by the EPA. Because of this, two major objectives of stream restoration plans are to implement measures to prevent bank erosion and to reduce the suspended sediment load (Prince George's County DEP, 2009**)**. To achieve these goals the traditional approach has been to either shore up eroding banks with rip rap or to completely channelize the stream by lining the channel with concrete or large boulders. Channelization can also be used as a flood control method by speeding up the conveyance of water through the channel during high flows, preventing it from spilling into the floodplain.

While these methods do effectively inhibit bank erosion and sediment transport in some cases, it may also initiate channel incision and remove the stream from its flood plain (Church, 2006**)**. This hinders or eliminates riparian function necessary for a healthy stream, reduces the perceived aesthetic and natural value, and may actually cause further erosion due to increased stream power (Church, 2006**)**. Most important, however, is that this approach completely ignores the other major source of sediment in urbanized streams and rivers: storm runoff. To successfully

reduce the sediment load and the associated toxic content we need to know: A) Where the sediment is coming from, and B) timing of the sediment from various sources, and whether there are sites of sediment storage in the watershed that could be enhanced.

Objectives

1. To determine the timing and amount of turbidity and suspended sediment load at three regions within the Northeast Branch watershed: A) the headwaters, B) the mouth of a major tributary, Little Paint Branch Creek, and C) near the mouth of the Northeast Branch..
2. To determine whether gravel bar formation, which results in channel widening and an increase in overbank flooding, significantly affects the suspended sediment load of the stream.
3. To determine the characteristics of storm runoff and rise time in the Anacostia River watershed.

Hypotheses

1. Bank erosion is a significance source of suspended sediment load. Therefore, turbidity and suspended sediment loads are highest for tributaries, such as Little Paint Branch tributary that are experiencing channel widening.

2. The formation of gravel bars causes flow divergence and bank erosion. Therefore, turbidity and suspended load are significantly higher at the downstream of the bar complex than upstream of the bar complex.
3. Storm runoff production will be greater in the more urbanized Northeast Branch drainage area, but peak discharge delays will be similar to those of the Little Paint Branch.

4.2 Previous Work

4.2.1 Empirical observations on sediment loads in urban watersheds

In 2007 a study was done by Allmendinger et al. to determine the sediment budget of the Good Hope Tributary in Montgomery County. The Good Hope Tributary is a third order stream in the Anacostia River watershed with a drainage area of 4.05 km^2 that has been progressively urbanized since the beginning of the 20^{th} century. The study used historical tax records to determine land use data, computations of historical peak discharges, statistical models derived from short-term channel surveys, and ergodic assumptions to estimate the components of the sediment budget.

The sediment budget showed that upland erosion in the watershed and the enlargement of the channel's area contributed significantly to the overall sediment flux in the watershed. The two each produced approximately 70 and 80% of the overall sediment yield. Around 50% of the total sediment yield was accounted for by floodplain deposits. In total floodplains stored around one-third of the total sediment production between 1951 and 1996, demonstrating their importance in sediment

retention in urbanizing watersheds. Remobilization of legacy sediments deposited in the 19th and early 20th century made up between 0 and 20% of the total yield, indicating that they are not a significant source in the region.

In 2000, Pizzuto et al. conducted a study of eight pairs of urban and non-urban gravel bed watersheds in southeastern Pennsylvania. The pairs were matched by drainage area and the urban watersheds were between 35 and 50 percent impervious. The main differences found were in the median bankfull widths and areas, pool depths, and sediment distributions. Median bankfull widths and areas ranged between being 26% and 180% larger in urban channels, while the median pool depths of urban watersheds were 31% smaller than the rural channels.

The overall median grain sizes did not differ significantly between the sets of watersheds, but the characteristic secondary mode of gravel bed rivers was lacking in the urbanized streams. A primary mode existed between 64 and 256 mm, but the secondary mode found between 2 and 64 mm in the non-urban watersheds was completely lacking in the urban ones. This indicates that the urban streams were depleted of sediment within that size range in comparison to the non-urban streams. The researchers concluded that the urban channels adjusted their areas and roughness to more efficiently transmit the increased peak discharges caused by the impervious surfaces. They also speculate that the erosion from the bed and upstream sources must be significant in order to supply the stream with enough sediment to maintain a bed sediment composition similar to that of the non-urban streams.

4.2.2 Suspended Sediment Theory

An estimate of depth integrated suspended sediment concentration can be determined with a measurement of concentration at one point and modeling the vertical variation of suspended sediment above the channel bed. Suspended sediment transport theory is based on boundary layer theory (law of the wall) and evaluates suspension as a balance between the downward settling of particles against the upward motion of turbulent eddies (Rouse, 1937). Simple versions of the theory require uniform flow, thus measurements should be made in straight reaches with stable cross sectional areas:

$$UH \equiv \int_0^H \bar{u}\, dz \tag{37}$$

$$UCH \equiv \int_0^H \bar{u}\,\bar{c}\, dz = q_s \tag{38}$$

where z = height from bed of interest (m), $\bar{u}$ = local stream flow velocity averaged over turbulence (m/s), $\bar{c}$ = local volume sediment concentration averaged over turbulence (liters), H = flow depth (m), q_s = volume transport rate of suspended sediment per unit width, U = vertically averaged stream flow velocity (m/s), and C = vertically flux-averaged volume concentration of sediment in suspension (liters).

To find the concentration, C, we can use the Rouse-Einstein equation. The Rouse-Einstein Equation is used to model the size of particles that are moved as suspended load for various discharge events. The Rouse number defines the balance between settling and turbulent suspension, it is essentially the ratio of the fall velocity to the shear velocity. A high value of the Rouse number indicates that the fall velocity is high and particles remain near the bed. If the shear velocity is increased and the particle size (fall velocity remains constant), then turbulence will serve to

keep the particles suspended in the flow. The Rouse-Einstein equation is formulated to evaluate the concentration of specified grain sizes at various depths above the channel bed.

$$\frac{C}{C_a} = \left[\frac{d-y}{y} \frac{a}{d-a} \right]^z \tag{39}$$

where, C is concentration, d is total depth, *y* is distance above the bed, and a is an arbitrary distance above the bed where measurement is made. The exponent Z is the Rouse number, which is determined as:

$$Z = \frac{w}{B\kappa U^*} \tag{40}$$

Where *w* is the settling velocity, B is a constant, k is von Karman's constant 0.4, and

$$U^* = \sqrt{gRS} \tag{41}$$

The settling velocity is largely a function of grain size and grain size distribution

$$W^2 = \frac{4gD}{3C_D} \frac{\gamma_s - \gamma}{\gamma} \tag{42}$$

where, C_D is the drag coefficient, which is a function of Reynolds number, g is the acceleration due to gravity, γ is the specific weight of water or sediment, and D is the median diameter of the grains.

If the constants are ignored, the Rouse exponent simplifies to a ratio of the fall velocity to the shear velocity. For a given sediment size, the smaller the exponent Z, (i.e. the higher the value of U*), the more evenly distributed the suspended sediment will be as a function of the flow depth. Thus, channel change may be driven by suspended sediment deposition as well as by erosion (a function of shear stress).

Dade and Friend (1998) used the ratio of the fall velocity to the shear velocity as a measure of the amount of sediment carried by bedload and suspended sediment load in rivers. They used field observations of bedload and suspended load transport rates and found that if the Rouse number was less than or equal to 0.3, suspended load was the dominant process. For Rouse numbers greater or equal to 3.0, bed load was the dominant transport mechanism. A river can be said to be dominated by suspended load if bedload is less than ten percent of the total load.

Suspended sediment load is commonly evaluated by determining the sediment load transported for a given discharge event, a relationship known as a sediment rating curve (Leopold and Miller, 1956). Available sediment concentration data (C, mg/l) and discharge measurements (Q, l/s) are used to calculate instantaneous load (Q_s, mg/s). The general equation for load is: $Q_s = QC$.

A sediment rating curve is the relationship between load and discharge:

$$Q_s = aQ^b \tag{43}$$

where Q_s is the total load (Leopold and Miller, 1956). The coefficient, a, and exponent, b, can be used to interpret relationships between a variety of sediment transport conditions and processes. The coefficient, a, and exponent, b, have no relation to the hydraulic geometry equations described earlier. Sediment rating curves have significant limitations. Most show a large scatter in the relationship and suspended load in rivers is almost always below the carrying capacity of the flow. As

a consequence, Q_s will change not only with Q, but with changes in the upstream sediment supply during a given storm.

4.3 Study Sites and Methods

4.3.1 Study Sites

A total of four sites were instrumented and used for analysis of suspended sediment load. The sites are distributed within NE Branch of the Anacostia, including sites in the headwater, at the mouth of Little Paint Branch Creek, and near the mouth of NE Branch, near the downstream end of the non-tidal portion of the Northeast of the Anacostia (fig 35). The instrumented sites are described below:

Greencastle Road (GCR): With a drainage area of 9.6 km^2, Greencastle Road is the furthest upstream site. It is the least urbanized, and much of the urbanization is mitigated with stormwater management. The site is located in a forested stream corridor downstream of Greencastle Road. The gauge and instrumentation at this site was installed for this project.

Upstream Cherry Hill (CHU): The Upstream Cherry Hill site is located 7.5 km downstream of Greencastle Road and it has a drainage area of 25.9 km^2. It is immediately upstream of a 500 meter reach of the stream called the Cherry Hill Bar Complex (CHBC) which, is characterized by a series of gravel bars. The gauge and instrumentation at this site was installed for this project.

Downstream Cherry Hill (CHD): The CHD site is located at the end of the gravel bar reach, 500 m downstream of CHU. There are no additional tributaries that enter the stream between the two sites, therefore, CHD has almost the same drainage area as the upstream site. The gauge and monitoring equipment at this was installed to document the effects of bar formation on bank erosion and suspended sediment load in the bar complex reach.

Northeast Branch (NEB): The Northeast Branch is a long-term discharge and sediment gauging station operated by the USGS. It is located within the channelized portion of the Northeast Branch of the Anacostia, and is 7.4 km downstream of the CHBC with a drainage area of 188.6 km^2. In addition to the discharge of the Little Paint Branch, it also receives flow from Paint Branch Creek, Indian Creek, and Beaverdam Creek. Paint Branch Creek and Indian Creek have amounts of urbanization that are similar to that of Little Paint Branch Creek and Little Paint Branch Creek has a watershed area intermediate in size of the other two.

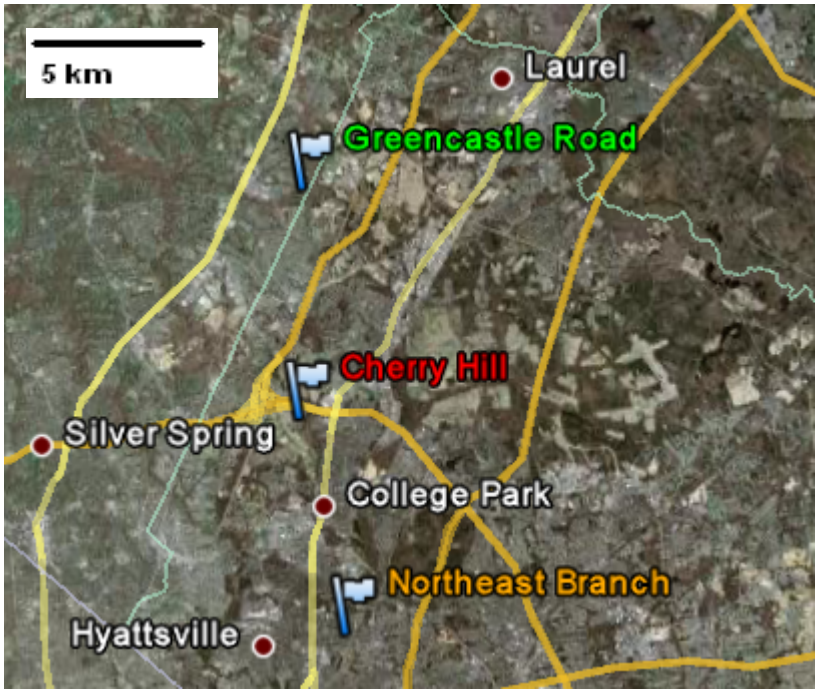

Figure 35. Aerial photograph of the study area, located northeast of Washington, DC. Taken from Google Earth, Source: DC GIS, USGS, Tele Atlas, 2009.

4.3.2 Turbidity and Gauge Height Measurement Methods

For the three upstream sites, Hydrolab MS5's were used to measure turbidity and gauge height during storms. The MS5's run under battery power and have a timed, synchronized gauging interval of 7.5 minutes so data could be compared directly with data from the Northeast Branch, which the USGS monitors at an interval of 15 minutes. Turbidity was measured in Nephelometric Turbidity Units, or NTU, and the gauge heights were measured in meters. The depth and turbidity probes were protected in PVC pipe casing with holes drilled into it to allow for adequate water circulation. The casing was then anchored to the stream bank with a coated metal cable and placed in a flat, deep, part of the channel. At the USGS

Northeast Branch gauging station turbidity is measured in FNU. The differences between FNU and NTU do not become significant until around 500 NTU or FNU. FNU data can be converted to NTU values.

The automatic sampling of depth and turbidity provided continuous measurements during storm and flood events that were too hazardous to be monitored manually. Gao (2008) noted that **"**this technique provides a cost effective way of in situ monitoring of continuous variation of suspended sediment concentration, which greatly improves the accuracy of determining the sediment yields compared with the traditional infrequent sampling."

Although the monitoring equipment provides the possibility for continuous monitoring, the gauges would have technical problems and either stop recording or record inaccurately. For this reason, not every storm has a complete or accurate set of depth and/or turbidity data. In particular, colder temperatures affected the accuracy of the gauge height readings. Therefore, winter storm data sets were not used for this study, but similar late winter, early spring storms were included in this study as well as fall and summer storm events. As previously mentioned, to verify accuracy the gauge height readings from the MS5's were checked against field readings of in-channel staff gauges periodically during storms at every gauged site.

4.3.3 Field Techniques

Discharge and turbidity data for storm events can be obtained directly from the USGS web site for NE Branch storm events. The other locations were gauged by the UMD team and required the measurement of discharge and establishment of a

discharge rating curve. To do this, stream cross-sections were surveyed at the three UMD gauge locations. The measurement interval for the cross-sections varied to fit the unique morphologies of each site and varied from 0.10 to 1.0 meters and at least 15 measurement points were included in each cross section measurement. During a range of flow events, discharge was determined by measurement of flow depth and average velocity (at 0.4 depth) at 10-15 locations within a channel cross section (Dunne and Leopold, 1978).

During individual storm events, the energy gradient and surface velocity of the stream was measured at each site. The energy gradient was measured by placing flags level with the stream surface at one meter increments into the bank. Elevations of the flood stage water surface was surveyed using these flagged elevations.

During high flows, current meter velocities could not be obtained and surface velocities were measured by timing the travel of floating particles over a set distance. These surface velocities were made for 3-4 locations in the channel cross section at bank and mid channel locations. Average velocity was taken to be 0.8 of the surface velocity. These measurements were combined with channel cross section of the flow to determine high flow discharge values.

4.3.4 Data Analysis

Discharge rating curves were developed for the three UMD sites using a combination of theory and empirical field data. Von Karman's boundary layer equation has been modified with empirical observations to determine the relationship

between flow resistance u/u* (u* = $(gRS)^{0.5}$) and relative depth (d/D84) to estimate velocity for gravel-bed streams (Leopold and Wolman, 1957)::

$$\frac{u}{u*} = 2.8 + 5.75 \times \log\left(\frac{d}{D_{84}}\right) \quad (44)$$

where u is the average cross sectional velocity (m/s) and d is average depth or hydraulic radius (m). This equation solves for the average flow velocity of the stream at a given average depth. At gauged sites, the relationship between average channel depth and cross sectional area is determined from the measured cross-section. Therefore, we can solve for discharge (m^3/s) using Q = VA.

Through the duration of recorded storm events, every MS5 and USGS gauge data point was used to calculate shear velocity (u*). The calculation used gauge height data taken and water surface gradient values that were derived from field data for multiple storm events at each gauged site. The gradients used for each site are as follows: Greencastle Road 0.0063, Upstream Cherry Hill 0.0055, Downstream Cherry Hill 0.007, and Northeast Branch 0.0016. These gradient values are representative of flows at bankfull stage to moderate flow levels. To ensure the accuracy of the gauge height data taken from the MS5 gauges, manually-read staff gauges were placed in the channels and the channel depth periodically recorded during high flows. The staff gauge data was then compared against the MS5 data and the latter was found to be accurate to $\pm$ 0.5 cm.

4.4 Results

4.4.1 Rating curves and discharge estimation

Field measurements of discharge were combined with model values of discharge derived using a flow resistance equation and field data gauge height, average flow depth, grain size and gradient. Results of these measurements and estimations generated rating curves for each of the gauged sites (figs. 36-38).

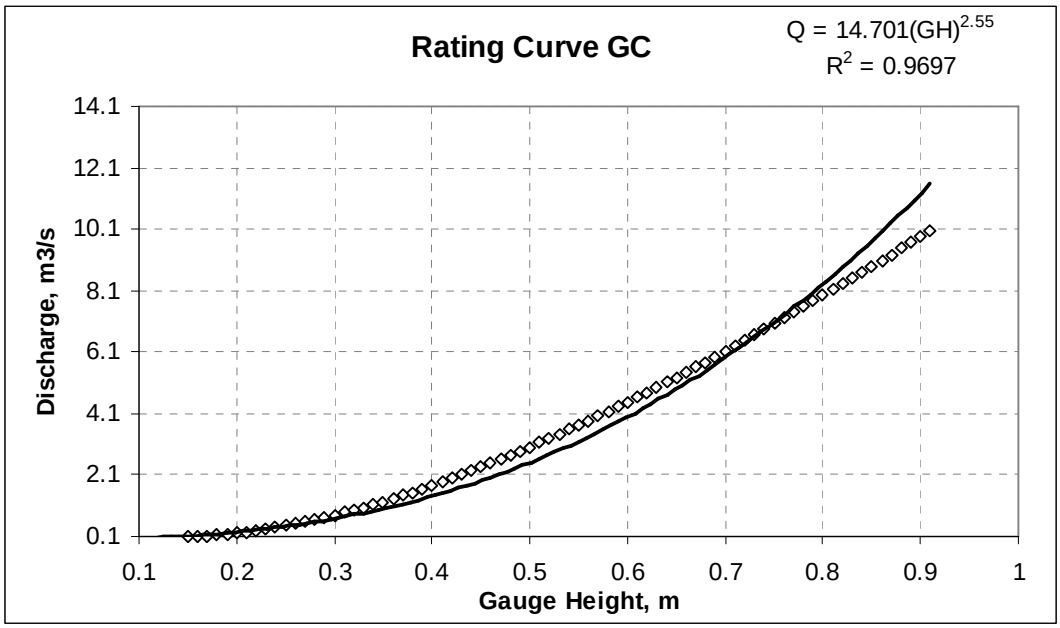

Figure 36. Rating curve for GC. Field-calibrated empirical curve shown in open circle, rating curve relationship shown in black.

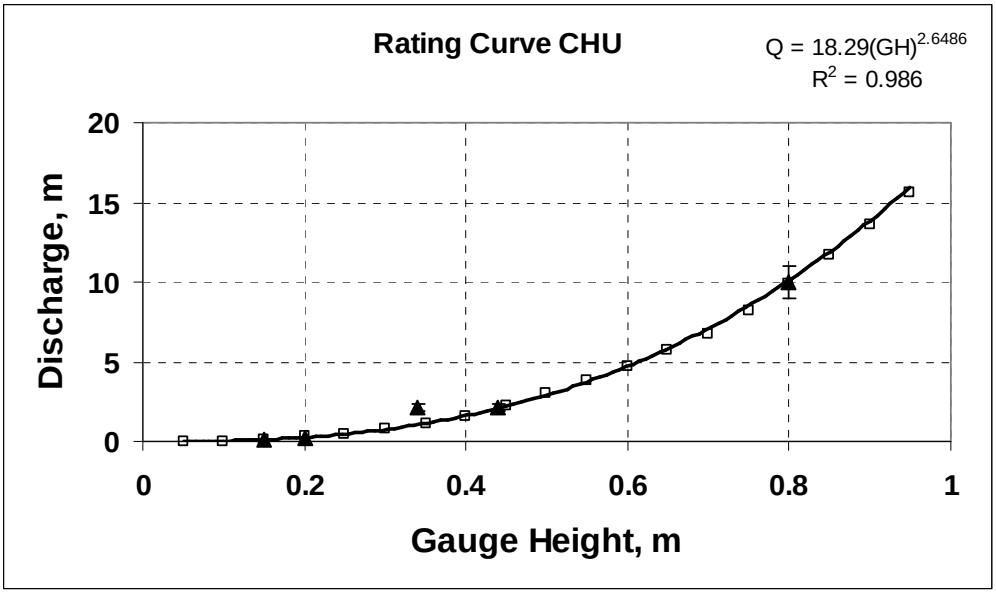

Figure 37. Rating curve for CHU. Field measurements of discharge are shown in triangles, discharge calculated from field data and an empirical velocity formula are shown in open squares, and the solid line shows the rating curve relationship given above.

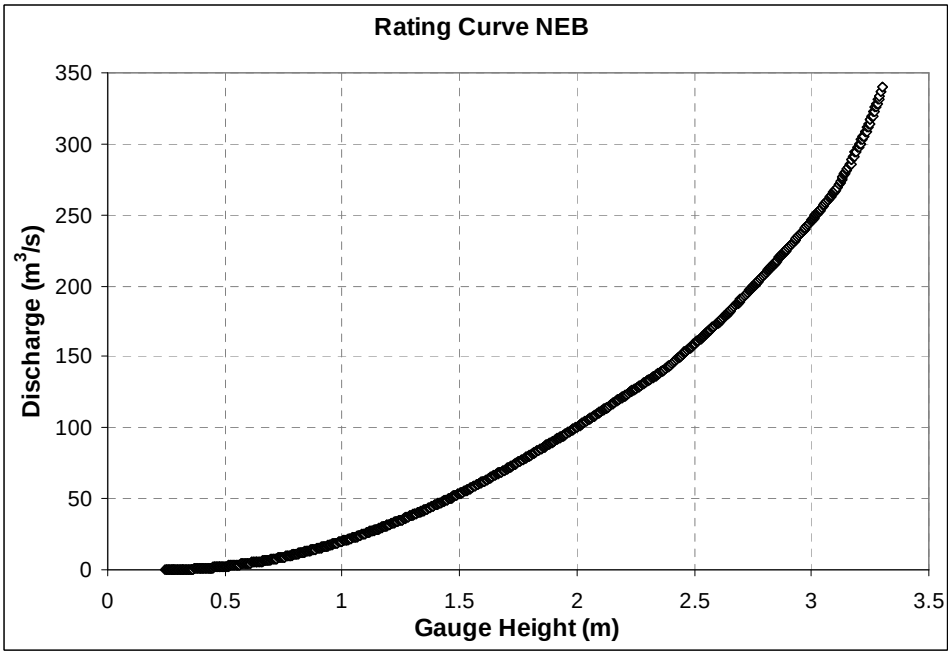

Figure 38. Rating curve for NEB, from USGS.

4.4.2 Storm Hydrographs and Runoff Production

Storm Hydrographs

The rating curves for each gauge can be used to create storm hydrographs for each gauge sites. Storm hydrograph data is then used to determine total volume of runoff from each site. Precipitation data from a weather station in College Park, were used to determine lag times (time interval between peaks or centroids of rainfall and runoff). The NE Branch watershed is large enough that some storm events do not affect the entire basin. Storm response can vary due to both the temporal intensity and spatial size of individual storm events. In natural humid temperate watersheds, the lag between peak storm precipitation and peak stream discharge is fairly long--from hours to days --because most runoff takes subsurface flow paths to the stream (Dunne and Leopold, 1978). Urbanization shortens lag times. This is evident in comparisons of the lag times for the Greencastle, Cherry Hill, and Northeast Branch gauges.

Storm hydrographs for NEB and Cherry Hill show synchroneity of peak runoff for some storm events. The storm that hit the Washington, D.C. metropolitan area on April 20th, 2009 produced hydrographs with similar response timing for both sites. Fig. 39 shows the storm hydrographs of the CHU and NEB gauges, as well as the rainfall rate and cumulative rainfall over time. During this storm, the peak precipitation rate was 0.23 inches per hour and the total rainfall was 1.13 inches. The lag time between the peak discharge at CHU and NEB was only fifteen minutes, but the travel time between these two stations should be about 90 minutes for the measured velocity values. This suggests that either rain began in the lower watershed

first or that rapid flow to the stream from the heavily urbanized lower portions of the NE branch watershed generated much of the NEB hydrograph peak (or a combination of these processes).

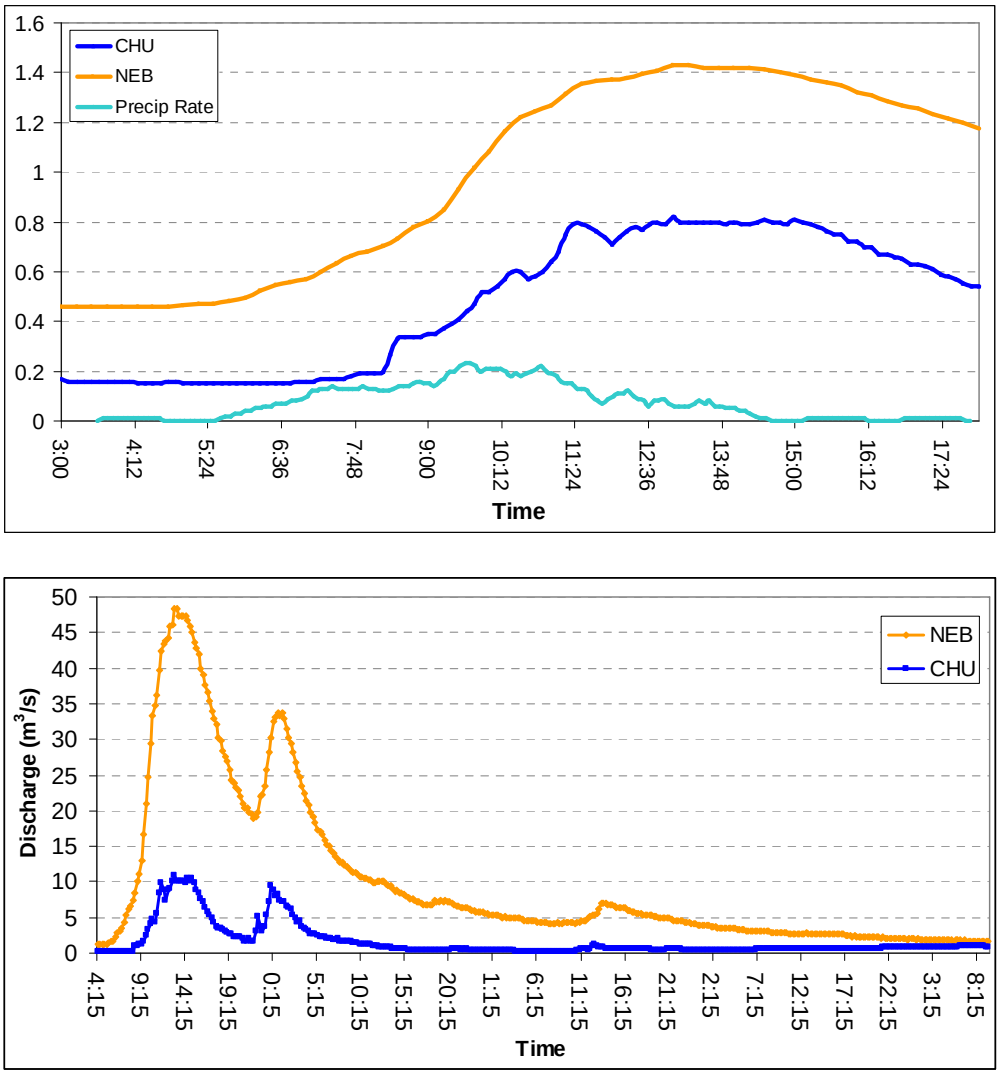

Figure 39 a) Initial gauge height (m) and hyetograph (in/hr) for the. April 20th Storm . b) Discharge hydrographs for the same storm; Orange is Northeast Branch discharge (m^3/s), Blue isCherry Hill discharge (m^3/s) note the synchroneity of the discharge peak

Similar synchroneity of peaks was observed between the Greencastle gauge and the Cherry Hill gauge during another similar storm on March 28th, 2009, seen in fig. 40. In this case, the upstream GC gauged peaked 15 minutes after the CHU gauge. This may have been due to the spatial distribution of storm rainfall. This storm event was similar in intensity to the April 20th storm, with a peak precipitation rate of 0.24 inches per hour and a total rainfall of 1.04 inches. The synchroneity of GC and CHU runoff peaks suggests that the storm hit the northern locations prior to the southern locations. For this storm, the NEB site experienced a longer hydrograph peak than the CHU site during this storm. Lag time between CHU and NEB peaks was 45 minutes lag in peak discharge between the sites.

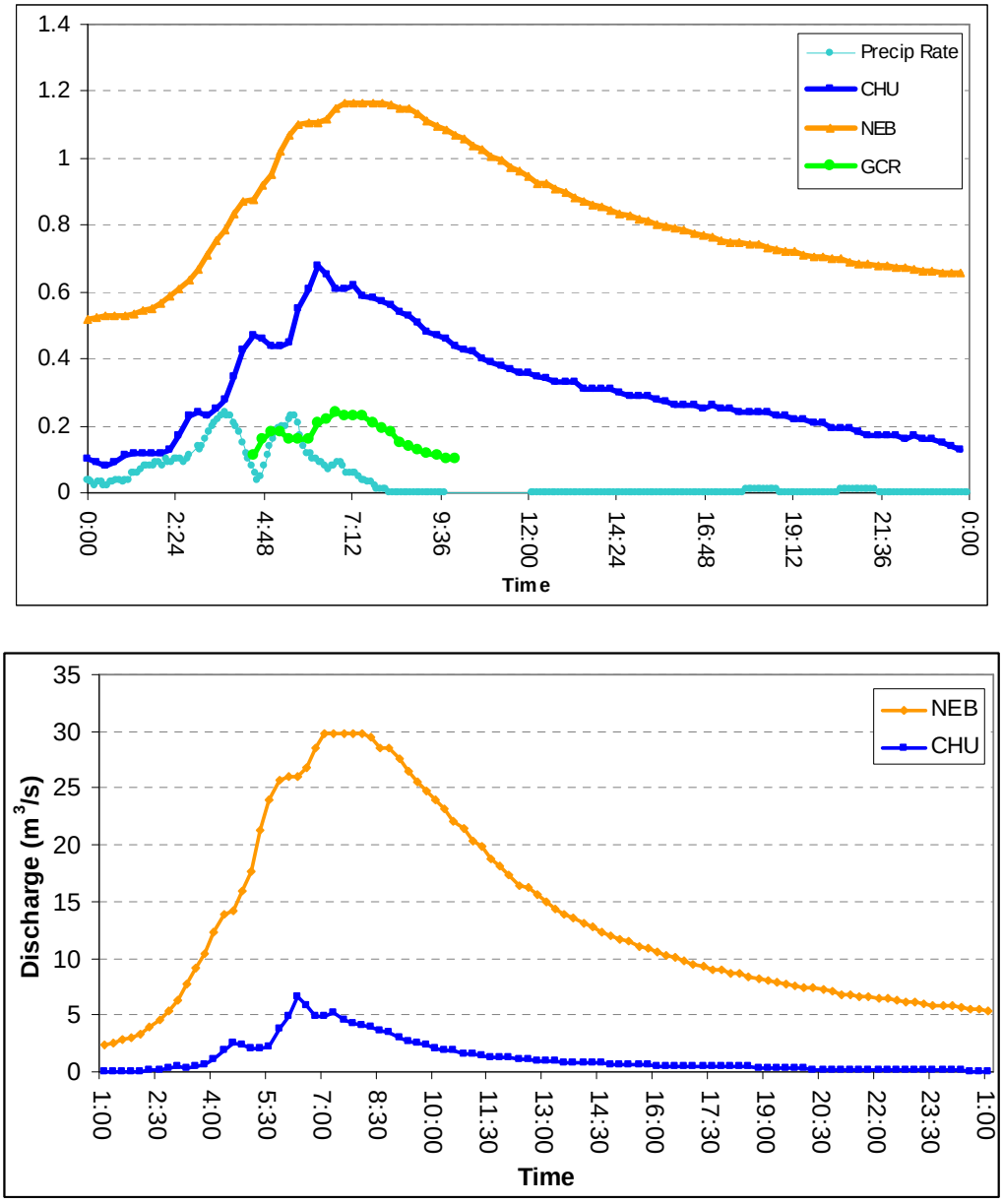

Figure 40. a) March 28th Storm Hydrograph. Orange is Northeast Branch gauge height (m), Blue is Upstream Cherry Hill gauge height (m), Light Blue is rainfall intensity (inches/hour). B) March 28th Storm Discharge Hydrograph. Orange is Northeast Branch discharge (m^3/s), Blue is Upstream Cherry Hill discharge (m^3/s).

The largest duration storm event measured was Tropical Storm Hannah (fig. 41), which produced intense rains in the area on September 6th, 2008. Total storm rainfall was 2.26 inches of rain, and for a period of time, the rainfall rate exceeded an inch (2.5 cm) per hour. Shortly after the peak rainfall intensity of the storm, the NEB site peaked in discharge about 30 minutes before the CHU site. These data suggest that the rapid transmittance of water from impervious surfaces and storm sewers in the lower watershed cause NEB to peak earlier than travel time from the upstream tributaries can allow.

Lag times between rainfall and runoff events can only be defined when the timing of the rainfall is well-known. The rain gauge location for the watershed is located in College Park, which is near the center of the watershed, but may not define the timing of storm events for localized storms. Therefore, rise time was used to determine hydrological response time at all locations. These data are shown in fig. 42 and they indicate that hydrograph rise time, the time from the start of precipitation to the peak discharge of the storm, is very similar for CHU and NEB and the rise times do not incorporate the travel times between the two sites. These data suggest that the initial peak of the hydrograph at the Northeast Branch gauge is generated by runoff from the local impervious surfaces, storm sewer systems, and channelized stream beds near the NEB gauge. Contributions from the upstream tributaries arrive at the downstream station later and contribute to the broad discharge peaks at the NEB gauge.

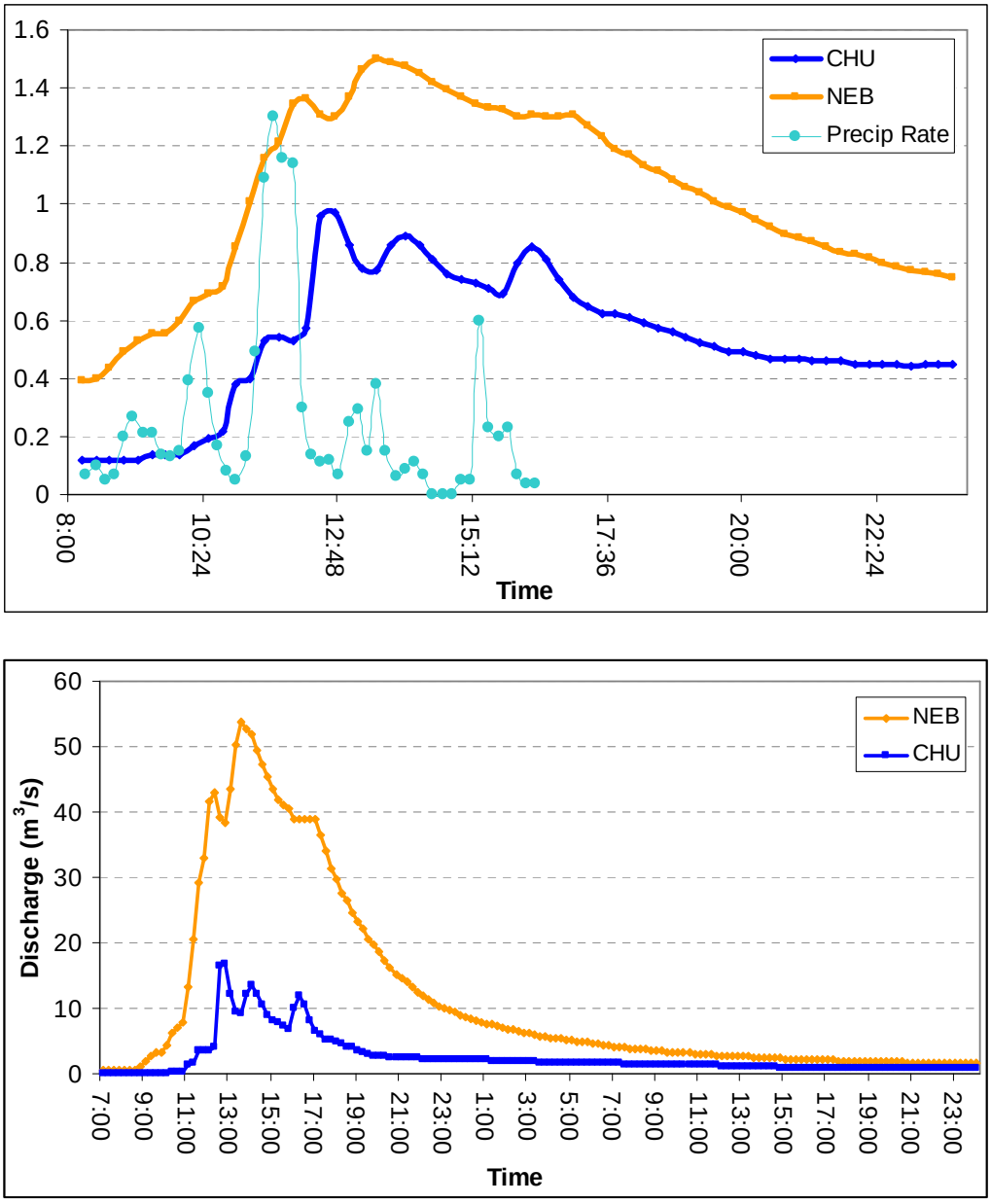

Figure 41 a) September 6 th Storm Hyetograph (in/hr) and gauge height, (m). B) Storm Discharge Hydrographs for Northeast Branch (orange) and Cherry Hill (blue).

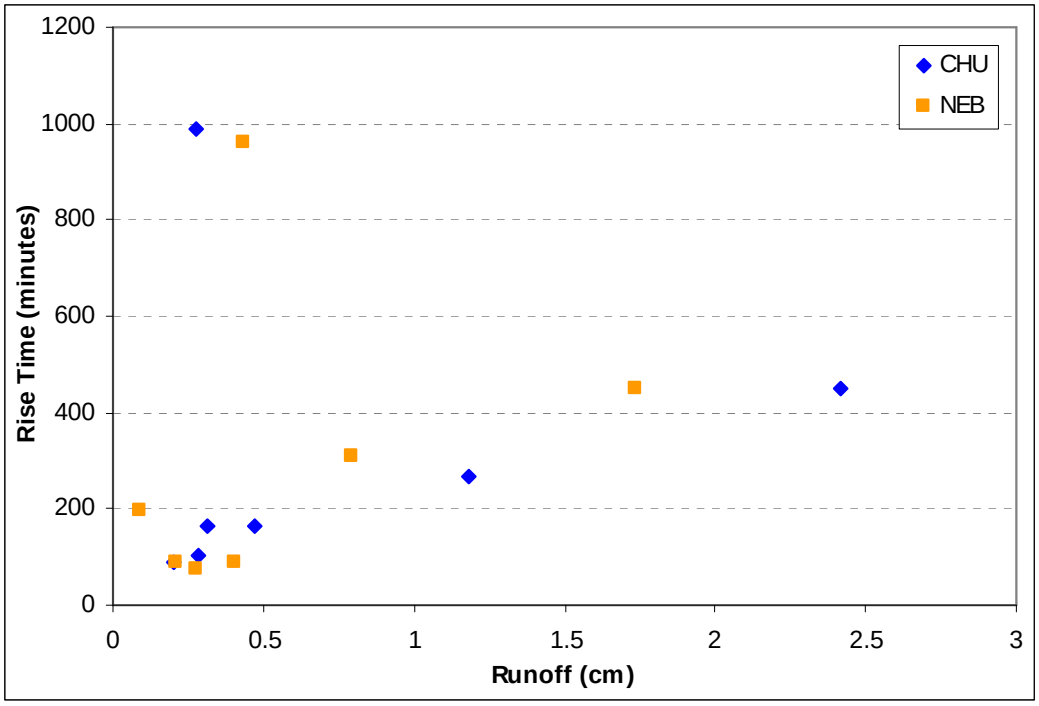

Figure 42. Hydrograph rise time for runoff events for both CHU and NEB. Runoff is calculated as total runoff volume divide by catchment area. Storm Rise Time v. Storm Runoff for CHU and NEB. Excluding the outliers, Rise Time increases with runoff volume and is similar for both sites.

Storm Rainfall-Runoff Relationships

Rainfall-runoff ratios are used to determine the amount of storm precipitation that immediately enters the stream system during a storm event. A high rainfall-runoff ratio can be caused by a precipitation event that wasn't absorbed into the ground due to intense rainfall, rapid transmittance of water to streams due to impervious surfaces and/or storm drains, or from a region's steep topography leading to nearby streams. To determine the total amount of storm runoff, streamflow hydrographs were used to obtain the total runoff volume at each gauged site. This can be done by calculating the total volume of water in a storm hydrograph and subtracting out the volume of the baseflow, the discharge that existed before the

storm event. This runoff volume was converted to a unit value of runoff by dividing total volume (m^3) by basin area (m^2. Stream runoff is the surface and groundwater that is delivered to the stream during a storm event. Table 10 summarizes the rainfall, runoff, runoff as a percent of the total storm volume, and rise time of seven storm events in the Anacostia River watershed that could be measured at both the CHU site and at the NEB gauge.

Table 10. Rainfall-runoff relationship data summary.

Storm	Rainfall (cm)	Site	Runoff (cm)	Ratio	Rise Time (minutes)
6/27/2008	1.45	CHU	0.20	0.14	90
		NEB	0.27	0.19	75
7/14/2008	1.65	CHU	0.47	0.28	165
		NEB	0.41	0.25	90
7/27/2008	2.29	CHU	0.28	0.12	105
		NEB	0.21	0.09	90
9/6/2008	5.74	CHU	1.18	0.20	265
		NEB	0.79	0.14	310
10/1/2008	1.12	CHU	0.32	0.29	165
		NEB	0.09	0.08	195
4/20/2009	2.87	CHU	2.42	0.84	450
		NEB	1.74	0.61	450
6/5/2009	1.80	CHU	0.28	0.15	990
		NEB	0.43	0.24	960

The relationship between runoff and rainfall is shown in fig. 43 and the ratio is given in Table 10. These data indicate that the runoff ratio for Little Paint Branch Creek (CHU) is 0.20 ± 0.07; that stream runoff is about 20% of storm precipitation. The amount of runoff generated from the entire NEB watershed is very similar; the average runoff ratio is 0.17 ± 0.07. This suggests that stream runoff is about 17% of precipitation. The difference in runoff ratios may be due to rainfall measurement accuracy over the basin. The April 20th storm generated unusually high runoff values at both locations. This storm event occurred after a series of large storms, which

generated very high antecendent moisture conditions. During this storm event, runoff was generated from lawns and other grassed surfaces in addition to streets and impervious surfaces. For this event, runoff ratio was 0.84 for CHU and 0.61 for NEB.

The significance of runoff is not only its volume, but also what the runoff carries. The studies by Allmendinger et al. (2007) and Pizzuto et al. (2000) suggested that a sizeable portion of the sediment budget in the urban streams that they studied was due to the erosion of upland areas in their respective watersheds. In the NEB watershed, the timing of runoff and erosion can be used to identify potential sources of sediment to the stream channel.

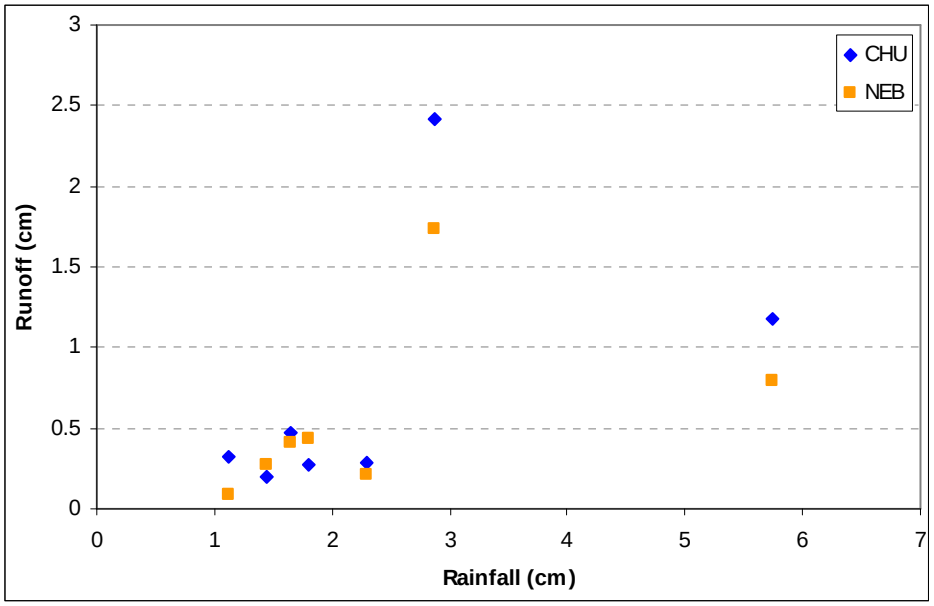

Figure 43. Storm Runoff v. Storm Rainfall at CHU and NEB. The average runoff ratio for CHU is 0.20 and the average runoff ratio for NEB is 0.17. The 4/20/09 storm generated much higher runoff.

Precipitation is a point measurement and it is therefore hard to determine accurately for large watersheds. Therefore, the runoff volumes for NEB and its tributary Little Paint Branch Creek were directly compared. The relationship between runoff at CHU and NEB is illustrated in fig. 44. It indicates that the total runoff volume for NEB gauge is about 72% of the runoff volume for CHU for all of the measured storm events.

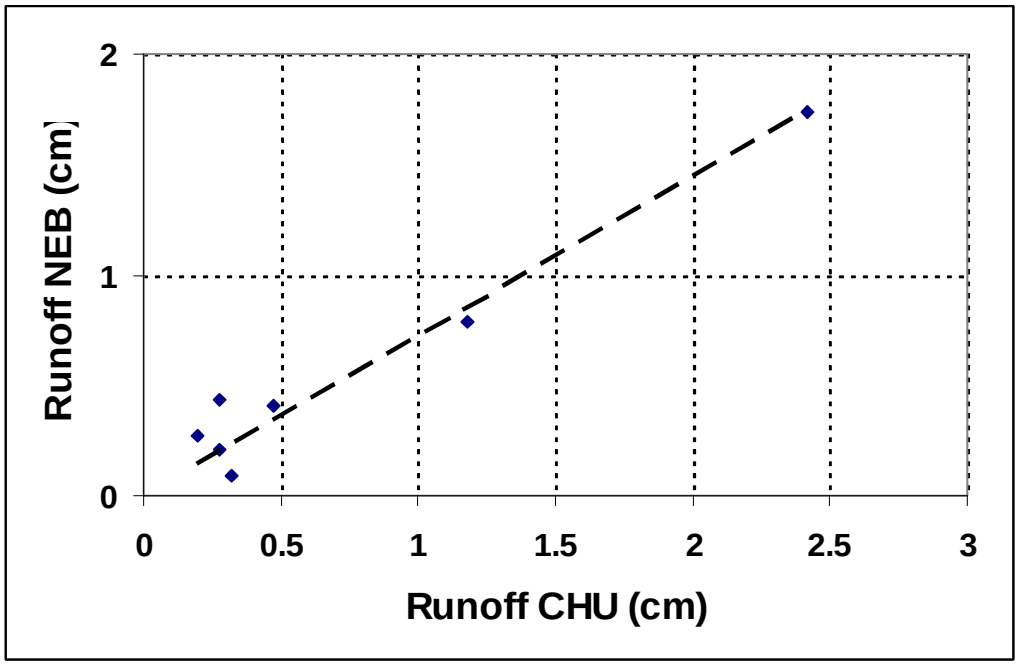

Figure 44. Relationship between storm runoff (cm) at CHU and NEB
$R_{NEB} = 0.72 (R_{CHU})$; R^2 value = 0.95.

4.4.3 Watershed Scale Turbidity

Watershed scale variations in turbidity

Continuous measurements of storm turbidity were used to examine the distribution of turbidity with time during a storm event. The previous examination of

the timing of runoff illustrated that proportionally more runoff was generated from the Little Paint Branch Tributary than the watershed as a whole, but that the timing of runoff at the NEB gauge illustrated that a significant runoff response was generated from the lower portions of the watershed. Similar procedures can be used to examine the timing of peak turbidity and total turbidity volumes at each of the gauge locations.

Turbidity measurements for all four gauged sites are shown in fig. 45. For these two storms, the Greencastle Road site had very different turbidity values when compared to the other sites. This may be due to localized storm intensity in this small watershed or variations in sources of sediment during storms. In general, turbidity data are the flashiest for the GC and the Cherry Hill Sites. NEB often shows an early turbidity flux that is probably associated with the early runoff from urban sites in the lower watershed. The total turbidity fluxes for all four sites in Table 11 and they indicate that the basin outlet, NEB, consistently has the largest turbidity flux.

Table 11. Comparison of Turbidity data for 4 stations

Storm	Site	Turbidity Flux	Avg.Turb.
12/19/2008	GCR	2541.7	8.92
	CHU	2991.1	9.44
	CHD	4351.1	13.73
	NEB	7540	23.79
1/28/2009	GCR	839.8	8.75
	CHU	3708.7	38.63
	CHD	2783.8	28.99
	NEB	4116	42.88
3/27/2009	GCR	13500.5	87.67
	CHU	11903.6	77.3
	CHD	13857.5	89.98
	NEB	17873	116.06

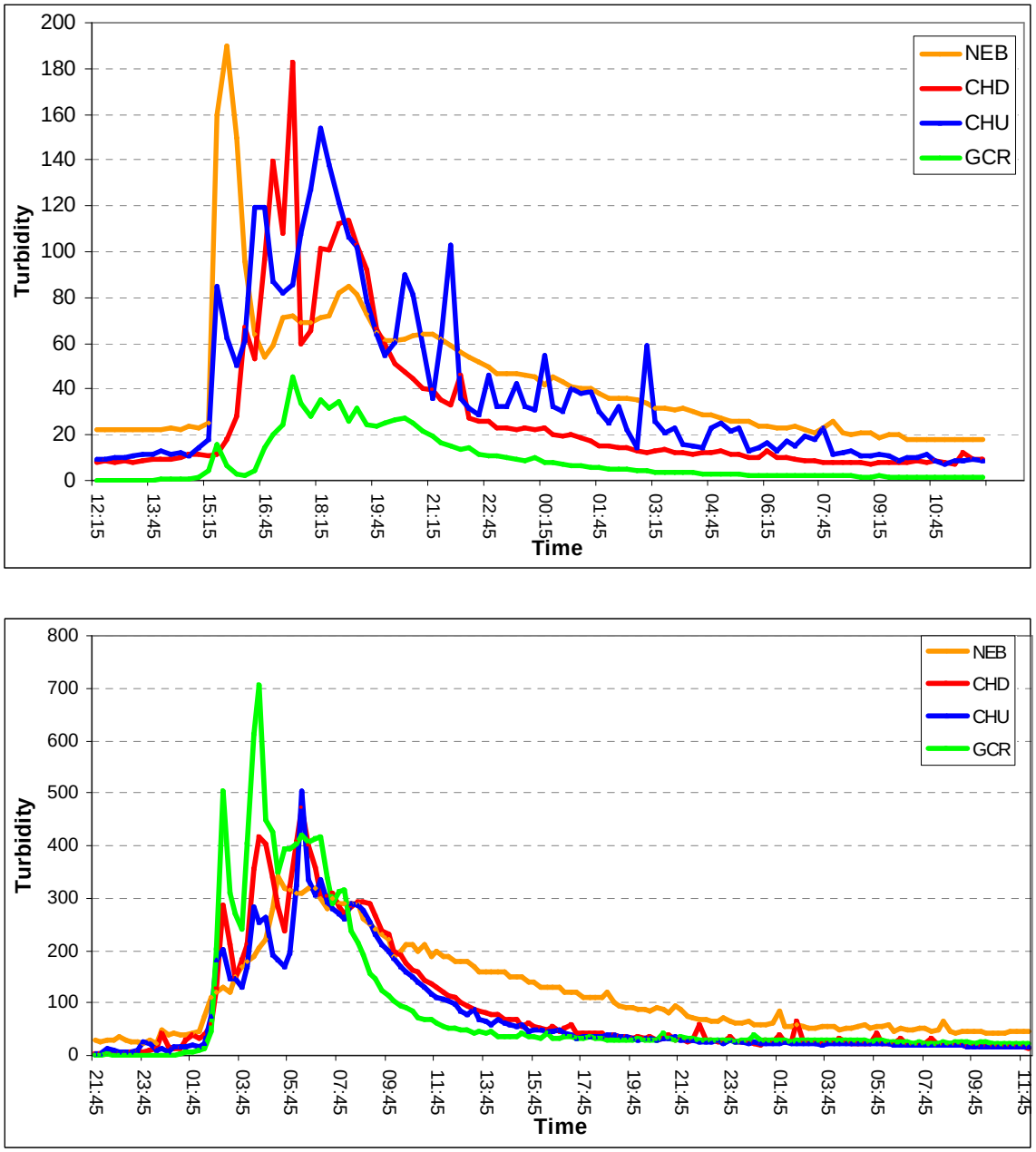

Figure 45. Turbidity at all gauges: A) 1/28/09 Storm. Total Rain: 0.38 inches. Average Rainfall Rate: 0.061 inches/hour. Turbidity Totals: GCR 839.8, CHU 3708.7, CHD 2783.8, NEB 4116 B) 3/28/09 Storm. Total Rain: 1.04 inches. Average Rainfall Rate: 0.088 inches/hour. Turbidity Totals: GCR 13500.5, CHU 11903.6, CHD 13857.5, NEB 17873

A comparison of the Cherry Hill and the NEB gauges is shown in fig. 36. The NEB gauge often has two turbidity peaks: a brief, short peak, that is associated with the heavily urbanized lower watershed that delivers water rapidly to the gauge and a broad peak, which is associated with tributary inputs. The two Cherry Hill gauges show very similar turbidity curves, with slightly higher peaks associated with the downstream gauge. Sources of sediment between these two gauges is limited to bank and bed erosion; there are no tributary or storm sewer inputs between the two sites. This suggests that bank erosion in the bar complex reach does provide an additional input of sediment.

Peak and total turbidity data at the two Cherry Hill Gauges and NEB for seven storms is summarized in Table 12. The total turbidity values indicate that the total flux of sediment is greater at the downstream NEB site. Peak turbidity values are often similar for both sites, with an average of 336 NTU for the CHU site and 290 FNU for NEB. This is significant because of the much greater stream power available at the NEB site to move sediment in comparison with the CHU site. Despite smaller shear stresses during storms, higher turbidity values are recorded at CHU than at NEB. This is probably due to a variety of causes. High turbidity values are likely associated with bank erosion in the Little Paint Branch drainage area, while bank protection in much of the lower watershed limits bank erosion processes. In addition, although the initial runoff from urbanized areas generates a turbidity peak, the contributed runoff also dilutes sediment concentrations.

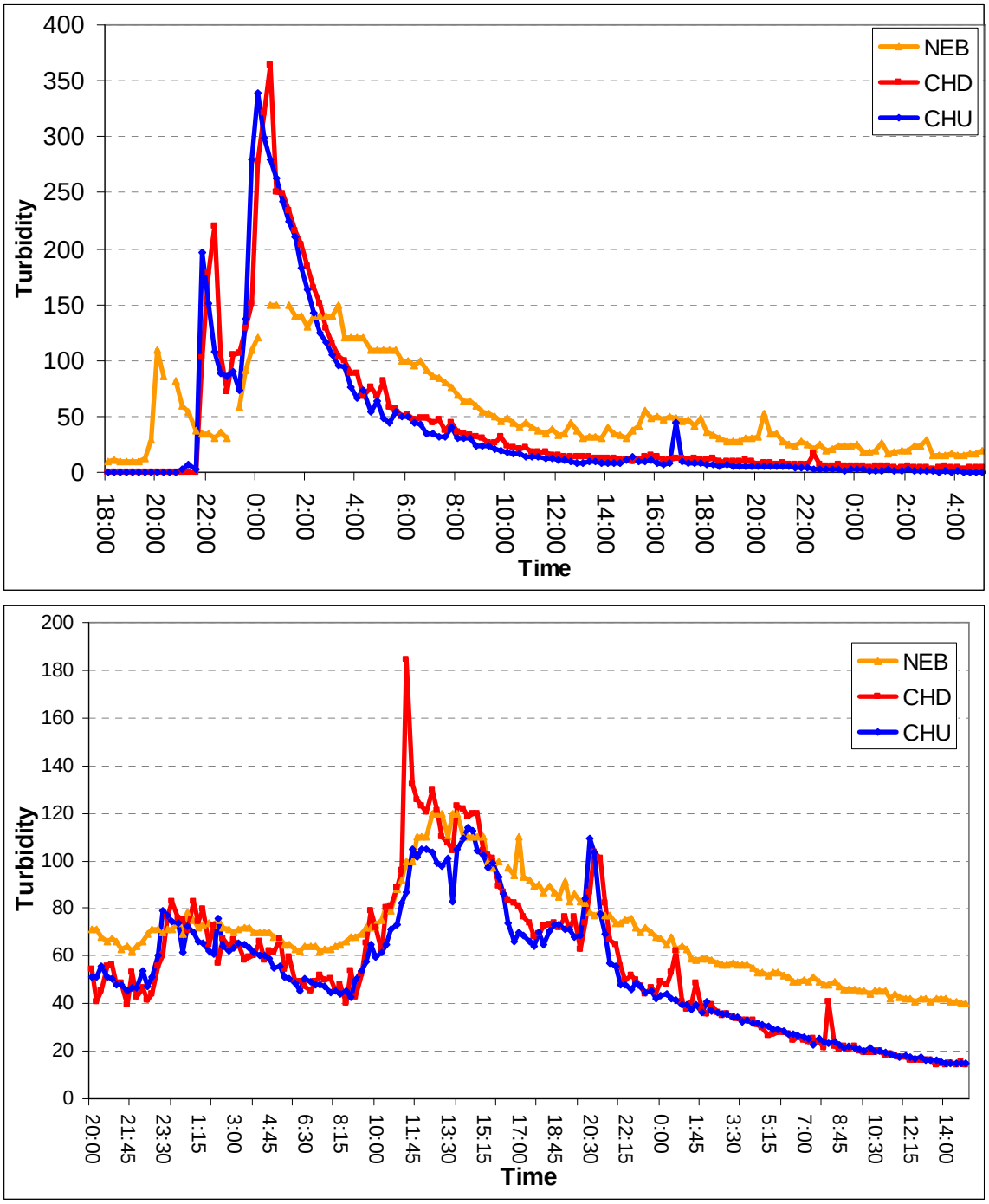

Figure 46. Comparison of Storm Turbidity Curves for the Cherry Hill and NEB sites. A) 10/1/08 Storm Turbidity Curve. B) 6/5/09 Storm Turbidity Curve

Table 12. Turbidity for NEB and CHU sites

Storm	Site	Peak Discharge (m^3/s)	Peak Turbidity	Total Turbidity
6/27/2008	CHU	6.3	514	6867.9
	NEB	45.3	460	11362
7/14/2008	CHU	3.6	180.5	2595.9
	NEB	19.3	180	8731.7
7/27/2008	CHU	10.1	270.5	3296.3
	NEB	16.9	340	9793.7
9/6/2008	CHU	16.9	386.2	6787.7
	NEB	53.8	370	11390
10/1/2008	CHU	5.38	364	5311.3
	NEB	10.1	150	5797
4/20/2009	CHU	10.8	520	23356.2
	NEB	48.4	410	29859.7
6/5/2009	CHU	5.38	113.7	7721
	NEB	33.4	120	9248

The relationships between turbidity and discharge for the Cherry Hill and NEB gauges are shown in fig. 47. The diagram of total turbidity versus discharge indicates that although discharge values are much higher for the downstream end of the reach, that total turbidity values are similar for both NEB and CHU. The tributary CHU has higher peak turbidity than NEB, this suggests either storage of sediment within the system and dilution of sediment concentrations.

.

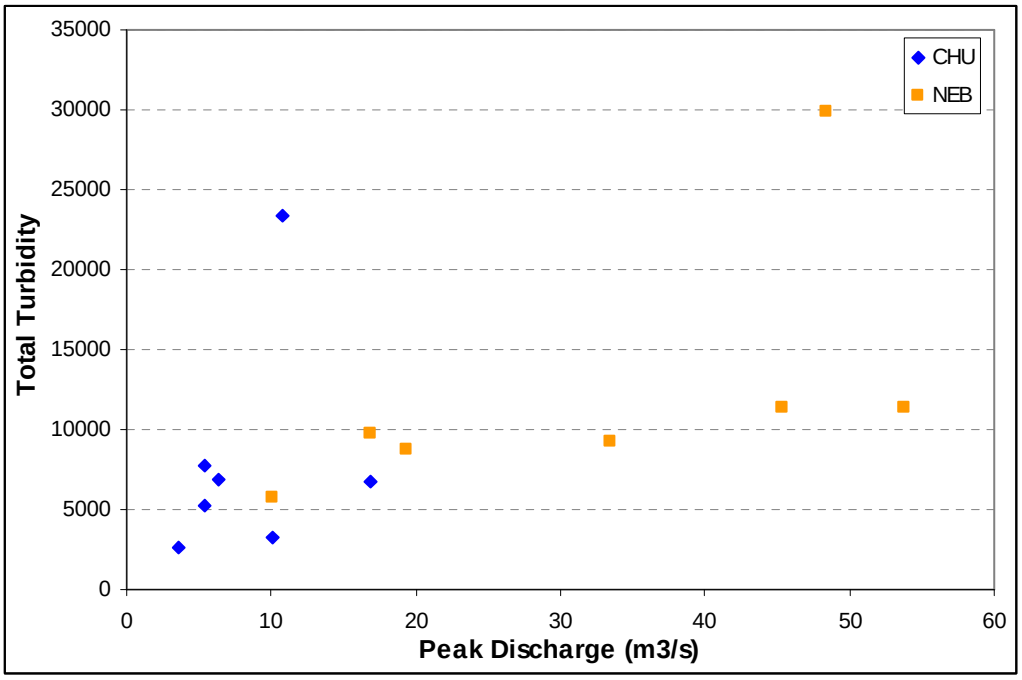

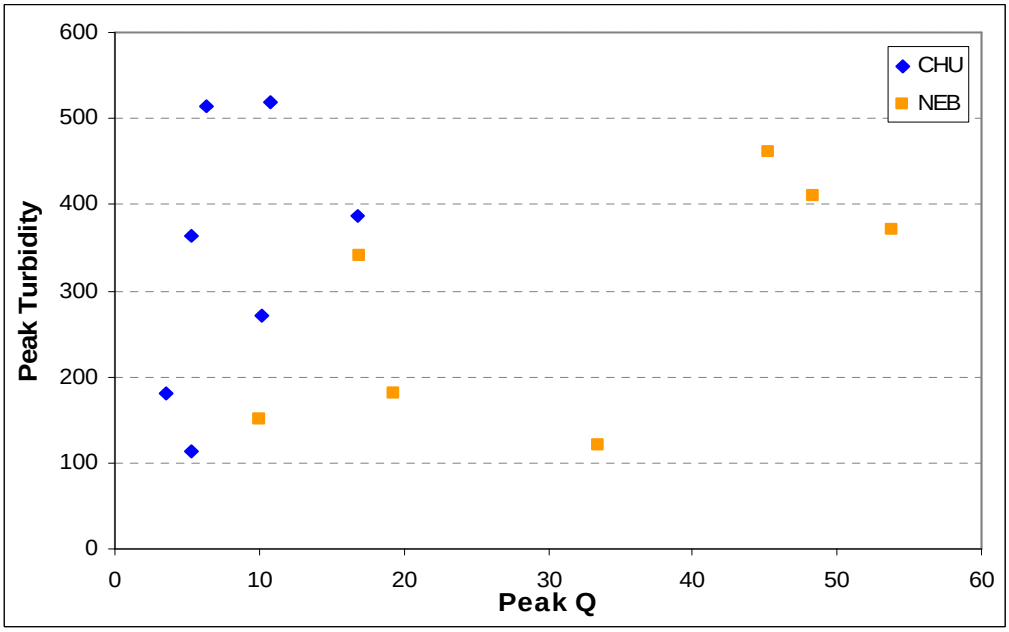

Figure 47 a) Total Storm Turbidity v. Peak Discharge at CHU and NEB and b)

Peak Storm Turbidity v. Peak Storm Discharge at CHU and NEB.

4.4.4 Bar Complex Turbidity

Gauges were placed up and downstream of the Cherry Hill Bar Complex to examine whether bank erosion in the gravel bar reach resulted in a significant input in turbidity.

Storm Turbidity Curves

Comparison of storm turbidity curves measured at the upstream and downstream Cherry Hill sites indicates that CHD generally has a larger turbidity flux and a slight delay in peak turbidity. Turbidity Curves for a variety of storms are shown in fig. 46 and fig. 48. Most of the data indicate that the CHD gauge consistently peaking later and at a higher NTU than the CHU gauge.

In addition to showing increased peak turbidities downstream of the bar complex, the gauges have shown evidence of mass failures of the banks after major storms such as the one between June 27th and 30th, 2008 (fig. 49). Over a period of a couple days after the storm the turbidity readings of the downstream gauge started peaking in comparison with the upstream gauge. As seen on the turbidity curve, this phenomenon occurred no less than three times with increasing intensity. Banks weakened by the bank erosion of major storms are likely to succumb more easily to the increased pore water pressure caused by subsurface flow during and after storms.

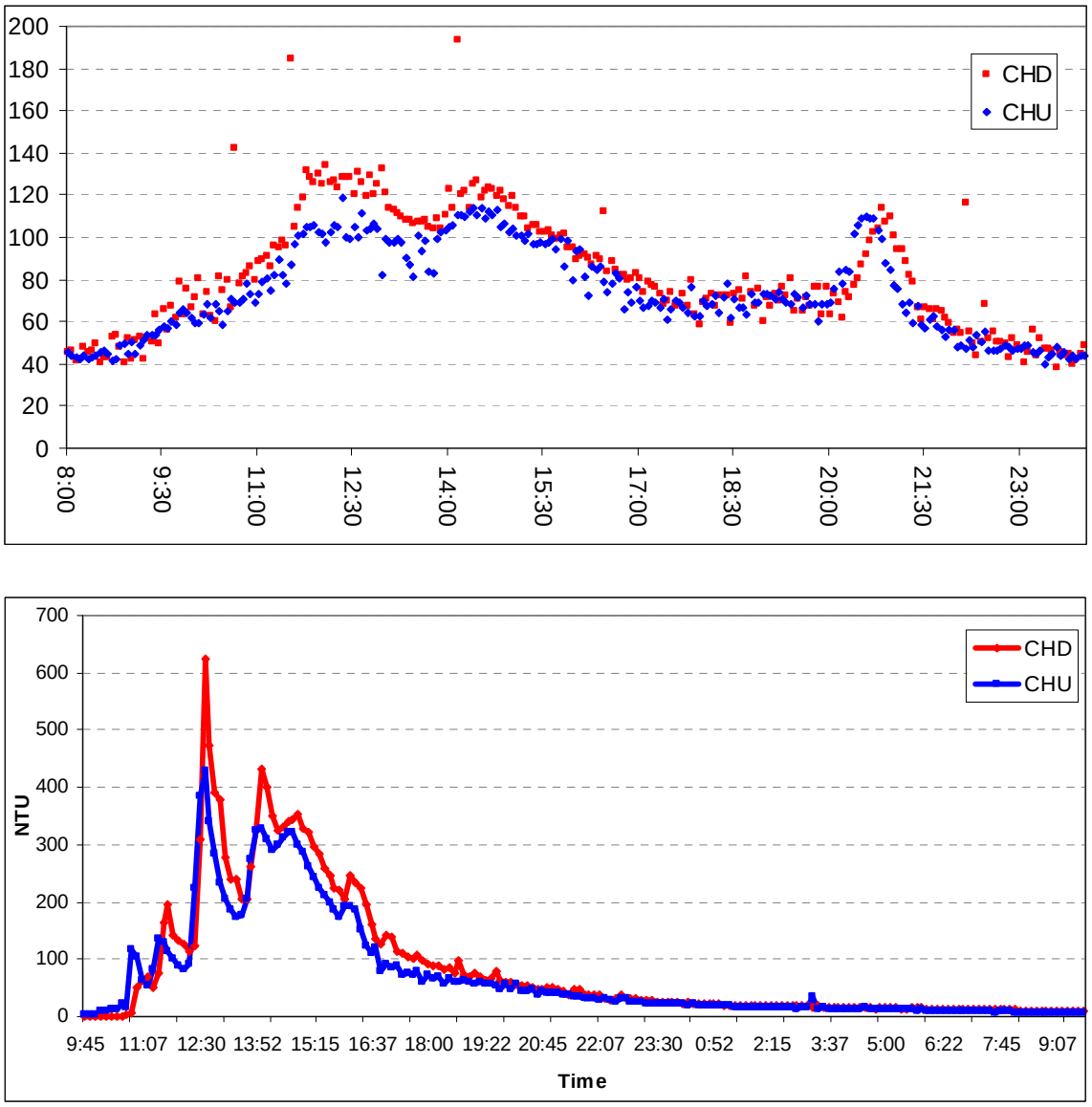

Figure 48 a) 6/5/09 Storm Turbidity Curve: CHU and CHD; b) 9/6/08 Storm Turbidity Curve: CHU and CHD

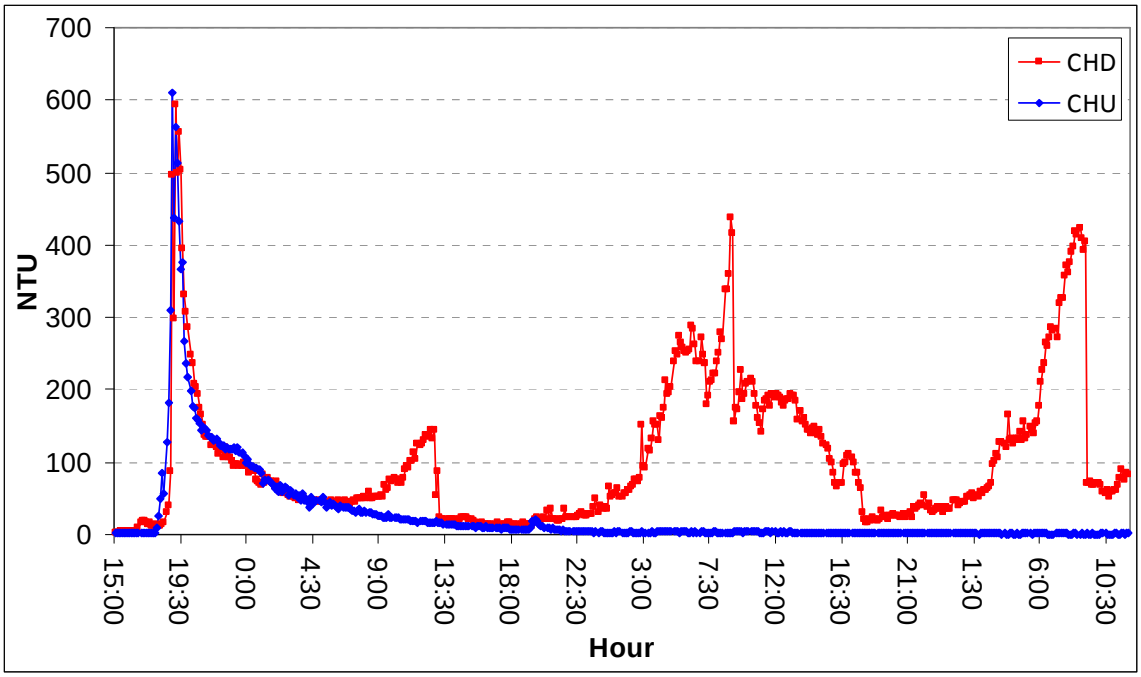

Figure 49. Turbidity measurements showing probable mass failures after 6/27-6/30/08 Storm

A gauge was temporarily placed downstream of the first bar in the bar complex in order to evaluate turbidity changes upstream and downstream of the bar. The data showed that in two out of three storms the overall turbidity flux decreased between CHU and the gauge downstream of the gravel bar, titled CHGB (see fig. 50). This effect may have been caused by the positioning in the channel, but it also suggests single bankfull gravel bars can attenuate fine sediment during storm events. When in place, CHU and CHGB appeared to experience different peak timings, but shared a similar overall shape of the turbidity curve.

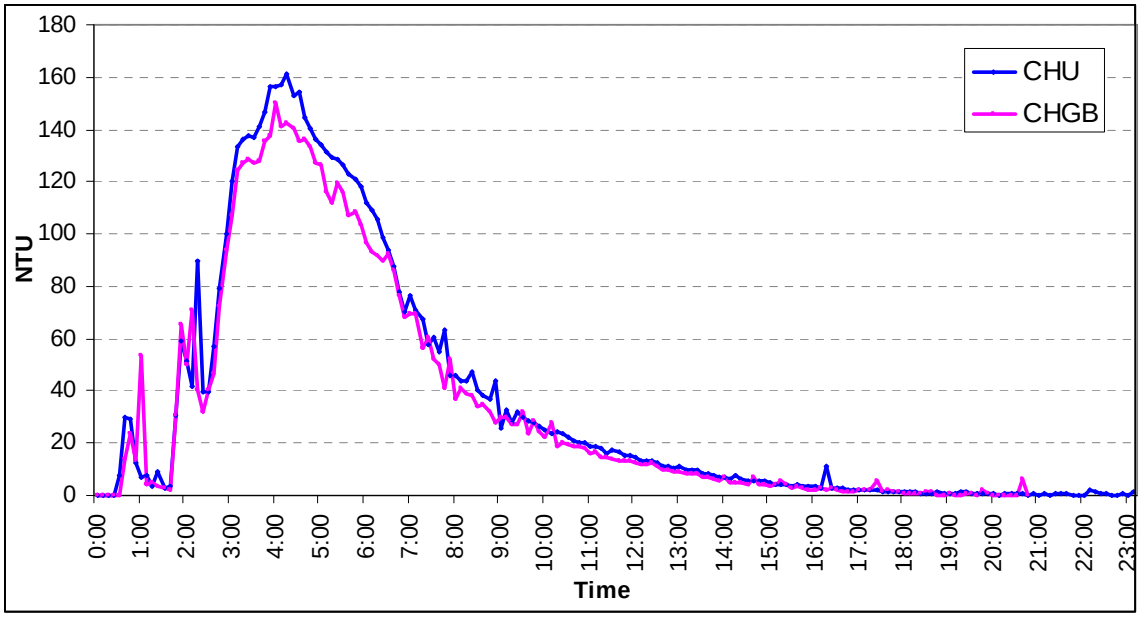

Figure 50. Turbidity curves upstream and downstream of a single gravel bars; 9/10/2008 Storm. Total NTU: CHU 6477.6, CHGB 5891

Turbidity Fluxes, Lag Times, and Peaks within the Bar Complex

Table 13 shows the turbidity fluxes and peaks between CHU and CHD. Of the nine storms analyzed, the net flux of CHU exceeded CHD only once. On average, the measured turbidity at CHU is ninety percent of that measured at CHD (see fig. 51). The magnitude of the peak turbidity measurements appear to correlate with the peak gauge height for each storm, as does the peak turbidity delay. This may be caused by the increase in stream velocity with increased depth and discharge. The size of the turbidity flux was directly proportional to the length and intensity of the particular storm events.

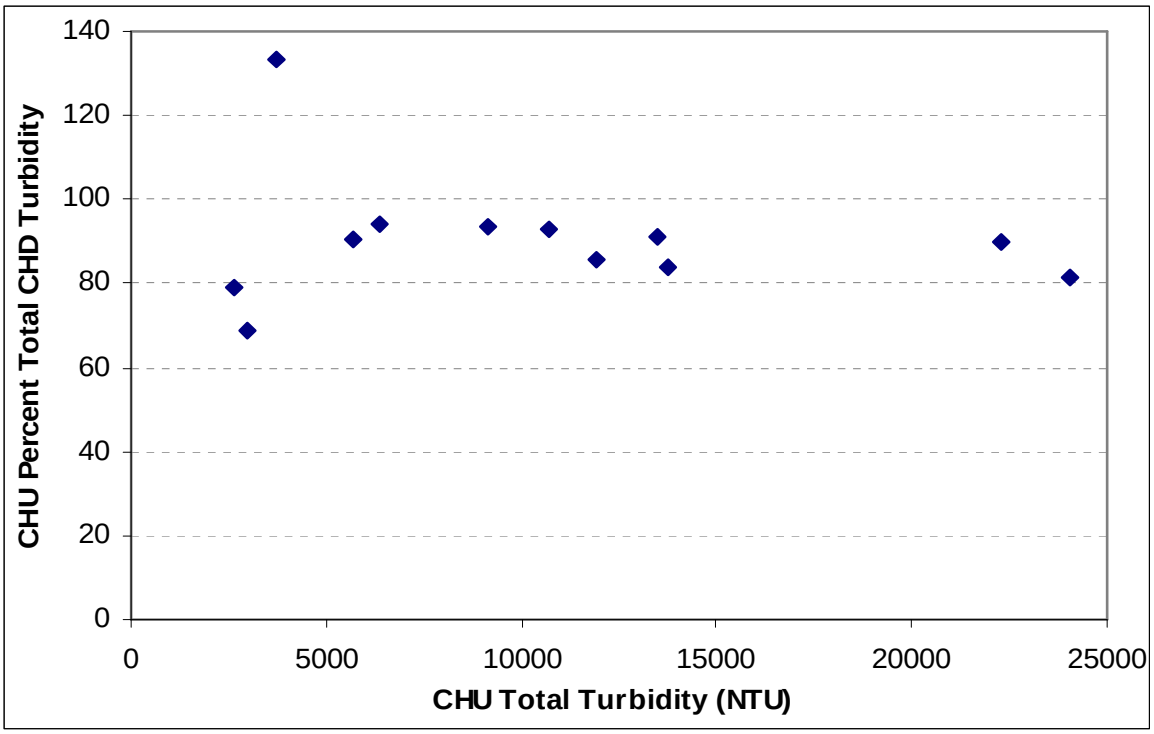

Figure 51. CHU Total Storm Turbidity as a percentage of CHD total storm turbidity. On average CHU's total turbidity is about 90% of CHD's.

The timing of peak turbidity varied with storm events, and at times was indistinguishable at the 7.5 minute gauging interval. Therefore, the gauging interval was decreased to 3:45 minutes to determine the travel time of turbidity though the system. For the June 5th Storm (see fig. 48) the peak turbidity delay could not be determined. This was because of how scattered the turbidity data points were between gauging intervals. Unfortunately it is not known at this time if that scattering was a product of the individual storm, or just something more easily observed with the smaller gauging interval of 3:45 compared with 7:30.

During the flow recession of a couple of the storms, "slugs" of turbidity flowed through the bar complex. The slugs were completely foreign to the system

and probably originated as a bank failure upstream or other point source further upstream. The instance where these were observed in the data allowed for it to be determined if the bar complex attenuates fine sediment after storms.

Table 13 Turbidity flux data for CHU and CHD.

Storm	Site	Average Turbidity	Peak Turbidity	Peak Turbidity Delay	Peak Gauge Height (m)	Turbidity Flux	Net Flux
	CHU	26.67	180.5		0.54	4721.3	
7/14/2008	CHD	31.70	154.7	7:30	0.44	5610.9	889.6
	CHU	60.44	304.8		0.81	6346	
7/27/2008	CHD	64.35	364.8	7:30	0.70	6756.8	410.8
	CHU	71.27	430		1.00	13754.8	
9/6/2008	CHD	85.14	623	0	0.86	16432.7	2677.9
	CHU	33.62	161.4		0.61	6488	
9/10/2008	CHD	31.48	130.6	15:00	0.47	6076	-412
	CHU	74.94	334		0.74	24055.1	
12/11/2008	CHD	91.98	537	7:30	0.70	29526.2	5471.1
	CHU	70.85	505		0.68	24947.6	
3/27/2009	CHD	81.30	480	7:30	0.50	28049.2	3101.6
	CHU	153.17	656		0.64	19605.3	
4/3/2009	CHD	169.77	1062	7:30	0.52	21730.3	2125
	CHU	96.49	525		0.82	37150.4	
4/20/2009	CHD	107.57	546	0	0.68	41415	4264.6
6/5/2009	CHU	74.68	118.4	NA	0.63	19193	2031.8

During the recession of a storm event on July 27th, 2008 a pair of distinctive bumps can be seen on the storm turbidity curve. Fig. 52 shows the slug of sediment in greater detail. The overall shape of the slug changes from trapezoidal upstream to a bell curve downstream. Between the two sites, a total of 10 NTU was reduced in the total flux, which cannot be regarded as significant due to potential gauging error and the small number of data points.

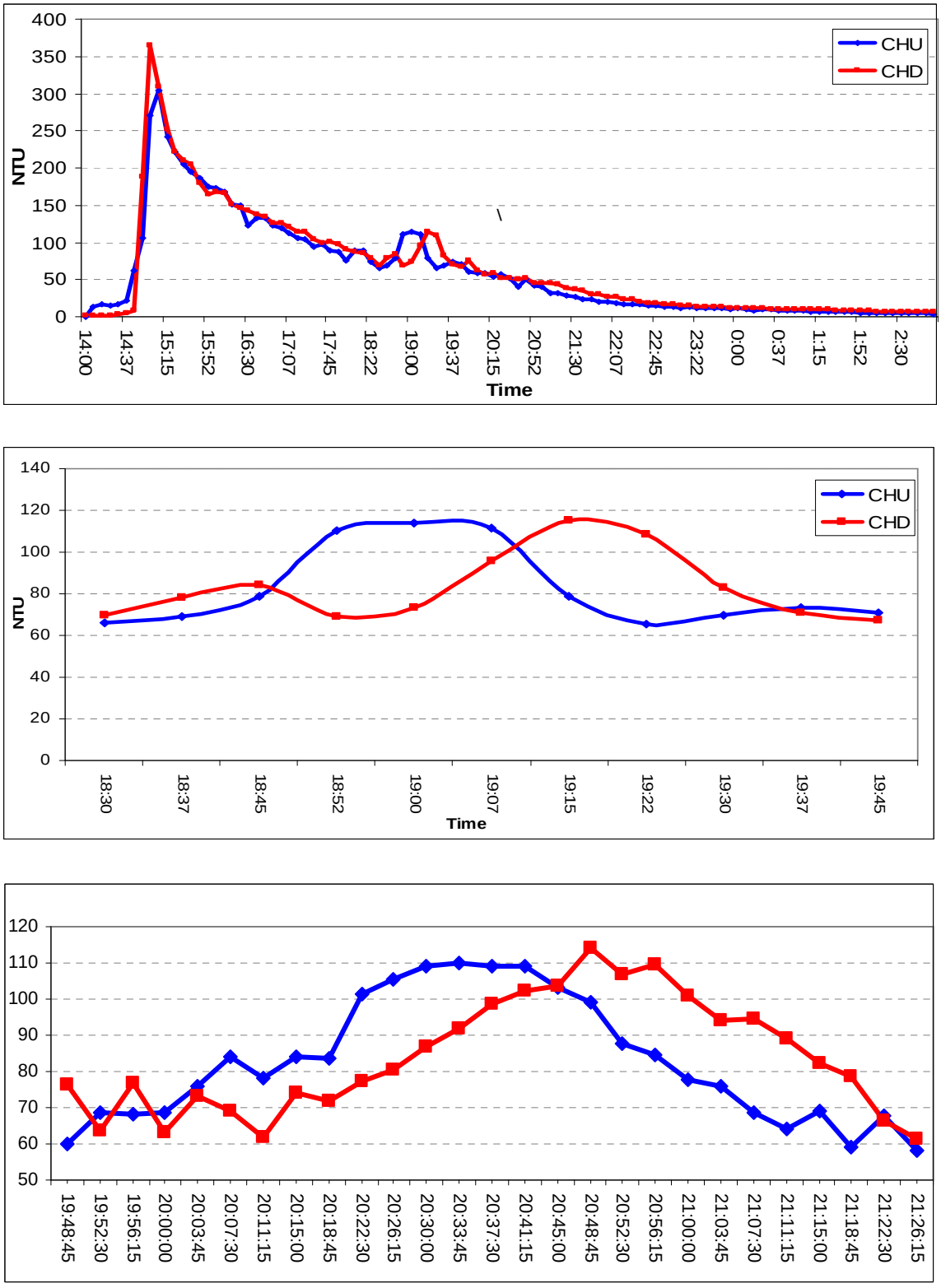

Figure 52. Travel times of turbidity through bar complex reach a) 7/27/08 Storm Turbidity Curve , b)7/27/08 Storm Mini-Peak. Total turbidity flux for CHU was 693.7 NTU, while for CHD it was 683.7 NTU.; c) 6/5/09 Turbidity Slug

Another natural slug was measured during the storm on June 5th 2009 (fig. 52). The slug of turbidity began shortly after 20:00 during the storm recession, and it produced the turbidity curve seen in fig. 52c. The net flux between the sites was 129.5 NTU's. Twenty-two minutes and thirty seconds elapsed between the start of the slug upstream and down, allowing the speed of its movement to calculated as 0.39 m/s. The elapsed time before the start and end of the slug at each site was 1:22:30 for CHU and 1:15:00 for CHD.

4.4.5 Potential Confounding Factors

For most storms the gauges were programmed to take a measurement of depth and turbidity every 7.5 minutes. This number was chosen so that the data obtained could be easily matched with data taken at the USGS run Northeast Branch gauge further downstream which has 15 minute measurement intervals. The speed and composition of water flowing through any channel varies constantly with turbulence and mixing, and because of this the turbidity is constantly changing. Depending on flow conditions, the actual stream conditions may change faster than the gauges take measurements. During especially intense storms, peak turbidities and depths may be missed entirely.

The velocity of water flow is dependent on the discharge of the stream. While some turbidity is being picked up within the bar complex, the ambient turbidity from upstream sources will have varying speeds of movement through the complex, depending on the magnitude of flow. Because of this, the peak turbidity lag times are

entirely dependent on the flow depth and during rising and falling limbs of the hydrograph the source of turbidity cannot be determined absolutely.

The gauges are located on the bed of the stream near the bank. They are located in the deepest part of the stream, but are nonetheless influenced by bank and bed roughness. The speed at which turbidity moves through the system is not necessarily reflected accurately by gauged data due to decreased flow velocity near the bed and banks of the stream. The actual depth of the different gauges is never the same and varies with discharge, so the near bed velocity upstream will usually be different than it is downstream.

4.5 Discussion

4.5.1 Summary and Implications

Storm events in the Anacostia River watershed cause a complex chain of events that can be traced from the headwaters through to the outlet into the Potomac. In this chapter I've determined that due to the extent of urbanization in the watershed, the storm response from the Northeast Branch has many properties similar to that of the Little Paint Branch. Their storm hydrographs follow a similar form, and lag times between peaks at the two sites are often only minutes apart when one could expect them to be around ninety minutes solely from the travel time of the water. This is due to the effects of stormwater management practices in both watersheds. While the practices may work to prevent flooding, they have also changed the hydrology of the area and provide a vehicle for the rapid transmittal of surface erosion and its

associated particulate to the rivers, which could be seen in the initial turbidity responses of some storms.

The proportions of storm runoff at NEB compared with CHU was surprising, as I expected that NEB, with its greater impervious area and many tributaries, to have a much higher proportion. This result was possibly simply due to the sheer size of the NEB drainage area in comparison with that of CHU, which would allow for more time for the retention and/or infiltration of storm water. Also, the overall gradient of the NEB drainage area is smaller, inhibiting the movement of runoff in comparison with the CHU drainage area which begins in the Piedmont.

The CHU site produced much flashier (rapidly peaking) storm turbidity values than the Northeast Branch gauging site did, indicating that there are one or more point sources upstream within the river or watershed. Per volume, the Little Paint Branch appears to be a major source of sediment; however, it is probable that much of this sediment is stored before it reaches NEB as the NEB watershed has several tributaries that are also considerable sources of sediment, such as Indian Creek. The turbidity flashiness was even more extreme at the GCR gauge, suggesting that the source of turbidity is storm runoff as there is no significant erosion upstream of the GCR site.

Within the Cherry Hill Bar Complex it was determined that during storms turbidity increased by only approximately ten percent between CHU and CHD. This was very likely due to bank erosion within the bar complex, as in Chapter 3 it was established that the gravel bars appear to selectively store fine sediment and the decreased shear stresses over the bar tops inhibit the initiation of sediment transport during storms, and also a mass failure event was recorded in the turbidity data after a

storm. By studying the foreign "slugs" of sediment moving through system, however, it appears that during flow recession the gravel bar complex reduces the sediment concentration of the flow, though this may also be due to natural settling.

Above all else this study has demonstrated the complexity of watershed storm response and sediment transport measurement. The Anacostia River watershed has been altered by urbanization such that the fundamental controls of its hydrology and morphology – water and sediment supply, are very difficult to model. Even given the complexities encountered however, some regional and general relationships could be established.

4.5.2 Future Work

The time series data on turbidity and depth can potentially be used to determine threshold values for shear velocity and turbidity. Preliminary analysis has been performed and found some strong initial relationships for sediment fall velocity and shear velocity thresholds for certain storms. With more refinement and water sample collection during storms, a relationship between turbidity and TSS should also be able to be determined.

Chapter 5: Conclusions

The Little Paint Branch is responding to changes in hydrology and sediment supply caused by urbanization through the formation of gravel bars and channel widening. Channel widening decreases flow depth and thus shear stress for bankfull and higher stages, thus flood discharges do not result in expected increases in sediment transport within the system. The decrease in flow depth caused by bar formation causes more frequent overbank flooding and it has reattached the Little Paint Branch to its floodplain. This last development may be crucial to the health of the Anacostia River and the entire Chesapeake Bay as a whole. Floodplains in coastal rivers are the last opportunity for storm sediments and their associated contaminants to be stored prior to discharge into estuarine and coastal systems.

Rosgen has suggested that river processes can be estimated from stream morphology. In the case of the Little Paint Branch Creek, the gravel bar reaches with their relatively high rates of stream bank erosion would be viewed as erosion problems. Due to their lack of entrenchment, however, they would be viewed as having higher stability than adjacent entrenched reaches according to Rosgen's classification scheme. This contradictory evidence of stability based on channel form and recent bank erosion can only be evaluated with data. This study provided an estimate of the amount of additional turbidity caused by bank erosion in the bar complex reach. The bank erosion caused a 10% increase in turbidity during this active phase of channel enlargement. The gravel bar formation, however, might provide a mechanism for channel change that results in increased overbank flooding and sediment storage on the floodplain.

More work needs to be done on the relationship between turbidity and sediment load in the Little Paint Branch so that more refined models of transport within the Little Paint Branch can be developed. It would also be beneficial for more monitoring of headwater streams in NE Branch Watershed and non-urban nearby watersheds in order to understand channel changes in urban watersheds. Storm water management practices in the area need to be evaluated for their contribution of suspended sediment to local streams.

Bibliography

Allmendinger, N.E., J.E. Pizzuto, G.E. Moglen, and M. Lewicki. 2007. A Sediment Budget for an Urbanizing Watershed, 1951-1996, Montgomery County, Maryland, U.S.A. *Journal of the American Water Resources Association* 43(6): 1483-1498.

Arnold, C.L., P.J. Boison, and P.C. Patton. 1982. Sawmill Brook: An Example of Rapid Geomorphic Change Realted to Urbanization. *Journal of Geology* 90: 155-166.

Ashworth, P.J., R.I. Ferguson, and M.D. Powell. 1992. Measurements in a braided river chute and lobe: II. Sorting of bedload during entrainment, transport, and deposition. *Water Resources Research* 28: 1887-1896.

Barry, J.J., J.M Buffington, and J.G. King. 2004. A general power equation for predicting bed load transport rates in gravel bed rivers. *Water Resources Research* 40: W10401

Behrns, K. 2006. Evaluation of Channel Adjustments to Urbanization on the Paint Branch Stream System. Unpublished Senior Thesis Paper, University of Maryland College Park.

Bernhardt, E.S. and M.A. Palmer. 2007. Restoring streams in an urbanizing world. *Freshwater Biology* 52: 738-751.

Bridge, J.S. 2003. Rivers and Floodplains: Forms, Processes, and Sedimentary Record. Blackwell Science Ltd., Malden, MA. 491pp.

Brierley, G. and K. Fryirs. 2005. *Geomorphology and River Management: Applications of the River Styles Framework*. Oxford, UK: Blackwell Publishing.

Brush, G.S. 1989. Rates and Patterns of Estuarine Sediment Accumulation. *Limnology and Oceanography* 34: 1235-1246.

Chesapeake Bay Program. Chesapeake Bay 2006 Health and restoration assessment. <www.chesapeakebay.net>

Chin, A. 2006. Urban transformation of river landscapes in a global context. *Geomorphology* 79: 460-487.

Church. 2006. Bed material transport and the morphology of alluvial river channels. *Annual Review of Earth and Planetary Sciences* 34: 325-354.

Cronin, T.M. and C.D. Vann. 2003. The Sedimentary Record of Climatic and Anthropogenic Influence on the Patuxent Estuary and Chesapeake Bay Ecosystems. *Estuaries* 26: 196-209.

Dade, W.B. and P.F. Friend. 1998. Grain size, sediment transport regime and channel slope in alluvial rivers. *Journal of Geology* 106: 661-675.

Dangol, A. 2009. Transport and Storage of Coarse and Fine Grained Sediment, Little Paint Branch Creek. Unpublished Senior Thesis Paper, University of Maryland College Park.

Dawdy, D.R. 1967. Knowledge of Sedimentation in Urban Environments. *Journal of Hydraulics Division, ASCE* 6: 235-245.

Dietrich, W.E., J.W. Kirchner, H. Ikeda, and I Fujiko. 1989. Sediment supply and the development of the coarse surface layer in gravel-bedded rivers. *Nature* 340: 20.

Dunne, T. and L.B. Leopold. Water in Environmental Planning. W.H. Freeman and Company, New York. 818pp.

Eaton, B.C. and R.G. Millar. 2004. Optimal alluvial channel width under a bank stability constraint. *Geomorphology* 62: 35-55.

EPA. Anacostia River Basin Watershed Sediment/TSS Maryland Approval Letter. PDF, Online.

Flintham, T.P. and P.A. Carling. 1993. Design of stable drainage networks in upland forestry plantations. *Hydrological Processes* 7(3): 335-347.

Gao, P. 2008. Understanding watershed suspended sediment transport. *Progress in Physical Geography* 32(3): 243-263.

Hammer, R.J. 1972. Stream channel enlargement due to Urbanization. *Water Resources Research* 8(6): 1530-1540.

Hession, W.C., J.E. Pizzuto, T.E. Johnson, and R.J. Horowitz. 2003. Influence of Bank Vegetation on Channel Morphology in Rural and Urban Watersheds. *Geology* 31: 147-150.

Hey, R.D. and C.R. Thorne. 1986. Stable Channels with Mobile Gravel Beds. *Journal of Hydraulic Engineering* 112(8): 671-689.

Huang, H.Q., G.C. Nanson, and S.D. Fagan. 2002. Hydraulic geometry of straight alluvial channels and the principle of least action. *Journal of Hydraulic Research* 40: 153-160.

Kemp, W.M., W.R. Boynton, J.E. Adolf, D.F. Boesch, W.C. Boicourt, G. Brush, J.C. Cornwell, T.R. Fisher, P.M. Gilbert, J.D. Hagy, L.W. Harding, E.D. Houde, D.G. Kimmel, W.D. Miller, R.I.E. Newell, M.R. Roman, E.M. Smith, and J.C. Stevenson. 2005. Eutrophication of Chesapeake Bay: Historical Trends and Ecological Interactions. *Marine Ecology-Progress Series* 303: 1-29.

Kosiba, A. 2008. Stability of Gravel Bars in Paint Branch Creek. Unpublished Senior Thesis Paper, University of Maryland College Park.

Leopold, L.B. and T. Maddock. 1953. The Hydraulic Geometry of Stream Channels and Some Physiographic Implications. *Geological Survey Professional Paper* 252

Leopold, L.B. and J.P. Miller. 1956. Ephemeral Streams: Hydraulic Factors and Their Relation to Drainage Net. *Geological Survey Professional Paper* 282-A

Leopold, L.B. and M.G. Wolman. 1957. River Channel Patterns: Braided, Meander and Straight. *Geological Survey Professional Paper* 282-B

Mclean, S.R. 1991. Depth-Integrated Suspended-Load Calculations. *Journal of Hydraulic Engineering* 117(11).

Millar, R.G. 2004. Theoretical regime equations for mobile gravel-bed rivers with stable banks. *Geomorphology* 64: 207-220.

Morisawa, M. and J.E. LaFlure. 1979. Hydraulic Geometry, Stream Equilibrium, and Urbanization. *Adjustments of the Fluvial System* 10: 333-350.

Neller, R.J. 1988. A comparison of Channel Erosion in Small Urban and Rural Catchments, Armidale, New South Wales. *Earth Surface Proces and Landforms* 13(1): 1-7.

Parker, G. 1978. Self-formed rivers with equilibrium banks and mobile bed: Part 2: The gravel river. Journal *of Fluid Mechanics* 89: 127-146.

Parker, G. 1979. Hydraulic Geometry of Active Gravel Rivers. *Journal of the Hydraulics Division* HY9: 1185-1201

Parker, G., P.C. Klingeman, D.G. McLean. 1982. Bedload and Size Distribution in Paved Gravel-Bed Streams. *Journal of the Hydraulics Division* 108(4): 544-571.

Paul, M. and J. Meyer. 2001. Streams in the urban landscape. *Annual review of Ecology and Systematics* 32: 333-365.

Pizzuto, J.E., W.C. Hession, and M. McBride. 2000. Comparing gravel-bed rivers in paired urban and rural catchments of southeastern Pennsylvania. *Geology* 28(1): 79-82.

Prince George's County DER. <www.princegeorgescountymd.gov/Government/AgencyIndex/DER>

Prestegaard, K.L., S. Dusterhoff, K. Houghton, K. Clancy, and E. Stoner. 2001. Hydrological and geomorphologic characteristics of Piedmont and Coastal Plain Streams, MD. *Maryland Department of Environment Report.*

Rosgen, D.L. 1994. A classification of natural rivers. *Catena* 22: 169-199.

Rouse, H. 1937. Modern conceptions of the mechanics of turbulence. *Trans American Soceity of Civil Engineering* 102: 436-505.

Simon, A., M. Doyle, M. Kondolf, F.D. Shields, B. Rhoads, and M. McPhillips. 2007. Critical evaluation of how the rosgen classification and associated "natural channel design" methods fail to integrate and quantify fluvial process and channel response. *Journal of the American Water Resources Association* 43(5): 951-956.

Ward, J., K. Tockner, U. Uehlinger, and F. Malard. 2001. Understanding natural patterns and processes in river corridors as the basis for effective river restoration. *Regulated Rivers: Research and Management* 17: 311-323.

Wiberg, P.L. and J.D. Smith. 1987. Calculations of the Critical Shear Stress for Motion of Uniform and Heterogeneous Sediments. *Water Resources Research* 23(8) 1471-1480.

Wilcock, P.R. 2001. Toward a practical method for estimating sediment-transport rates in gravel-bed rivers. *Earth Surface Process Landforms* 26: 1395-1408.

Wilcock, P.R. and J.C. Crowe. 2003. Surface-based transport model for mixed-size sediment. *Journal of Hydraulic Engineering* 129(2): 120-128.

Wolman, M.G. 1955 A method of sampling coarse river-bed material. *Transactions, American Geophysical Union* 35(6).

Wolman, M.G. 1967 A cycle of sedimentation and erosion in urban river channels. *Geografiska Annaler* 49A: 385–95.

Wolman, M.G. and A.P. Schick. 1967. Effects of Construction on Fluvial Sediment, Urban and Suburban Areas of Maryland. *Water Resources Research* 3(2): 451-464.

Yang, C.T., C.C.S. Song, and M.J. Woldenberg. 1981. Hydraulic geometry and minimum rate of energy dissipation. *Water Resources Research* 17: 1014-1018.